ucc

Coláiste na hOllscoile Corcaigh, Éire
University College Cork, Ireland

Design of Digital Differentiators

Xiaoli Yang, B.E.

A thesis presented to the National University of Ireland, Cork

for the degree of Ph.D.

January 2014

School of Engineering ,

University College Cork,

Ireland

head of School: Prof. *Nabeel A. Riza*

Supervisor: Dr. Richard C. Kavanagh

Acknowledgments

I am indebted to Dr. Richard C. Kavanagh, whose encouragement, guidance and support over the past four years has enabled me to understand and research the subject matter of this project. His keen and vigorous academic observations were enlightening, not only in this project but also for my future study. I appreciate his vast knowledge and skill in many areas, and his assistance in writing this report.

I would especially like to thank Liu Yuping and Yang Donghua, my mother and father, for the support they provided me through my entire life. I also express my sincere appreciation to the staff of the School of Engineering and my friends, fellow students, and former and current colleagues, for their assistance and never-ending encouragement. I also most gratefully acknowledge the financial support of UCC, particularly the School of Engineering, which assisted me throughout much of my Ph.D. studies.

Declaration

I declare that this thesis is the product of my own work, which it has not been submitted before for any degree or examination in any other university, either at University College Cork, or elsewhere.

Abstract

A digital differentiator simply involves the derivation of an input signal. This work includes the presentation of first-degree and second-degree differentiators, which are designed as both infinite-impulse-response (IIR) filters and finite-impulse-response (FIR) filters. The proposed differentiators have low-pass magnitude response characteristics, thereby rejecting noise frequencies higher than the cut-off frequency. Both steady-state frequency-domain characteristics and Time-domain analyses are given for the proposed differentiators. It is shown that the proposed differentiators perform well when compared to previously proposed filters. When considering the time-domain characteristics of the differentiators, the processing of quantized signals proved especially enlightening, in terms of the filtering effects of the proposed differentiators.

The coefficients of the proposed differentiators are obtained using an optimization algorithm, while the optimization objectives include magnitude and phase response. The low-pass characteristic of the proposed differentiators is achieved by minimizing the filter variance, which provides a measure of the ability of the filter to attenuate noise corruption on an input signal. The low-pass differentiators designed show the steepest roll-off when compared with a number of other previously proposed differentiators of the same order, as well as having highly accurate magnitude response in the pass-band. The proposed differentiators can be designed for a particular group delay or roll-off characteristics, by choosing an application-dependent weight vector when defining the goals.

While having a history of over three hundred years, the design of fractional differentiator has become a ‘hot topic’ in recent decades, because many authors have pointed out that these mathematical phenomena allow for

the description of a real object more accurately than the classical integer-degree model. One challenging problem in this area is that there are many different definitions to describe the fractional model, such as the Riemann-Liouville and Caputo definitions. Some new fractional degree differentiators are designed using both of the above definitions. Through use of a feedback structure, based on the Riemann-Liouville definition. It is shown that the performance of the fractional differentiator can be improved in both the frequency-domain and time-domain. Further time-domain analyses show that the Caputo differentiators have better performance than other Fractional degree (FD differentiators when the initial value of the input signal is not zero.

Two applications based on the proposed differentiators are described in the thesis. Specifically, the first of these involves the application of second degree differentiators in the estimation of the frequency components of a power system. A linear phase FIR second degree differentiator replaces a previously proposed IIR differentiator in a frequency-estimation algorithm, to avoid the error caused by the variable group delay. The second example concerns for an image processing, edge detection application. In this application, it is shown that IIR FD differentiators can be used to advantage when applied to the edge detection application, with the Caputo-based FD differentiators showing particular advantages.

Contents

Nomenclature

h_n : component of the impulse response, equivalent to the filter coefficients for an FIR filter.

N : filter order; an N^{th} order filter has $P = N + 1$ terms.

b_n and IIR filter coefficients(numerator and denominator, respectively).

$H\left(e^{j\omega}\right)$: frequency response of a filter.

$\beta\left(e^{j\omega}\right)$: phase response of a filter.

$\tau\left(e^{j\omega}\right)$: group delay.

$x(n)$: input signal.

$y(n)$: output signal.

R : output noise power gain or variance of the filter.

$E(\omega)$: maximum absolute value of the error function.

$\mathbf{F}$: the set of prescribed frequency bands.

r : radius of a pole.

ε : the total weighted least-squares error . λ, w_n, v_n are the weighting factors.

Ls : the number of frequency components of an FIR filter.

$H_{des}\left(\omega_n\right)$: desired magnitude response of a low-pass differentiator.

$H_d(\omega)$: ideal magnitude response of a full-band differentiator.

$\sigma^2(\omega)$: variance of the group delay.

m_g : mean of the group delay.

p : number of filter coefficients.

α : fractional delay.

I : integer delay.

$H_d(\omega)$: ideal full-band second-degree differentiator.

$O(\alpha^{k+1})$: error term of decays as fast as α^{k+1} .

$\delta(\cdot)$: the delta function.

$PI^{\rho_1}D^{\rho_2}$: fractional degree controller.

$\Gamma(z)$: Euler's gamma function.

v : degree of fractional differentiator.

${}_aD_t^v f(t)$: Riemann-Liouville or Grunwald-Letnikov derivative.

${}_a^C D_t^v f(t)$: Caputo derivative.

Chapter 1 Introduction

Determining the derivative of a given applied signal is a traditional and well known problem in many applications. In control systems, differentiator is a fundamental element of the proportional-integral-derivative controller (PID). In image processing, edge detection can be implemented by using a differentiator. In biomedical engineering, the sharpness of some biological signals, such as the electroencephalogram (EEG) and electrocardiogram (EKG), can be measured by using second-degree differentiator. Additionally, in power systems, the second-degree differentiator is used to estimate the fundamental frequency. The derivatives of a given signal can often be determined explicitly using basic mathematical functions. However, there is frequently no simple expression for the derivative of the given signal when it is interfered with by noise. As a result, the design of digital differentiators remains an important topic in practical systems. Many articles are found on the design of first-degree differentiators, while significantly lesser attention has been paid to second degree or higher degree differentiators. Additionally, the fractional-degree differentiator has attracted significant attention in recent years, because of the increased use of fractional calculus in the modeling and control of physical phenomena. It is assumed in the thesis that the signals being considered are stationary, so that the noise characteristics of the signals do not vary greatly over the time interval considered. At the very least, it is assumed that a single differentiator will be applied to the input signals over the time interval.

The following section of the introduction chapter contains an overview of some basic concepts of digital signal processing and relevant mathematical tools. In this thesis, both finite impulse response (FIR) and Infinite impulse response (IIR) differentiators are designed, so the concepts of FIR and IIR filters will be

introduced. For an IIR filter, group delay is one of the most important characteristics to be considered, so that an expression is given by which the group delay can be calculated. In this thesis, some differentiators are designed using an optimization technique to calculate the filter coefficients. Therefore, an introduction to the mathematical tool employed, the sequential quadratic programming method (which is included in the Matlab optimization toolbox) is provided in the final section of this chapter.

This work focuses on the field of the design of digital differentiators – first-degree and second-degree FIR or IIR low-pass differentiators. The most basic, and common, concepts relating to digital differentiators are introduced in Chapter 2, one aspect of which concerns the ideal magnitude response of a first-degree differentiator. Then, an IIR low-pass first-degree digital differentiator is designed using an optimization technique: the sequential quadratic programming method. This is applicable to nonlinear functions, and is used for computing the optimized filter coefficients. A vector of weight coefficients is set, as part of the minimization process, to define the relative importance of different objectives for IIR differentiators: magnitude response, variance, and flatness of group delay response. Additionally, a FIR low-pass differentiator is designed using a similar method, for which the optimization objectives include magnitude response and variance. The proposed FIR differentiator has linear-phase characteristics of either Type III or Type IV form. The proposed differentiators have low-pass characteristics and steep roll-off transition-bands, achieved by minimizing the filter variance. The variance provides a measure of the ability of the filter to attenuate noise corruption on an input signal. In this thesis, the cut-off frequency of low-pass differentiator is defined as the frequency where the magnitude response of the differentiator starts being attenuated significantly (e.g. by 3 dB), compared with the ideal

full-band differentiator. The FIR implementation differs from some implementations by allowing a variable cut-off frequency. The proposed differentiators exhibit highly accurate magnitude response in the pass-band, which is obtained by optimizing the squared error of the magnitude response, relative to that of the ideal differentiator. In particular, the proposed IIR differentiator has almost linear phase response in the pass-band, as well as being characterized by the minimization of the variation of the group delay. Test and analysis of the proposed differentiators are considered in both the frequency-domain and time-domain, and compared with some existing methods. In the frequency-domain, the proposed differentiators show the steepest roll-off when compared with a number of other differentiators of the same order, as well as having highly accurate magnitude response in the pass-band. For time-domain testing, the proposed differentiators show very good performance in terms of noise filtering. In addition, another advantage of the proposed method is that the designer can design a differentiator for a particular group delay or roll-off characteristics, by choosing an application-dependent weight vector when defining the goals.

It is shown that the techniques employed for the first-degree differentiator are easily applied for the second-degree differentiator. In Chapter 3, a new method for the design of low-pass second-degree digital differentiators is presented. The proposed FIR differentiator exhibits better attenuation performance on the transition band and stop band, though some high-frequency ripple exists. The proposed differentiators show good performance when testing the time-domain behavior, especially when evaluating the response to input noise. Because the second-degree differentiator is particularly sensitive to noise, such differentiators have a stricter requirement (relative to first-degree differentiators) in terms of the

attenuation required in the transition band and stop band.

Additionally, the fractional-degree differentiator is designed and discussed. The proposed differentiator can be based on one of the standard definitions of the fractional calculus, such as the Riemann-Liouville, Grunwald-Letnikov and Caputo definitions. A classical IIR fractional-degree differentiator and a fractional-degree integrator are combined using a proportional feedback loop. This structure is found to improve the performance of the proposed differentiator, in terms of both its frequency-domain and time-domain characteristics. In addition, the fractional degree differentiator based on the Caputo definition also been designed. It is shown that the proposed Caputo differentiator exhibit better performance when the initial value of input is no zero.

The applicability of the proposed differentiators is presented. For example, a second–degree differentiator-based algorithm is applied to the problem of frequency estimation in power systems. The proposed structure result exhibits good performance using a specifically designed proposed FIR second-degree differentiator. Additionally, in image processing, the edge detection problem is introduced and discussed. The proposed fractional degree IIR differentiators, based on Riemann-Liouville and Caputo definition, are used for this detection, and show good results. Especially, the Caputo-based edge-detector has a better visual appearance when compared with the Riemann-Liouville edge detector.

1.1 Review of Established Work on Digital Signal Processing

This review includes the following four sections which concern:

1. The concept of finite impulse response (FIR) filters;
2. The concept of Infinite impulse response (IIR) filters;
3. The concept of group delay;
4. The optimization toolbox of Matlab.
5. Performance metrics of low-pass differentiators.

1.1.1 The concept of finite impulse response (FIR) filters

In digital signal processing, the impulse response $h(n)$ of the FIR filter is finite $(0 \le n \le N)$. The transfer function of a FIR filter is defined by the following equation:

$$H(z) = \sum_{n=0}^{N} h_n z^{-n} \tag{1.1}$$

where :

- h_n is a component of the impulse response, equivalent to the filter coefficients,

- N is the filter order; an N^{th} order filter has $p = N + 1$ terms.

The FIR filter has the following properties [1]: The FIR filter can be designed to possess linear phase, when the phase response of the filter is a linear function of frequency. A FIR filter is linear phase if and only if the filter coefficients are symmetrical or anti-symmetrical. The FIR filter is always stable, because the impulse response has a finite number of terms and is therefore absolutely summable.

1.1.2 The concept of the Infinite impulse response (IIR) filter

The Infinite Impulse Response (IIR) filter is another primary type of digital filter used in digital signal processing. The impulse response of such a filter is infinite due to the feedback nature of the system. The transfer function of an N^{th} order IIR filter is defined by the following equation:

$$H(z) = \frac{B(z)}{A(z)} = \frac{b_n z^{-n}}{a_n z^{-n}} = \frac{b_0 + b_1 z^{-1} + b_2 z^{-2} + \ldots + b_N z^{-N}}{a_0 + a_1 z^{-1} + a_2 z^{-2} + \ldots + a_N z^{-N}} \qquad (1.2)$$

where b_n and a_n are the IIR filter coefficients,

In designing an IIR filter, it is necessary to constrain all complex poles to have an absolute magnitude of, at most, slightly less than unity, to ensure the filter's stability [2]. One expects an IIR filter to achieve a similar given magnitude response specifications with one-fifth (or less) of the order of corresponding FIR filter [3].

1.1.3 The concept of, and expression for, group delay

In telecommunications applications, group delay is one of the most important characteristics to be considered, because a filter with constant group delay passes a square wave with little distortion [4]. Thus, the variation of the group delay with frequency, which can be obtained from [5], is an important aspect of IIR filter design.

The frequency response $H\left(e^{j\omega}\right)$ can be expressed as:

$$H\left(e^{j\omega}\right)=\left|H\left(e^{j\omega}\right)\right|e^{j\beta\left(e^{j\omega}\right)}=\mathrm{Re}\left[H\left(e^{j\omega}\right)\right]+j\,\mathrm{Im}\left[H\left(e^{j\omega}\right)\right] \qquad (1.3)$$

Thus, the phase response $\beta\left(e^{j\omega}\right)$ of the filter is:

$$\beta\left(e^{j\omega}\right)=\arctan\left(\frac{\mathrm{Im}\left[H\left(e^{j\omega}\right)\right]}{\mathrm{Re}\left[H\left(e^{j\omega}\right)\right]}\right) \qquad (1.4)$$

The group delay $\tau\left(e^{j\omega}\right)$ is expressed as:

$$\tau\left(e^{j\omega}\right)=-\frac{d\,\beta\left(e^{j\omega}\right)}{d\,\omega}$$

It can be rewritten as:

$$\begin{aligned}\tau(e^{j\omega}) &= -\frac{d\beta(z)}{dz}\frac{dz}{d\omega}\bigg|_{z=e^{j\omega}} \\ &= -jz\frac{dz}{d\omega}\bigg|_{z=e^{j\omega}}\end{aligned}$$

because

$$\ln\left[H(e^{j\omega})\right] = \ln\left|H\left(e^{j\omega}\right)\right| + j\beta\left(e^{j\omega}\right)$$

where $\ln(\cdot)$ corresponds to the natural logarithm, and

$$\beta\left(e^{j\omega}\right) = \mathrm{Im}\left\{\ln\left[H\left(e^{j\omega}\right)\right]\right\}$$

The expression for group delay is:

$$\begin{aligned}
\tau\left(e^{j\omega}\right) &= -\mathrm{Im}\left[\frac{d}{d\omega}\left\{\ln[H(e^{j\omega})]\right\}\right]_{z=e^{j\omega}} \\
&= -\mathrm{Im}\left[\frac{d\left\{\ln\left[H(z)\right]\right\}}{dz}\frac{dz}{d\omega}\right]_{z=e^{j\omega}} \\
&= -\mathrm{Im}\left[j\,z\frac{d\left\{\ln\left[H(z)\right]\right\}}{dz}\right]_{z=e^{j\omega}} \\
&= -\mathrm{Re}\left[z\frac{d\left\{\ln\left[H(z)\right]\right\}}{dz}\right]_{z=e^{j\omega}} \\
&= -\mathrm{Re}\left[z\frac{dH(z)}{dz}\frac{1}{H(z)}\right]
\end{aligned} \tag{1.5}$$

The group delay of a digital filter is constant when the filter exhibits a linear phase characteristic.

1.1.4 Optimization algorithm utilized for differentiator

In this work, optimization techniques are needed to enable the calculation of differentiator coefficients, which is a nonlinear optimization problem. The Matlab Optimization toolbox provides widely used algorithms for standard and large-scale optimization problems. These algorithms solve constrained, and unconstrained, continuous and discrete problems.

The Matlab solver *fgoalattain*, which concerns the minimization of multi-objectives simultaneously, is used for computing the optimized filter coefficients. This solver, *fgoalattain*, uses a sequential quadratic programming (SQP) method, which addresses the problem of solving nonlinear functions [6][7]. A vector of weight coefficients must be set to define the relative importance of different objectives. Compared with traditional linear or nonlinear methods, the advantage of using this solver is: The goals can be defined more clearly, and the resultant differentiator has exactly constrained magnitude and phase response performance, as desired.

It is necessary to use a suitable optimization algorithm which ensures the avoidance of local minima. In [13], the iterative quadratic programming approach is used. Alternatively, other authors pay attention to unconventional algorithms such as the genetic algorithm (GA), simulated annealing (SA) or neural networks [3][13][14][22].

The probability of finding local minima will be decreased by the use of judiciously chosen constraints. Specifically, the use of a nonlinear constraint method, such as the SQP method, to optimize a nonlinear function, can be problematical in ensuring the avoidance of local minima. A practicable method is to find suitable starting points (initial 'guess' for the filter parameters) and to include constraints that ensure the system's stability. A convenient method of choosing the start points is to utilize filter parameters of some existing differentiators, such as the differentiators in [3], [9] and [18], with similar requirements (cut-off frequency, order of the filter and stop band attenuation). If problems due to the local minima still occur, the parameters from another existing differentiator are instead chosen, with the resulting new design being evaluated.

1.1.5 Performance metrics of low-pass differentiator

A desired low-pass differentiator can be designed to approximate closely to an ideal differentiator in the pass-band, but it should attenuate the magnitude response (ideally to zero) in the transition-band and stop-band. Additionally for the IIR differentiator, a differentiator that provides close to linear phase is also very important. Thus, the performance metrics of low-pass differentiators in the frequency domain include: (1) percent error in pass-band; (2) attenuation in transition band and stop band and (3) the variation (if any) of the group delay. For time-domain performance, (1) the output should be the derivatives of input signal, (2) and should exhibit good noise rejection performance.

Chapter 2 Design of a First-Degree Digital Differentiator

2.1 Introduction

An ideal discrete-time differentiator is a linear system. When samples of a band-limited continuous signal are used as input, the output samples represent the derivative of the continuous signal. Given a continuous-time signal $x(t)$ and its corresponding sampled version $x(n) = x(nT)$, which can be assumed to be input to an ideal differentiator, an output signal $y(n)$ can be produced, for which [8]:

$$y(n) = \left.\frac{dx(t)}{dt}\right|_{t=nT} \tag{2.1}$$

If the Fourier transform of a continuous time input signal is denoted by $X(j\omega)$, the Fourier transform of its derivative is obviously given by $j\omega X(j\omega)$. Thus, the ideal discrete-time differentiator has the following frequency response:

$$H\left(e^{j\omega}\right) = j\omega, \quad |\omega| \le \pi \tag{2.2}$$

The corresponding magnitude are shown on Figure 2.1. Note that the normalized frequency is typically scaled to one at the Nyquist frequency, the corresponding normalized magnitude being π.

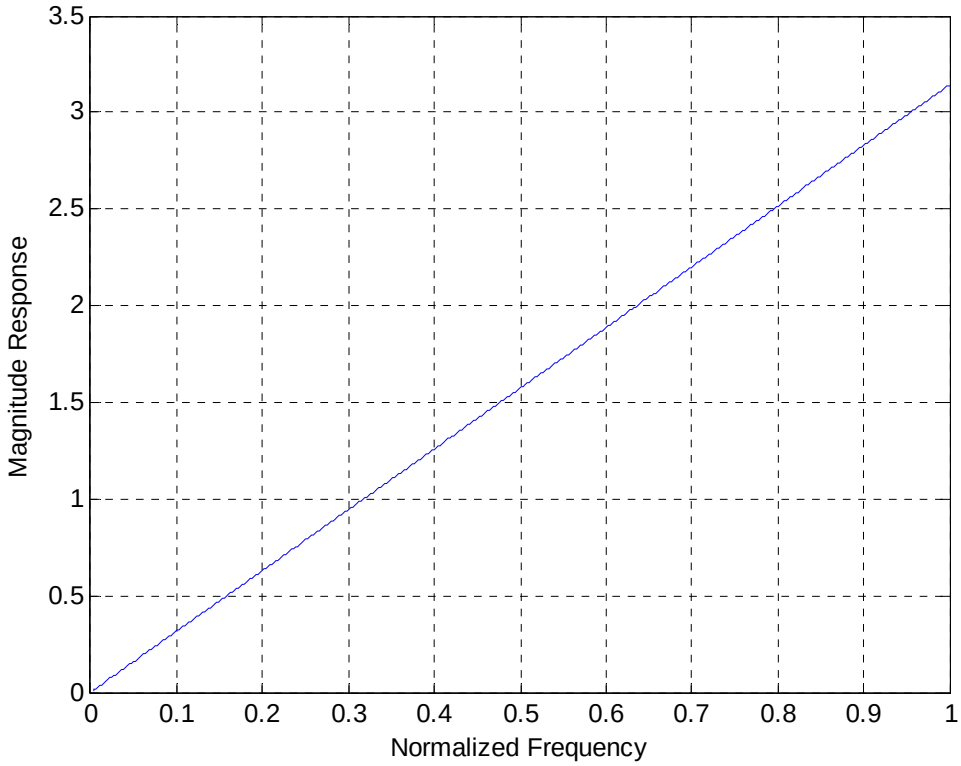

Figure 2.1 *Ideal magnitude response of ideal, normalized first-degree differentiator.*

2.2 Literature review

Many methods and possibilities have been proposed in the literature for the design of first-degree digital differentiators. For FIR differentiators, Kavanagh describes a method of using time-domain-based differentiator input/output sequences to design the FIR first-degree differentiator [24]. As described by Vainio et al, such FIR differentiators can be designed to provide optimum noise attenuation [9]. In [8], and in many other texts, the FIR differentiator

approximation that is obtained from window functions is described. Alternatively, it has been shown in the literature [10][11][12] that a first-degree differentiator can be designed using the numerical integration rule. The design method proposed by Al-Alaoui in [3] is based on the use of a numerical integration rule to design a low-pass IIR differentiator, by cascading a low-pass filter with an all-pass differentiator. With the development of optimization algorithms, many authors have designed both FIR and IIR digital differentiators using such optimization techniques [3][11][13][14]. Sections 2.2.1 to 2.2.4 provide the literature review for the design of FIR differentiator, while Sections 2.2.6 to 2.2.7 contain the literature review of the design of IIR differentiator.

2.2.1 Design using time-domain-based differentiator using input/output sequences

For a FIR differentiator, which consists of a transversal filter of order N with coefficients $h(n)$, the transfer function of a differentiator should preferably be represented by the equations [9] [24]:

$$\sum_{n=0}^{N} h(n) = 0 \tag{2.3}$$

$$\sum_{n=0}^{N} nh(n) = -1 \tag{2.4}$$

Equations (2.3) and (2.4) can be used to define a digital differentiator that exhibits:

- zero gain for d.c. input, and

- an output equal to the slope for a ramp input.

(2.3) and (2.4) can be rewritten in the following matrix form:

$$\mathbf{V_1}\, h = \mathbf{V_2} \tag{2.5}$$

where $h = [h(0), h(1), \ldots, h(N)]^T$, and $\mathbf{V}_1$, and $\mathbf{V_2}$ are given by:

$$\mathbf{V}_1 = \begin{bmatrix} 1 & 1 & 1 & \ldots & 1 & 1 \\ N & N-1 & N & \ldots & 1 & 0 \end{bmatrix} \tag{2.6}$$

and

$$\mathbf{V_2} = \begin{bmatrix} 0 \\ -1 \end{bmatrix} \ . \tag{2.7}$$

As commonly defined for FIR filters, when $h_n = -h_{N-1-n}$, the differentiator is a Type III or Type IV filter (filter coefficients anti-symmetrical) which exhibits a linear-phase characteristic. In [9], an FIR differentiator was designed with optimum noise attenuation. Assuming that the additive noise has a flat power response, the output noise power gain is given by:

$$R_s = \sum_{n=0}^{N} h^2(n) \tag{2.8}$$

Thus, the problem is to minimize the quantity R_s with the two constraints (2.3) and (2.4). The authors solved the optimization problem above, by using the method of Lagrange multipliers. The filter coefficients are given by [9], with transfer function:

$$h(n) = \frac{6}{(N+1)(N+2)}\left(1 - \frac{2n}{N}\right), \quad n = 0, 1, \cdots, N \tag{2.9}$$

The magnitude responses are plotted using the Matlab function '*dbode*', as shown in Figure 2.2. The *y*-axis is zoomed to 1 to provide a clear view of the response. The linear equations (2.5) can be solved using the Moore-Penrose pseudoinverse matrix, for example, in [28], a linear-phase second-degree FIR differentiator is obtained using this method. The Moore-Penrose pseudoinverse computes a 'best fit' (least squares) solution to a system of linear equations that lacks a unique solution. Thus, the differentiators designed using the Moore-Penrose pseudoinverse and those obtained using Lagrangian multipliers [9] give exactly the same results.

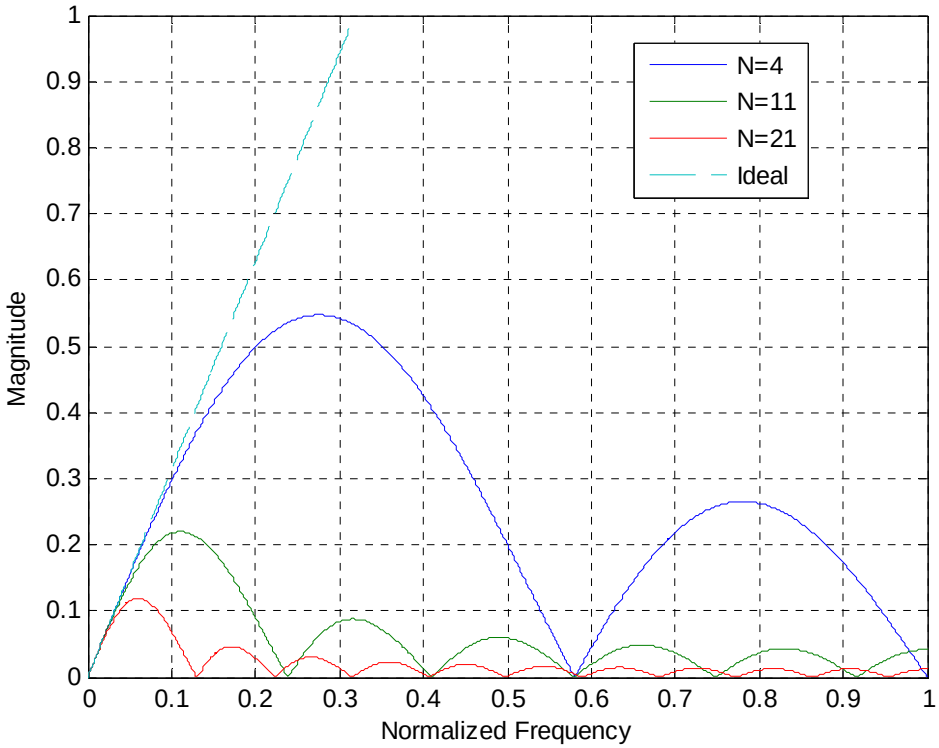

Figure 2.2 *Magnitude responses of the FIR differentiator with orders N = 4, N = 11, N = 21, and ideal digital differentiators.*

2.2.2 Design of a FIR differentiator using window functions

From the Fourier transform of an FIR filter, the relationship between the frequency response $H(e^{j\omega})$ and the coefficients $h(n)$ is given by the following equations:

$$H(e^{j\omega}) = \sum_{n=-\infty}^{\infty} h(n)e^{-j\omega n} \tag{2.10}$$

$$h(n) = \frac{1}{2\pi}\int_{-\pi}^{\pi} H(e^{j\omega})e^{j\omega n}d\omega \tag{2.11}$$

Using equation (2.2), the corresponding impulse response is given by:

$$\begin{aligned} h(n) &= \frac{1}{2\pi}\int_{-\pi}^{\pi} j\omega e^{j\omega n}d\omega \\ &= \begin{cases} 0, & for \quad n = 0 \\ \dfrac{1}{2\pi}\left[e^{j\omega n}\left(\dfrac{\omega}{n} - \dfrac{1}{jn^2}\right)\right]\Bigg|_{-\pi}^{\pi} = \dfrac{(-1)^n}{n} & for \quad n \neq 0 \end{cases} \end{aligned} \tag{2.12}$$

An example is provided here of using rectangular, triangular, Hamming, Hanning, and Blackman windows, for an order $N = 44$. The filter coefficients are obtained from the convolution of the impulse response of the differentiator (shown in (2.12)) and different window functions. Figure 2.3 represents the magnitude responses of different windows, which shows the outputs of some FIR differentiator designs. Each window is applied to an all-pass differentiator. Obviously, the rectangular window and triangular window don't show good magnitude response characteristics. Figure 2.4 gives the percentage errors of the FIR differentiators that make use of the other windows. Based on the above, the Blackman window is found to exhibit the smallest percentage error of magnitude responses amongst these windows.

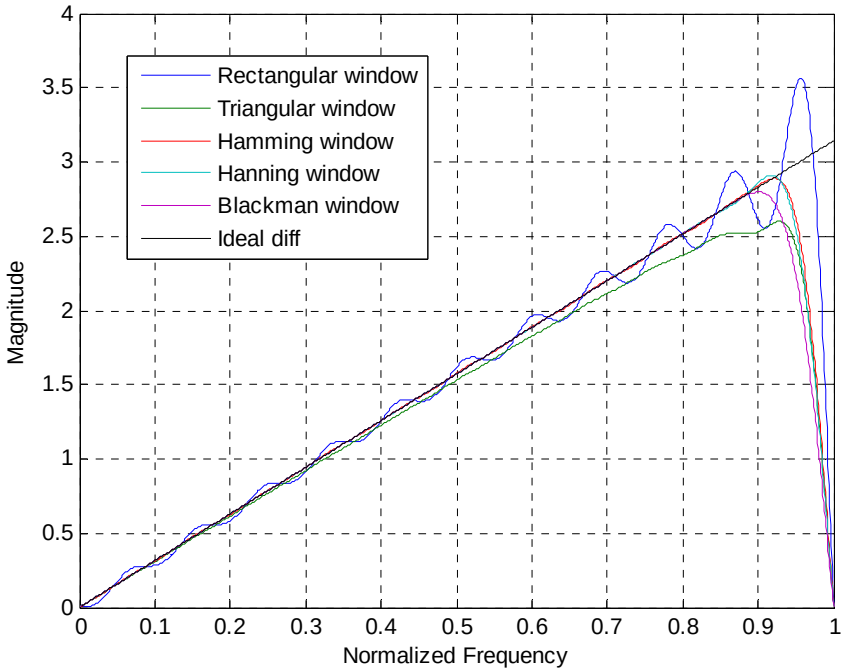

Figure 2.3 *Magnitude responses of the FIR differentiators with rectangular, triangular, Hamming, Hanning, and Blackman windows.*

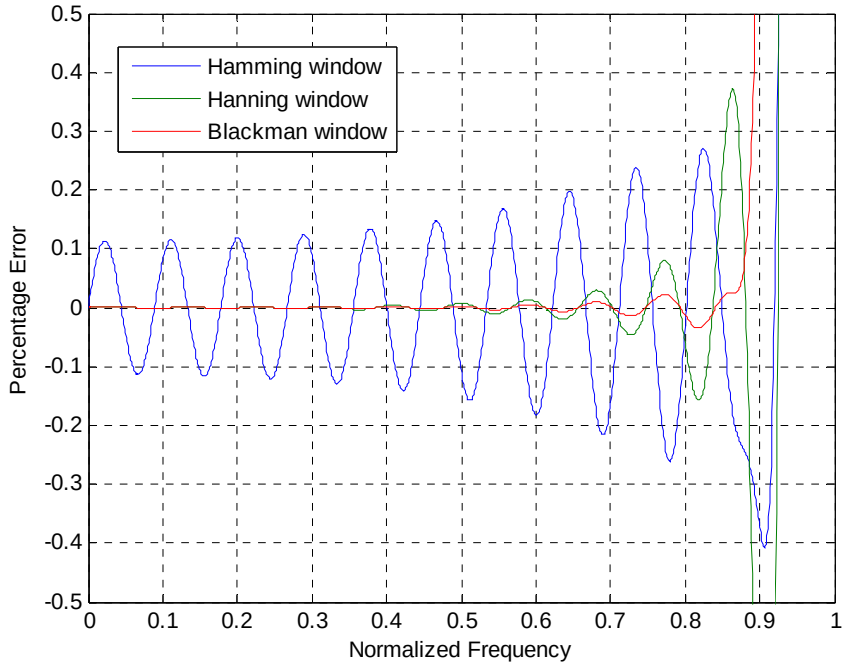

Figure 2.4 *Percentage error of the FIR differentiators with Hamming, Hanning, and Blackman windows.*

Another example shows the magnitude response of the Blackman window with different even orders $N = 6$, $N = 10$, $N = 20$, and $N = 40$. Figure 2.5 shows that the frequency range over which one obtains a small percentage error, relative to the ideal passband response, changes with the order of the differentiator.

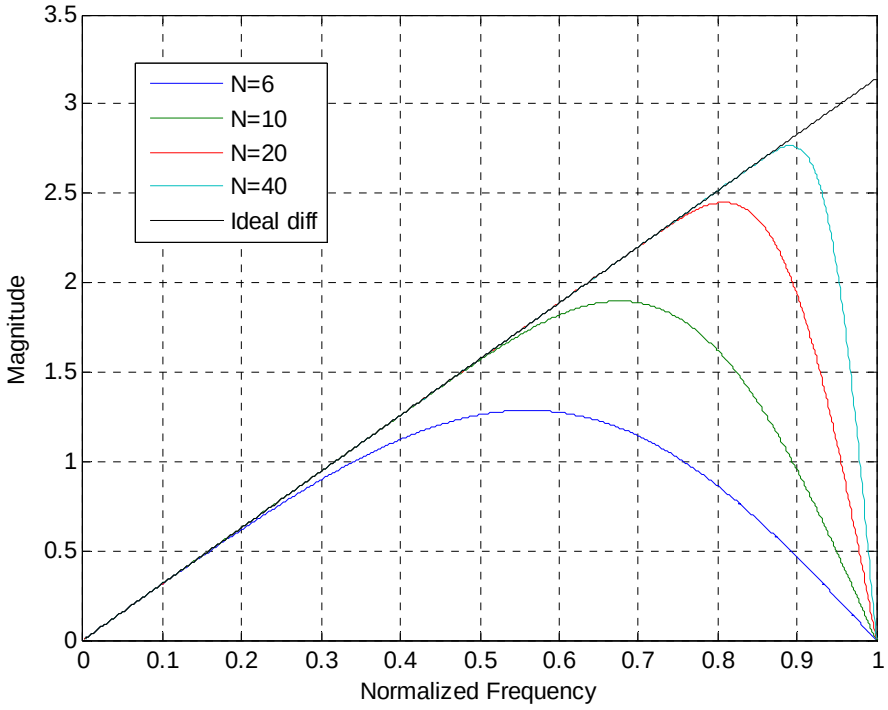

Figure 2.5 *Magnitude responses of FIR differentiators using the Blackman window, for* $N = 6, N = 10, N = 20$ *and* $N = 40$.

2.2.3 Design of maximally flat low-pass digital differentiators

There are many papers [15][16][17] on the design of full-band maximally flat digital differentiators, for which the approximation is highly accurate. However, to avoid the undesirable amplification of noise in digital differentiation, [18] introduce the design of a maximally flat low-pass digital differentiator, which satisfies the following constraints:

$$\left|H(e^{j\omega})\right| = 0, \quad \omega = 0 \tag{2.13}$$

$$\frac{d}{d\omega}\left|H(e^{j\omega})\right| = 1, \quad \omega = 0 \tag{2.14}$$

$$\frac{d^k}{d\omega^k}\left|H(e^{j\omega})\right| = 0, \quad \omega = 0 \quad 2 \le k \le 2L \tag{2.15}$$

$$\frac{d^k}{d\omega^k}\left|H(e^{j\omega})\right| = 1, \quad \omega = \pi \quad 0 \le k \le 2M \tag{2.16}$$

Let C denote the number of zeros of the transfer function at $z = -1$. For a Type IV filter, the transfer function always has an even number of zeros at $z = -1$. Selesnick, [18] gives the solution to this problem, using the nomenclature $C = 2M$ for Type IV transfer functions, and $C = 2M + 1$ for Type III transfer functions. The combined formula for Type III and Type IV, maximally flat low-pass differentiators is shown to be given by:

$$H(z) = \left(\frac{1 - z^{-1}}{2}\right)\left(\frac{1 + z^{-1}}{2}\right)^C z^{-L} \times \sum_{n=0}^{L} s(n)\left(\frac{-z + 2 - z^{-1}}{4}\right)^n \tag{2.17}$$

where

$$s(n)=\frac{(8n^2+4Cn-10n-C+3)s(n-1)-(2n+C-3)s(n-2)}{2n(2n+1)} \quad (2.18)$$

for $n\geq 2$, with $s(0)=2$, and $s(1)=C+1/3$. When C is even, $H(z)$ is a Type IV transfer function; when C is odd, while $H(z)$ is a Type III transfer function. In either case, the length of the impulse response is $p=C+2L+2$, so that $L=(p-C)/2-1$, which determines how many values of $s(n)$ are needed in (2.17). Figure 2.6 and Figure 2.7 show the magnitude response of Selesnick's proposed differentiators. The cut-off frequency depends on the values of C and L. When $C=0$, a full band differentiator is obtained.

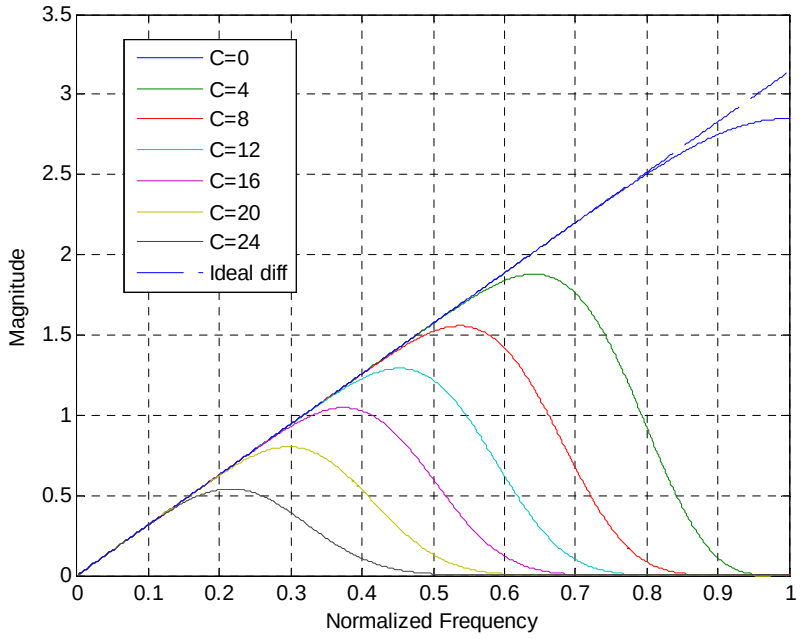

Figure 2.6 *Magnitude responses of Type IV FIR maximally flat low-pass differentiators with length of the impulse response* $p=30$.

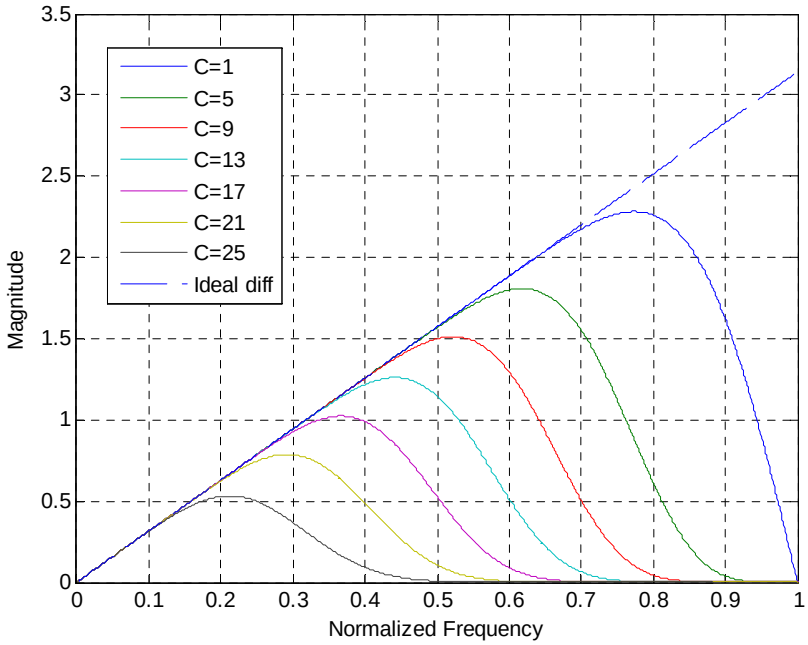

Figure 2.7 *Magnitude responses of Type* III *FIR maximally flat low-pass differentiators with length of the impulse response* $p = 31$.

2.2.4 Design of an FIR low-pass digital differentiator using the Chebyshev method

A linear-phase FIR filter can be designed using the Chebyshev method, or Parks-McClellan algorithm. The goal of this method is to design a FIR filter with an optimal fit between the desired and actual frequency responses, by minimizing the maximum absolute value of the error function $E(\omega)$ [8][19]. The proposed filters designed by this method exhibit an equiripple behavior in their frequency response, and are sometimes called equiripple filters. This method can be described as in [8]:

$$\min\left\{\left\|E(\omega)\right\|_{\infty}\right\} = \min\left\{\max_{\omega\in F}\left\|E(\omega)\right\|_{\infty}\right\} \qquad (2.19)$$

where F is the set of prescribed frequency bands. This method (with some

improvements to speed up the overall convergence routine) is made available in the MATLAB function firpm.

An example is given to show the magnitude response and percentage error of the proposed differentiators with cut-off frequency $\omega_c = 0.4$ of the normalized frequency, corresponding of magnitude vector $\mathbf{Ad} = [0 \quad 0.4\pi \quad 0 \quad 0]$ and different frequency vectors $\mathbf{F}_1 = [0 \quad 0.4 \quad 0.45 \quad 1]$, $\mathbf{F}_2 = [0 \quad 0.4 \quad 0.5 \quad 1]$, $\mathbf{F}_3 = [0 \quad 0.4 \quad 0.6 \quad 1]$, $\mathbf{F}_4 = [0 \quad 0.4 \quad 0.7 \quad 1]$ and $\mathbf{F}_5 = [0 \quad 0.4 \quad 0.8 \quad 1]$. For example, using $\mathbf{F}_1$, the magnitude of the filter output is 0.4π at a normalized frequency of 0.4, while the desired magnitude gain is zero at normalized frequencies of 0, 0.45 and 1 , as indicated in the vector $\mathbf{Ad}$.

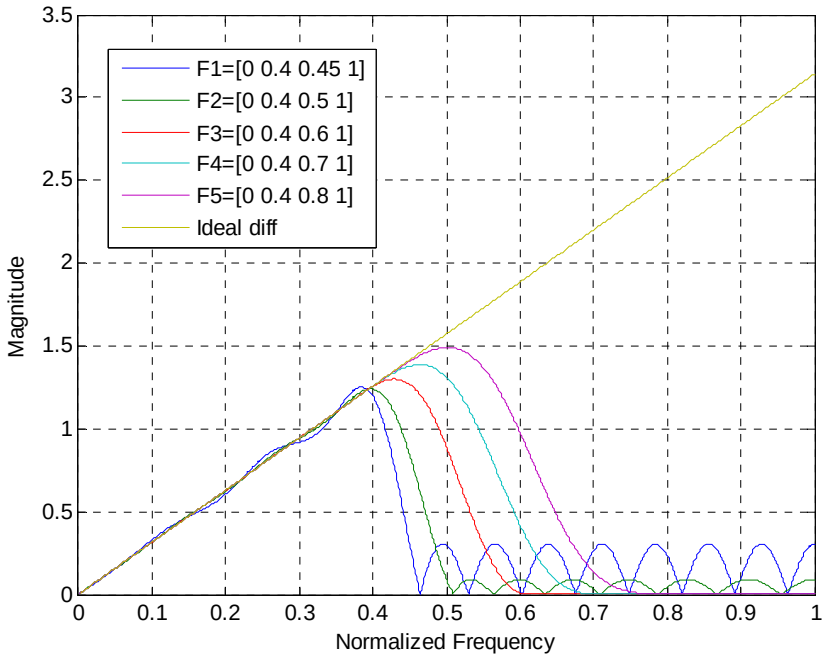

Figure 2.8 *Steady-state magnitude responses of the FIR differentiators design using the chebyshev method, with different frequency specifications.*

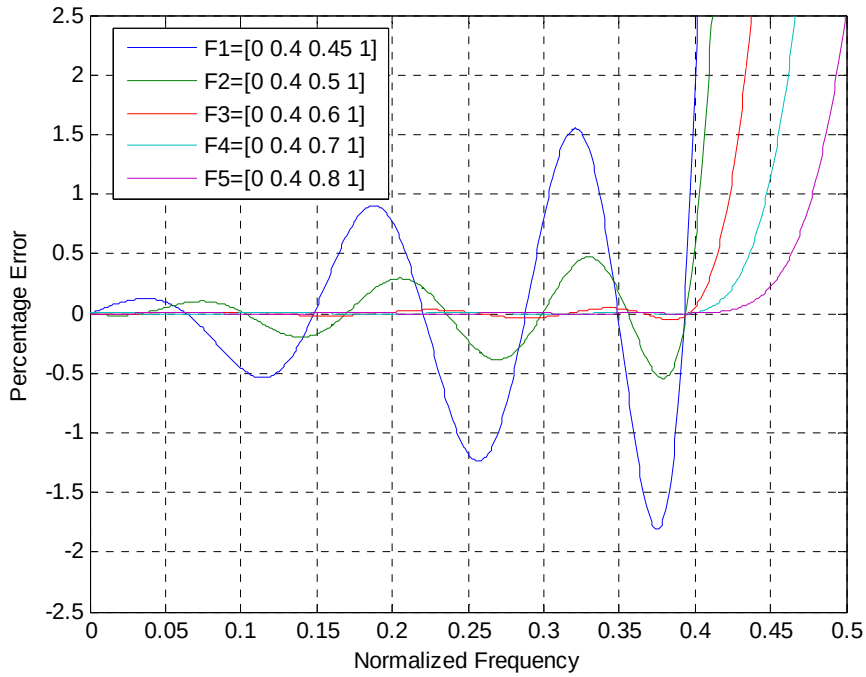

Figure 2.9 *Percentage error of the FIR differentiators design using the Chebyshev method, with different frequency -band specifications.*

The resulting differentiators exhibit identical cut-off frequencies, but different roll-off characteristic. It can be concluded from Figure 2.8 and Figure 2.9 that increased steepness is associated with bigger magnitude response error in the pass-band, and smaller attenuation in the stop-band. In addition, the attenuation in the stop-band shows equiripple performance.

2.2.6 Design of an IIR differentiator using Newton-Cotes numerical integration rules

Al-Alaoui has published many papers on the design of IIR differentiators, based

on the Newton-Cotes numerical integration rules [10][11][20][21][12][3]. The following are the numerical rules considered:

- The Trapezoidal Rule:

$$\int_a^b f(t)dt \approx \frac{l}{2}\left[f(a) + f(a+l) \right]; \quad l = (b-a) \quad . \tag{2.20}$$

- The Simpson Rule:

$$\int_a^b f(t)dt \approx \frac{l}{3}\left[f(a) + 4f\left(\frac{a+b}{2}\right) + f(b) \right]; \quad l = \frac{b-a}{2}. \tag{2.21}$$

- The Simpson three-Eight Rule:

$$\int_a^b f(t)dt \approx \frac{3l}{8}\left[f(a) + 3f(a+l) + 3(b-l) + f(b) \right]; \quad l = \frac{b-a}{3} \tag{2.22}$$

- The Boole Rule:

$$\int_a^b f(t)dt \approx \frac{2l}{45}\left[7f(a) + +32f(a+l) + 12f\left(\frac{a+b}{2}\right) + 32f(b-l) + 7f(b) \right]; \quad l = \frac{b-a}{4}. \tag{2.23}$$

The transfer functions of Newton-Cotes base integrators of the above rules are given by:

$$H_T(z) = \frac{T}{2}\frac{\left(1+z^{-1}\right)}{\left(1-z^{-1}\right)} \tag{2.24}$$

$$H_{S1/3}(z) = \frac{T}{3}\frac{\left(1+4z^{-1}+z^{-2}\right)}{\left(1-z^{-2}\right)} \tag{2.25}$$

$$H_{S3/8}(z)=\frac{3T}{8}\frac{\left(1+3z^{-1}+3z^{-2}+z^{-3}\right)}{\left(1-z^{-3}\right)} \tag{2.26}$$

$$H_{B}(z)=\frac{2T}{45}\frac{\left(7+32z^{-1}+12z^{-2}+32z^{-3}+7z^{-4}\right)}{\left(1-z^{-4}\right)} \tag{2.27}$$

where T is the sample interval.

The proposed differentiators are obtained by inverting the transfer function of integrators [10]. Note that if a pole of the proposed differentiator lies outside the unit circle at a radius of r, it should be replaced by a pole that lies inside the unit circle at a radius of $1/r$, in order to provide stability. The resulting transfer function should be multiplied by $1/r$ to compensate for the resulting change in magnitude.

In [21], a differentiator is obtained by inverting the transfer function of the Simpson integrator of (2.25). A pole that lies outside the unit circle at $z=-3.7321$ is replaced by $z=-1/3.7321=-0.2679$, and multiplication by $1/3.7321$ is implemented to compensate for the change of magnitude. The proposed transfer function is obtained by:

$$H_{diff\_S1/3}(z)=\frac{3(1-z^{-2})}{3.7321(1+0.5358z^{-1}+0.0718z^{-2})}. \tag{2.28}$$

In [10], an integrator obtained by the rectangular and trapezoidal rules is given as:

$$H_{N}(z)=\frac{7\left(1+\frac{1}{7}z^{-1}\right)}{8\left(1-z^{-1}\right)} \tag{2.29}$$

After taking the inverse of this integrator, the resulting differentiator transfer function is:

$$H_{diff\_N}(z) = \frac{8\left(1-z^{-1}\right)}{7\left(1+\frac{1}{7}z^{-1}\right)} \tag{2.30}$$

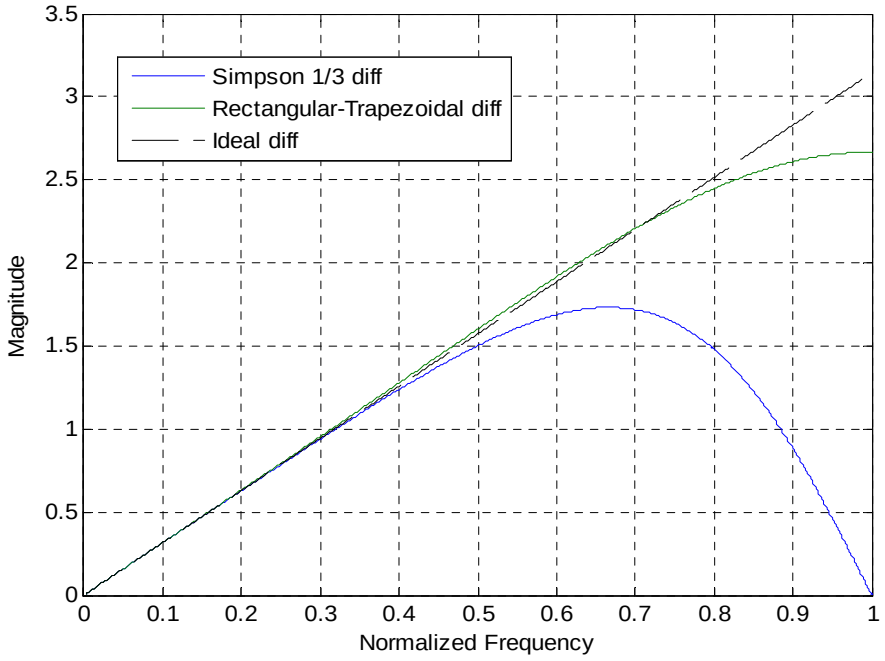

Figure 2.10 *Magnitude responses of the IIR differentiators designed using the Simpson and rectangular-trapezoidal rules.*

In [11], a non-minimum phase integrator is generated by Al-Alaoui for interpolating the Simpson integrator and trapezoidal integrator:

$$\begin{aligned} H_{ST} &= qH_S(z) + (1-q)H_T(z) \\ &= \frac{(3-q)\left(1+r_1 z^{-1}\right)\left(1+r_2 z^{-1}\right)}{6(1-z^{-2})} \end{aligned} \tag{2.31}$$

where q is the desired weight parameter, $r_1 = \frac{\left(3+q+2\sqrt{3q}\right)}{(3-q)}$, $r_2 = \frac{\left(3+q-2\sqrt{3q}\right)}{(3-q)}$, and $0 \le q \le 1$.

The minimum phase characteristic can be obtained by applying the

approach outlined in [10], and noting that $r_2 = 1/r_1$. The transfer function is:

$$H_{diff\_ST} = \frac{6\left(1-z^{-2}\right)}{r_1\left(3-q\right)\left(1+r_2 z^{-1}\right)^2} \tag{2.32}$$

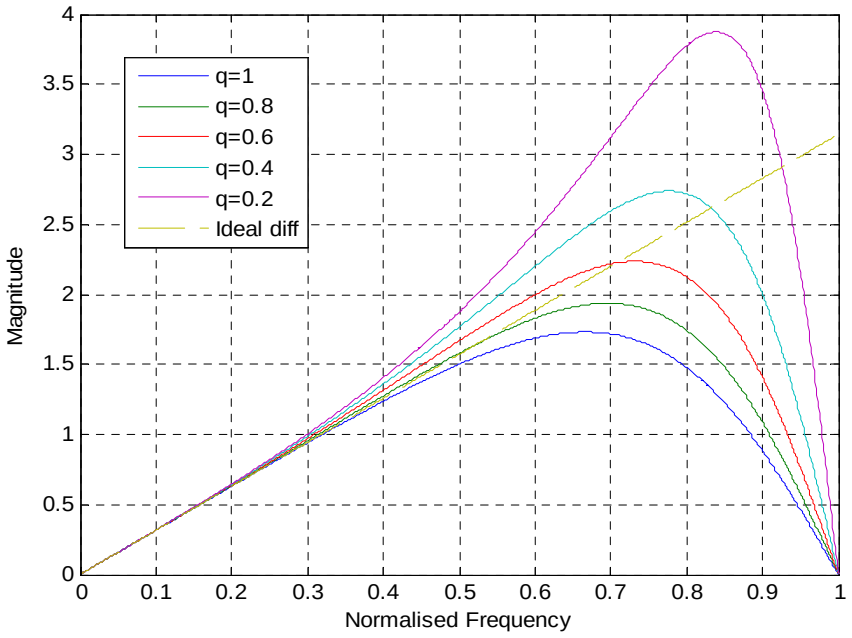

Figure 2.11 *Magnitude responses of the IIR differentiator design using the Simpson*-trapezoidal rule with different interpolation weights (ratios).

2.2.7 Design of IIR low-pass differentiator using the cascade method

A low-pass digital differentiator should usually exhibit steep roll-off for the magnitude response of the frequency response. For an IIR filter, the linearity of the phase in the pass-band is also a very important goal. Thus, Al-Alaoui obtained a low-pass differentiator, [3] by cascading the differentiator presented above (2.28) or (2.30) with an IIR low-pass filter whose numerator also represents a close-to linear phase IIR filter. As examples, some third-order Chebyshev Type 1, low-pass filters, having 0.1 dB attenuation in the pass-band, were chosen. The corresponding desired, normalized cut-off frequencies were 0.35, 0.42, 0.52, and 0.7 of full band, respectively [3]. The magnitude responses are shown in Figure 2.12, the group delays are shown in Figure 2.13 and the differentiator coefficients are given in Table 2.1:

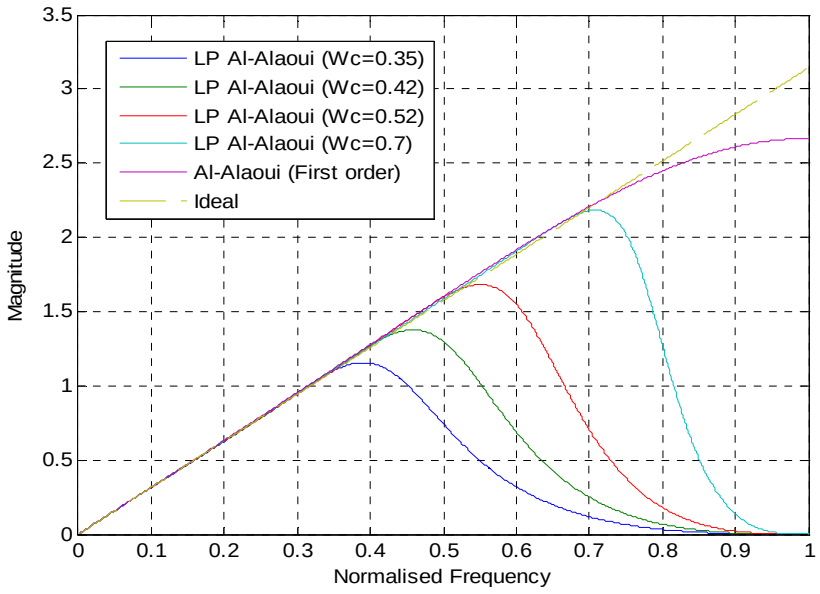

Figure 2.12 *Magnitude responses of the IIR Al-Alaoui low-pass differentiators and rectangular-trapezoidal rule based differentiator , presented in (2.30).*

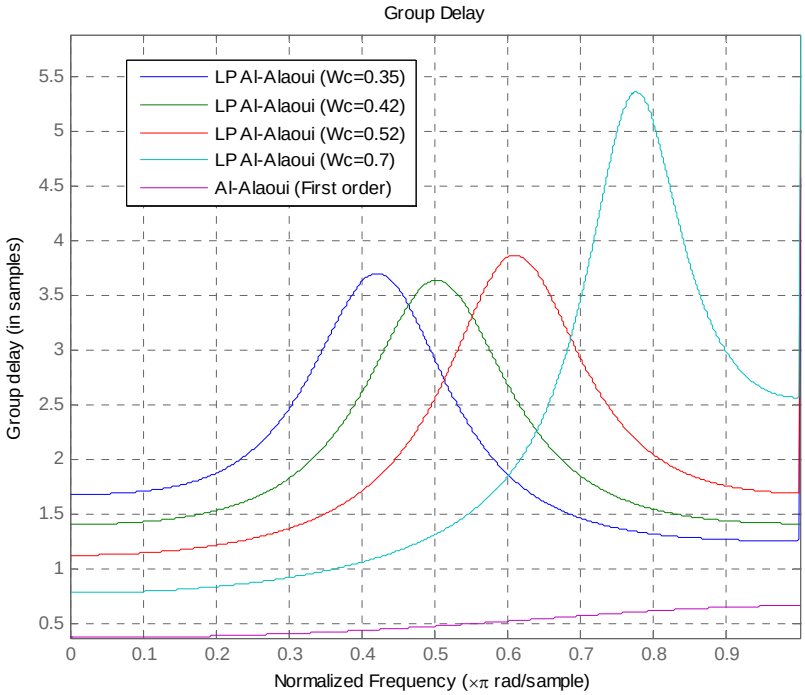

Figure 2.13 *Group delay of the Al-Alaoui low-pass differentiators and the rectangular-trapezoidal rule based differentiator.*

In paper [22], a differentiator is proposed by Tahmasbi and Shokouhi for approximating Parks-McClellan low-pass differentiators by modifying the above method. Different low-pass filters are chosen as the cascade filter, such as the Chebyshev 1, Chebyshev 2, Butterworth and Elliptic low-pass filters. The result shows that the proposed fourth-order low-pass differentiators yield a magnitude response which is close to that obtained for 30^{th} order Parks-McClellan low-pass differentiators.

Table 2.1 Coefficients of the Al-Alaoui low-pass, fourth-order IIR differentiator

$\omega_c(rad/s)$	0.35	0.42	0.52	0.7
$b(0)$	0.0386	0.0573	0.0897	0.1649
$b(1)$	0.0772	0.1147	0.1794	0.3298
$b(2)$	0.0000	0.0000	0.0000	0.0000
$b(3)$	-0.0772	-0.1147	-0.1794	-0.3298
$b(4)$	-0.0386	-0.0573	-0.0897	-0.1649
$a(0)$	1.0000	1.0000	1.0000	1.0000
$a(1)$	-0.4398	0.0133	0.6228	1.6240
$a(2)$	0.4672	0.4366	0.5531	1.1710
$a(3)$	-0.0403	0.0003	0.0768	0.3223
$a(4)$	-0.0170	-0.0092	0.0011	0.0265

2.2.8 Design of differentiator using the optimization technique

Many authors have designed digital differentiators using an optimization technique. This method can be broken down to a number of components [3][13][14][22].

In [3], a constrained optimization method is introduced. The first step is to choose one of the following equations as the transfer function, depending on

the required filter order, with the frequently appropriate orders four and five being assumed in this work:

$$H(z)=\frac{K\left(1+2z^{-1}-2z^{-1}-z^{-4}\right)}{1+a(1)z^{-1}+a(2)z^{-2}+a(3)z^{-3}+a(4)z^{-4}} \tag{2.33}$$

$$H(z)=\frac{K\left(1+3z^{-1}+2z^{-2}-2z^{-3}-3z^{-4}-z^{-5}\right)}{1+a(1)z^{-1}+a(2)z^{-2}+a(3)z^{-3}+a(4)z^{-4}+a(5)z^{-5}} \tag{2.34}$$

Then the gain K and the coefficients of the denominator polynomials will be allowed to vary in such a manner as to satisfy the optimization criterion. The cost function employed and the magnitude and phase responses are important characteristics of a digital differentiator. An optimality criterion to minimize the error is given in [3] [22]:

$$\varepsilon=(1-\lambda)\sum_{n=1}^{Ls}w_n\left[H(\omega_n)-H_{des}(\omega_n)\right]^2+\lambda\sum_{n=1}^{Ls}v_n\left[\tau_g(\omega_n)-\tau_g(\omega_0)-\tau_d(\omega_n)\right]^2 \tag{2.35}$$

where ε is the total weighted least-squares error over all frequency bands (usually a large set of discrete frequencies is used), $\omega_1,\omega_2,?..\ \omega_{Ls}$ in $0\le\omega\le\pi$. λ, w_n, v_n are the weighting factors selected by the designer, and Ls is the number of frequency components considered. The magnitude error at a frequency like ω_n is $H(\omega_n)-H_{des}(\omega_n)$, where $H_{des}(\omega_n)$ is the desired magnitude response, the group delay error is $\tau_g(\omega_n)-\tau_g(\omega_0)-\tau_d(\omega_n)$, where $\tau_g(\omega_0)$ is the filter delay at some nominal center frequency in the pass band, and $\tau_d(\omega_n)$ is the desired delay response of the filter relative to $\tau_g(\omega_0)$ [3][22].

The resulting differentiators obtained from (2.33) and (2.34) are labelled “Optimized Al-Alaoui 1” and “Optimized Al-Alaoui 2”, respectively. The filter

coefficients are given in [3].

Table 2.2 Coefficients of the optimized Al-Alaoui low-pass IIR differentiators

	K	$a(1)$	$a(2)$	$a(3)$	$a(4)$	$a(5)$
Opt diff 1 $\omega_c = 0.3$	0.0953	-0.6744	0.5425	-0.0777	-0.0272	0
Opt diff 1 $\omega_c = 0.5$	0.2918	0.6524	0.5687	0.0454	-0.0008	0
Opt diff 1 $\omega_c = 0.7$	0.5324	1.6901	1.2187	0.3095	0.0276	0
Opt diff 2 $\omega_c = 0.3$	0.0660	-0.3332	0.3041	0.1178	-0.0454	-0.0137
Opt diff 2 $\omega_c = 0.4$	0.1178	0.3021	0.4396	0.1430	-0.0093	-0.0053
Opt diff 2 $\omega_c = 0.5$	0.2032	0.9515	0.8383	0.2321	0.0255	-0.0004

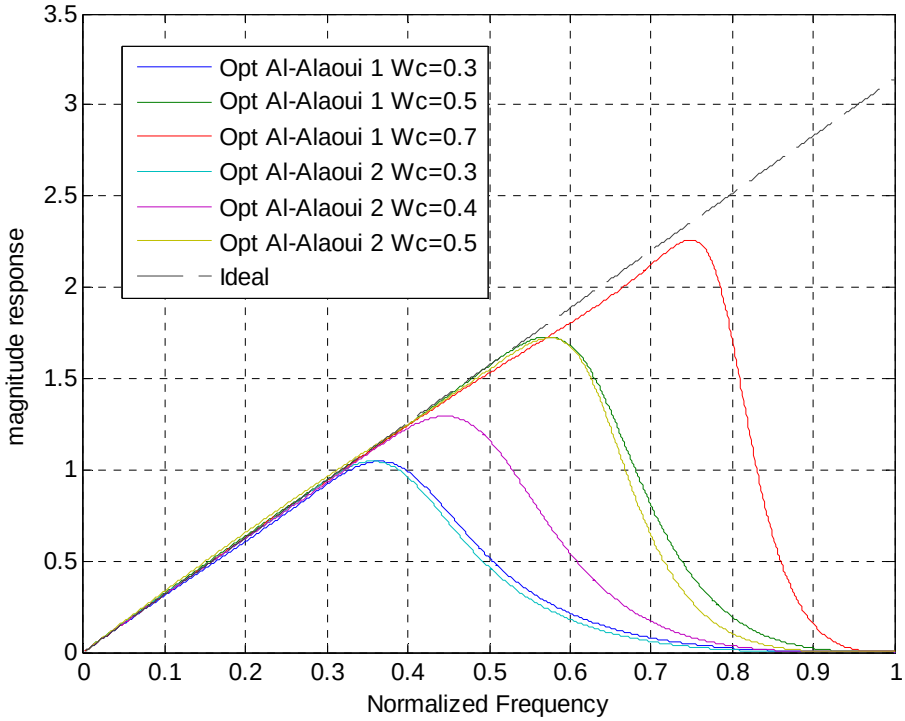

Figure 2.14 *Magnitude responses of the optimized Al-Alaoui low-pass differentiators.*

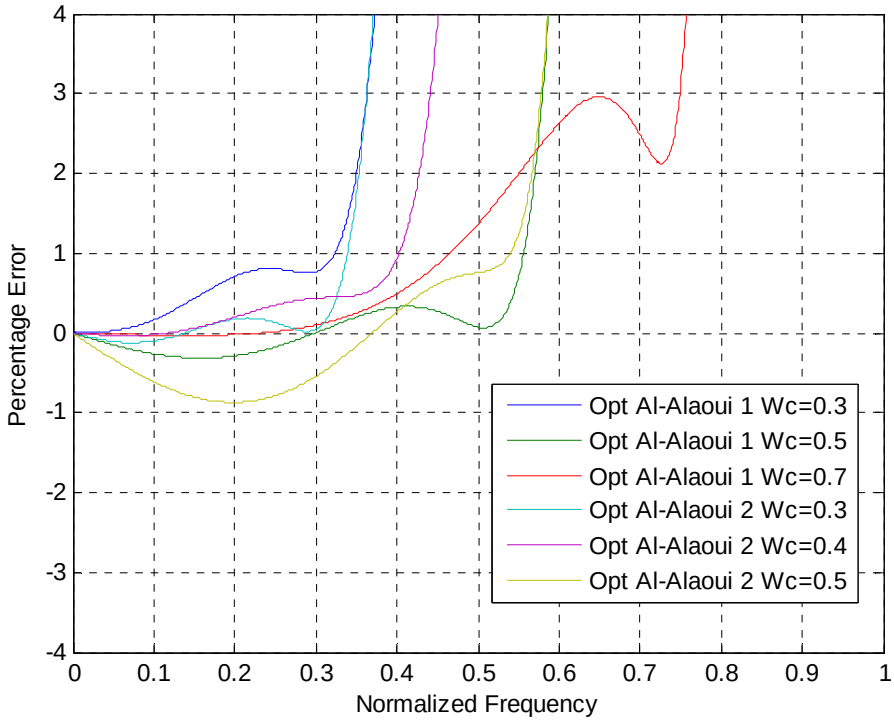

Figure 2.15 *Comparison of the percentage error of magnitude responses of optimized Al-Alaoui low-pass differentiators.*

The magnitude response and percentage error of the optimized Al-Alaoui differentiators are shown in Figure 2.14 and Figure 2.15. Some obvious errors can be seen in the pass-band of the magnitude response, especially for the optimized Al-Alaoui differentiator 2, when $\omega_c = 0.7$, which gives approximately 3% maximum percentage error.

2.2.9 Conclusions for previous work in this field

This section introduced several papers described in the literature, on the design of both FIR and IIR digital differentiators. The methods of FIR differentiator design through the consideration of time-domain-based differentiator input/output sequences, and that considering optimum noise attenuation are shown to give the same result, with good performance in the low-frequency-band, and high attenuation in the stop-band. Design using window functions is also an important method, with the Blackman window exhibiting the best magnitude response performance. Selesnick describes the design of the maximally flat FIR low-pass differentiator, which exhibits the smallest error magnitude response in the pass-band. Design via the Chebyshev method is the most popular method, because the proposed differentiator performance criteria, such as magnitude response, roll-off and stop-band attenuation are dependent on a set of magnitude and frequency vectors that are easily defined by the user.

For IIR differentiators, Al-Alaoui has published many papers based on the Newton-Cotes numerical integration rules. From these, methods have been presented on the design of a low-pass IIR differentiator by cascading the resulting differentiator with a low-pass filter. On the other hand, the design methods that are based on the use of an optimization technique have become very popular recently. These consider both magnitude and phase responses.

2.3 Design of the new IIR low-pass differentiator

After the literature review section, the new method for the design of a low-pass IIR differentiator is presented in this section. The design method is based on the definition of the IIR differentiator, while the filter coefficients are computed by the constraint optimization technique. The components of the cost function are the square error of the magnitude response, the variance of the filter, and the group delay.

2.3.1 IIR digital differentiator

The transfer function of an IIR filter which is shown at (1.2) can be described by the recursive difference equation:

$$\sum_{i=0}^{N} a_i y(n-i) = \sum_{i=0}^{N} b_i x(n-i), \quad a_0 = 1 \tag{2.36}$$

where $x(n)$ and $y(n)$ are the input and output sequences, respectively. For a digital differentiator, the output should clearly be the derivative of the input. Assuming the input to be the form $p_i = p_0 + v_i$ (at some arbitrary time-index i), where p_0 represents some initial signal value, the filter output at sample i is the rate estimate v. Therefore, the output $y(n)$ will be a constant value (the slope of the input) for a ramp input, and the output $y(n)$ should decay to zero for a constant input. Therefore, the constraints can be described using the following equations:

$$\sum_{n=0}^{N} b_n = 0 \tag{2.37}$$

$$\sum_{n=0}^{N} n b_n = -\sum_{n=0}^{N} a_n \tag{2.38}$$

2.3.2 The transfer function of the IIR differentiator

For an IIR filter, the numerator part can be regarded as an FIR filter, which will have a linear phase characteristic when $b(n) = -b(N-n)$, corresponding to a Type III or Type IV linear phase FIR filter.

The transfer function of digital differentiator can be rewritten as $d_n = \frac{1}{G} b_n$ with constraints (2.37) and (2.38):

$$H(z) = \frac{B(z^{-1})}{A(z^{-1})} = G \frac{1 + d_1 z^{-1} + d_2 z^{-2} + \ldots - d_1 z^{-N+1} - z^{-N}}{1 + a_1 z^{-1} + a_2 z^{-2} + \ldots + a_{N-1} z^{-N+1} + a_N z^{-N}} \tag{2.39}$$

where

$$\begin{aligned} G &= \frac{1 + \sum_{n=1}^{N} a_n}{N + \sum_{n=1}^{\frac{N-2}{2}} (N-2n) d_n}, \quad \text{for} \quad N \quad \text{even}, \\ G &= \frac{1 + \sum_{n=1}^{N} a_n}{N + \sum_{n=1}^{\frac{N-1}{2}} (N-2n) d_n}, \quad \text{for} \quad N \quad \text{odd} \end{aligned} \tag{2.40}$$

The effect of the constant G here is to meet the equation (2.38), which constrains the gain of the differentiator in such a way as to ensure that the output signal is the instantaneous rate of change of the input signal.

2.3.3 The variance of the IIR filter

The variance of a filter is the measure of the average power output for a white-noise input. Hence, it provides a measure of the ability of the filter to attenuate noise corruption on an input signal. The expressions for variances of signals can be written as [23]:

$$\begin{aligned} R_s &= \frac{1}{2\pi}\int_{-\pi}^{\pi}\Phi_s(\omega)e^{i\omega\tau}d\omega \\ &= \frac{1}{2\pi}\oint\frac{B(z)B\left(\frac{1}{z}\right)}{A(z)A\left(\frac{1}{z}\right)}z^{-1}dz \end{aligned} \tag{2.41}$$

where $\Phi_s(\omega)$ is the spectrum of the qusi-stationary signal.

The efficient algorithm from [23] can be used to compute (2.41), either numerically or symbolically, as follows:

$$\begin{aligned} A(z) &= a_0 + a_1 z^{-1} + a_2 z^{-2} + \ldots + a_N z^{-N}, \\ B(z) &= b_0 + b_1 z^{-1} + b_2 z^{-2} + \ldots + b_N z^{-N} \end{aligned}$$

Letting $a_i^N = a_i$, $b_i^N = b_i$ and defining a_i^N, b_i^N recursively by:

$$\begin{aligned} a_i^{N-n} &= \frac{a_0^{N-n+1}a_i^{N-n+1} - a_{N-n+1}^{N-n+1}a_{N-n+1-i}^{N-n+1}}{a_0^{N-k+1}}, \\ b_i^{N-n} &= \frac{b_0^{N-n+1}b_i^{N-n+1} - b_{N-n+1}^{N-n+1}b_{N-n+1-i}^{N-n+1}}{b_0^{N-n+1}}, \end{aligned} \tag{2.42}$$

$$i = 0,1,\ldots,N-n \quad \text{and} \quad n = 1,2,\ldots,N$$

eventually allows computation of the output variance:

$$R_s = \frac{1}{a_0}\sum_{n=0}^{N}\frac{\left(b_n^n\right)^2}{a_0^n} \tag{2.43}$$

It should be noted that the variance of an FIR filter is simply;

$$R_s = \sum_{n=0}^{N} h_n^{\,2} \tag{2.44}$$

2.3.4 Design method for IIR differentiators

A design method, using an optimization algorithm based on a number of required or desirable characteristics of an IIR differentiator, is described in this Section. It is found to be possible to define constraints and design rules that ensure the stability of the optimization and the good performance of the filter. The proposed differentiator should have high accuracy in the pass-band and fast roll-off in the transition-band (when considering the magnitude response), with as linear as possible phase response. For an IIR filter, all poles must be placed within the unit circle in the z-domain, to ensure filter stability. The nonlinear constraint function of this solver can be used to constrain all the poles to have an absolute magnitude of less than 0.98, to allow for some quantization of both coefficients and calculations.

The cost function includes three functions:

- Magnitude response

A disadvantage of the ideal digital differentiator, or all-pass differentiator, is its high pass characteristic, which means that the high-frequency noise will be amplified, which is a problem in many applications. This implies the usefulness of a low-pass differentiator, which approximates closely to an ideal differentiator in the pass-band, but which should attenuate the magnitude response to zero in the transition-band and stop-band. A good pass-band characteristic is realized by minimizing the square-error in the pass-band between the proposed

differentiator and an ideal one:

$$g_1 = \sum_{n=1}^{Ls} \left(H(\omega_n) - H_d(\omega_n) \right)^2 \qquad (2.45)$$

where $\omega_1, \omega_2, \omega_3 \ldots \omega_{Ls}$, Ls is the number of frequency components considered, at specific points within the range $0 \le \omega \le \omega_c$. Note that ω_c is the cut-off frequency, and $H_d(\omega_n)$ is the ideal magnitude response. Above the cut-off frequency, the goal of minimizing the variance will implicitly minimize the magnitude gains in the transition and stop bands.

- Variance

The low-pass character of the IIR differentiator is ensured by minimizing the variance of the filter. The magnitude response in the pass-band should be maintained as close to ideal as possible, using the constraint (2.45). For the proposed low-pass differentiator, the attenuation of magnitude response in the transition-band and stop-band is obtained by minimizing the variance of the filter, as this will lead to a steeper roll-off of the magnitude of the frequency response.

- Group delay

Constant group delay implies linear phase of the frequency response of an FIR filter. While exactly linear phase is not possible for an IIR filter, the associated optimality criterion is intended to minimize the variance of the group delay, as follows:

$$\sigma^2 = \frac{1}{Ls}\sum_{n=1}^{Ls}(\tau_g(\omega_n) - m_g)^2 \tag{2.46}$$

where the angular frequencies considered are $\omega_1, \omega_2\ \omega_3 \ldots \omega_{Ls}$, for $0 \le \omega \le \pi$, Ls is the number of frequency components considered, τ_g is the group delay, which expression is shown in (1.5), and m_g is the mean of the group delay τ_g:

$$m_g = \frac{1}{Ls}\sum_{n=1}^{Ls}\tau_g(\omega_n) \tag{2.47}$$

Therefore, the cost functions to be utilized are:

$$F_1 = g_1 \tag{2.48}$$

$$F_2 = \sigma^2 \tag{2.49}$$

$$F_3 = R_s \tag{2.50}$$

- Cost function

The filter coefficients of the transfer function can be computed using an optimization technique. The cost function of the optimization is:

$$\varepsilon = w_1F_1 + w_2F_2 + w_3F_3 \tag{2.51}$$

where $\mathbf{W} = \begin{bmatrix} w_1 & w_2 & w_3 \end{bmatrix}$ is a weight vector. To ensure filter stability, an additional constraint on the optimization is included to constrain all complex poles to have an absolute magnitude of, at most, slightly less than unity [9].

2.3.5 Design example 1

Fourth order IIR differentiators, with the number of frequency components $Ls = 1000$ are chosen in this design example. Therefore, the transfer function of (2.39) and (2.40) can be rewritten as:

$$H_4(z) = \left(\frac{1 + a_1 + a_2 + a_3 + a_4}{4 + 2d_1} \right) \left(\frac{1 + d_1 z^{-1} - d_1 z^{-3} - z^{-4}}{1 + a_1 z^{-1} + a_2 z^{-2} + a_3 z^{-3} + a_4 z^{-4}} \right) \quad (2.52)$$

To compare with the differentiators presented by Al-Alaoui [3], 4th order differentiators with normalized cut-off frequencies of 0.35, 0.42, 0.52, and 0.7 of the full band frequency, respectively, are chosen. The proposed filter coefficients and optimization parameters are listed in Table 2.3. Figure 2.16 shows that the proposed differentiator exhibits steeper roll-off than that of Al-Alaoui. Figure 2.17 shows the percentage error of the magnitude response of the proposed low-pass differentiator and that of the Al-Alaoui differentiator labeled 'Diff 1', for $\omega_c = 0.52$, clearly demonstrating that the proposed low-pass differentiator has much lower percentage error in the pass-band region than Al-Alaoui's filter. The 0.1% error is felt to be acceptable. Figure 2.18 shows that the group delay of the proposed low-pass differentiator is slightly inferior to that of Al-Alaoui, but that both have an almost constant group delay in the pass-band, with a sample delay difference of approximately 1.9 samples from zero frequency to the cut-off frequency $\omega_c = 0.52$. The new differentiator is felt to be acceptable for most applications.

Table 2.3 Coefficients and optimization parameters of the proposed IIR low-pass differentiator

$\omega_c(rad/s)$	0.1	0.35	0.42	0.52	0.7
$b(0)$	0.0354	0.1098	0.1488	0.2685	0.5032
$b(1)$	0.0637	0.1976	0.2678	0.4832	0.9759
$b(2)$	0.0000	0.0000	0.0000	0.0000	0.0000
$b(3)$	-0.0637	-0.1976	-0.2678	-0.4832	-0.9759
$b(4)$	-0.0354	-0.1098	-0.1488	-0.2685	-0.5032
$a(0)$	1.0000	1.0000	1.0000	1.0000	1.0000
$a(1)$	-0.7724	-0.6317	-0.3491	0.4251	1.5315
$a(2)$	-0.1620	0.5786	0.5990	0.5881	1.1140
$a(3)$	0.0797	-0.1127	-0.1507	-0.0026	0.2900
$a(4)$	0.1235	-0.0001	0.0315	0.0296	0.0289
F_1	0.001	0.001	0.001	0.001	0.001
F_2	1	0.7	0.84	1	2
F_3	0.023	0.29	0.44	0.78	1.47
Weight vector	[1 1 1]	[1 1 1]	[1 1 1]	[1 1 1]	[1 1 1]

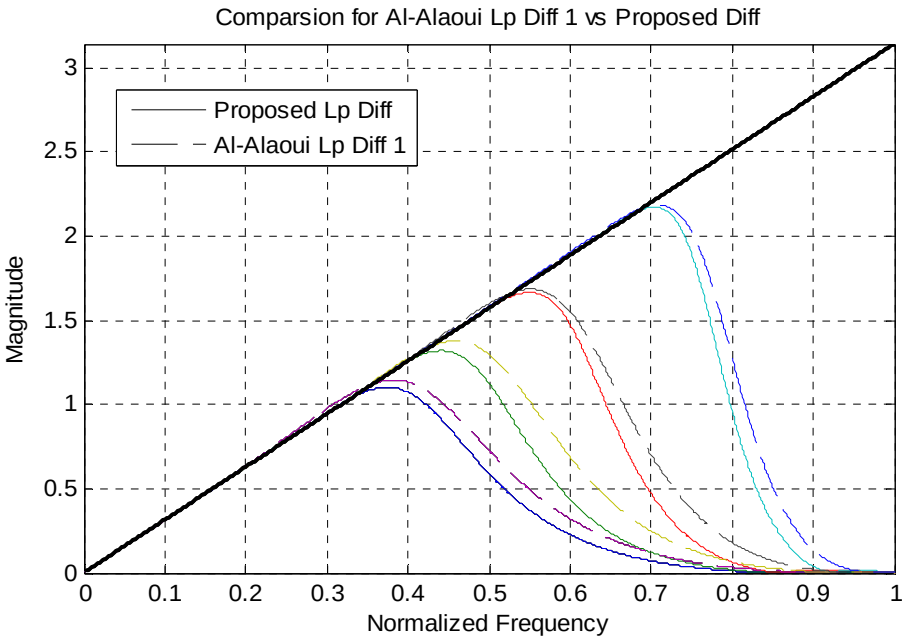

Figure 2.16 *Magnitude responses of fourth order proposed differentiator and fourth-order Low-Pass Al-Alaoui Differentiators, for the values of* ω_c *listed in Table 2.3.*

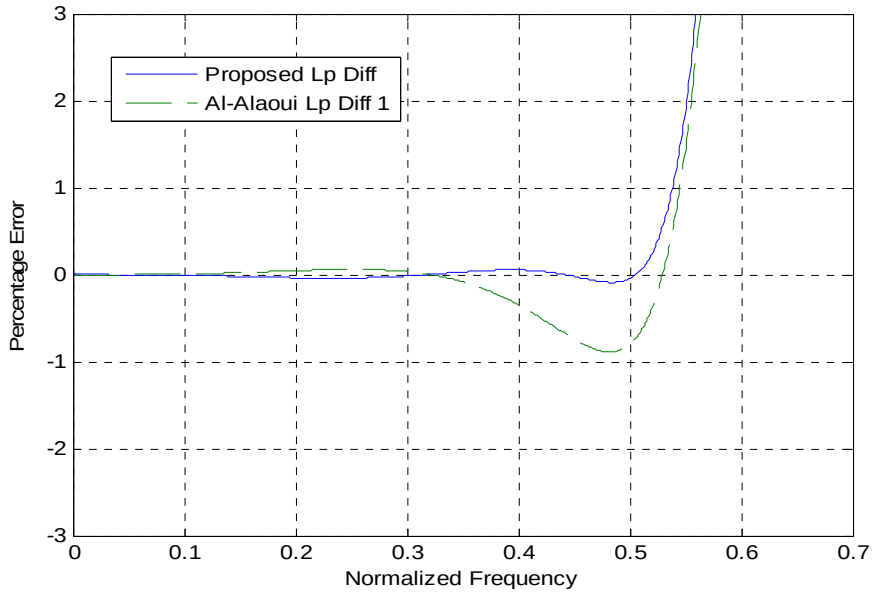

Figure 2.17 *Comparison of the percentage error of magnitude responses of proposed low-pass differentiator and the low-pass Al-Alaoui differentiator (termed Diff 1 by Al-Alaoui), for* $\omega_c = 0.52$ *.*

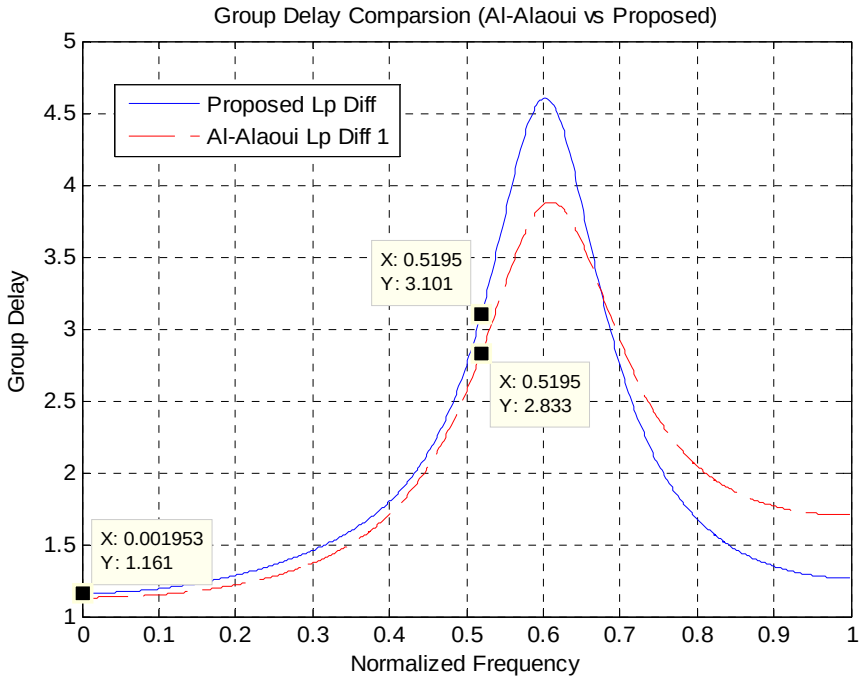

Figure 2.18 *Comparison of the group delay of frequency responses of proposed low-pass differentiator and low-pass Al-Alaoui Differentiator, for* $\omega_c = 0.52$.

Then, the comparisons of the proposed low-pass differentiator and the optimized Al-Alaoui differentiators will be given. The differentiators will be comprised include: (1) proposed differentiator $\omega_c = 0.52$ (filter coefficients shown in Table 2.3); (2) Al-Alaoui differentiator 1 $\omega_c = 0.52$ (filter coefficients shown in Table 2.1); (3) optimized Al-Alaoui differentiator 1 for $\omega_c = 0.5$ and optimized Al-Alaoui differentiator 2 for $\omega_c = 0.5$ (filter coefficients shown in Table 2.2). From Figure 2.19 and Figure 2.20, it can be seen that the proposed differentiator exhibits the smallest percentage error amongst the four differentiators.

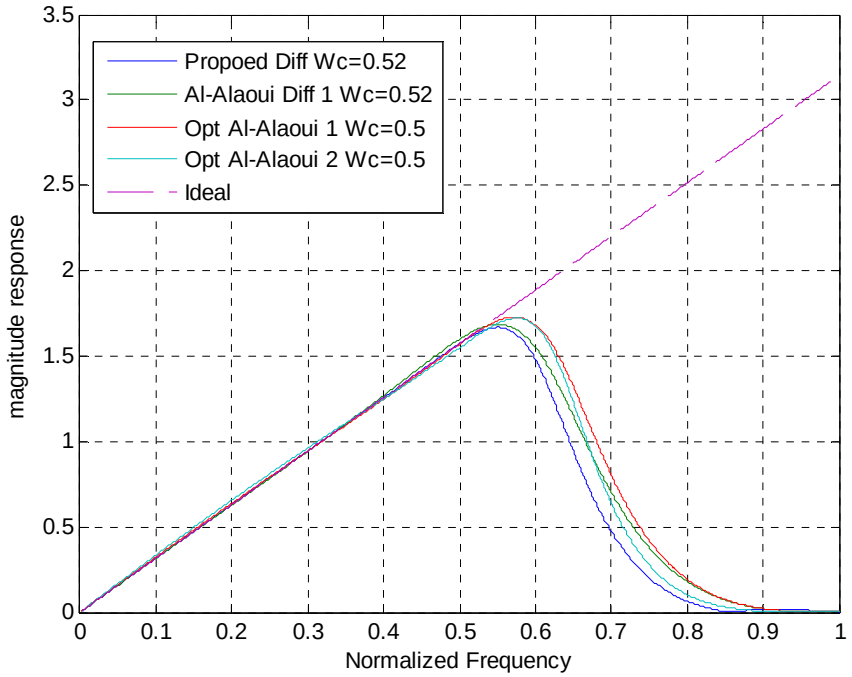

Figure 2.19 *Comparison of the magnitude responses of proposed differentiator, Al-Alaoui Differentiators 1 and optimized Al-Alaoui differentiators.*

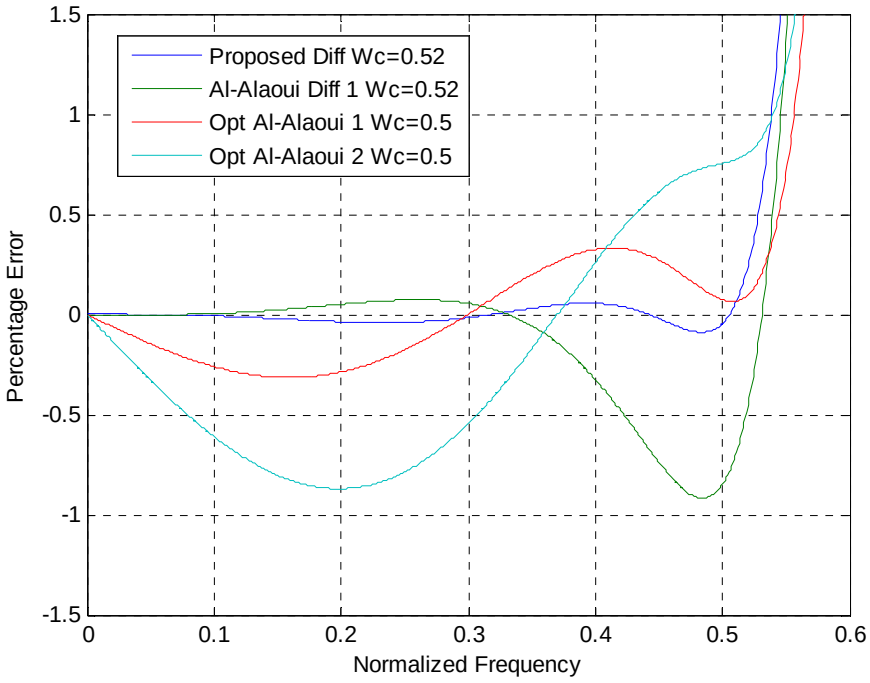

Figure 2.20 *Comparison of the percentage error of proposed differentiator, Al-Alaoui Differentiators 1 and optimized Al-Alaoui differentiators.*

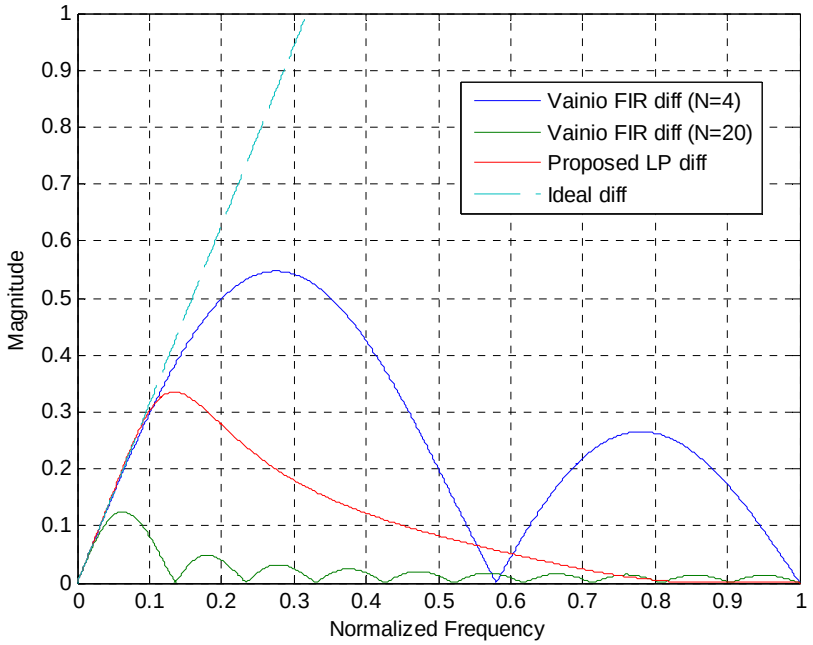

Figure 2.21 *Comparison of the magnitude responses of the proposed low-pass IIR differentiator and Vainio's FIR Differentiator, for* $\omega_c = 0.1$.

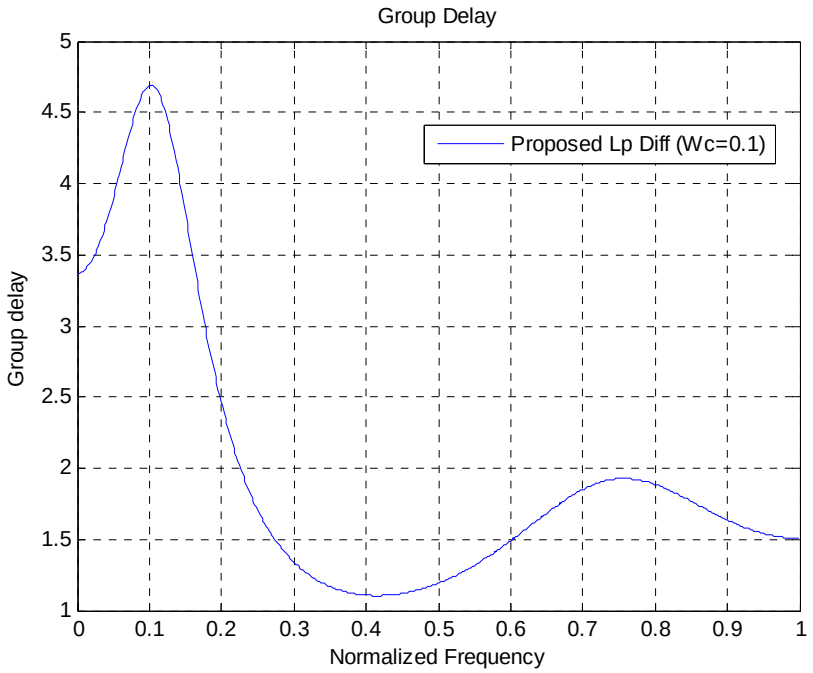

Figure 2.22 *Group delay of the proposed low-pass differentiator, for* $\omega_c = 0.1$.

Another comparison is given for the low-frequency-band performance. The cut-off frequency of the proposed IIR differentiator is $\omega_c = 0.1$. FIR differentiators of an identical cut-off frequency, with fourth and twentieth orders, obtained by equation (2.9) is also included in the comparison. An IIR filter that approximates a FIR filter should have an order of perhaps up to one fifth the order of the FIR filter. The comparison on Figure 2.21 shows that Vainio's FIR differentiator has a minimum cut-off frequency that depends on the order of the filter. It is found experimentally that the minimum cut-off frequency for the proposed IIR differentiator cannot be less than a FIR of the corresponding order. (including a minimum assumed ratio of five between the orders of the FIR and IIR filters, to strive for some similar performance characteristics). However, the potential cut-off frequencies of the proposed IIR differentiators can be chosen over a very wide range, with higher cutoff frequencies attainable than with previous designs.

2.3.6 Design example 2

Different goals will result in a low-pass differentiator with different magnitude and phase responses. The example shows the low-pass differentiator with different goals for $\omega_c = 0.6$. The optimized filter coefficients are shown in Table 2.4. Specifically, two goals are used in this example. In general such goals (and goal vectors) will be application dependent.

Table 2.4 Coefficients and optimization parameters of the proposed low-pass differentiator for different goals

$\omega_c = 0.6$	Goal 1	Goal 2
$b(0)$	0.1972	0.3034
$b(1)$	0.6288	0.5462
$b(2)$	0.0000	0.0000
$b(3)$	-0.6288	-0.5462
$b(4)$	-0.1972	-0.3034
$a(0)$	1.0000	1.0000
$a(1)$	0.5596	0.5912
$a(2)$	0.4794	0.6596
$a(3)$	-0.0222	0.0096
$a(4)$	0.0295	0.0459
F_1	0.01	0.1
F_2	0.7	1.4
F_3	1.1	0.9
Weight vector	[1 1 1]	[1 1 1]

Goal 1 places more weight factor on the filter variance, but less on the group delay, as shown below. Thus, as shown in Figure 2.23 and Figure 2.24, the differentiator with Goal 1 exhibits a shorter transition band and better stop band than that with Goal 2, but with worse group delay performance.

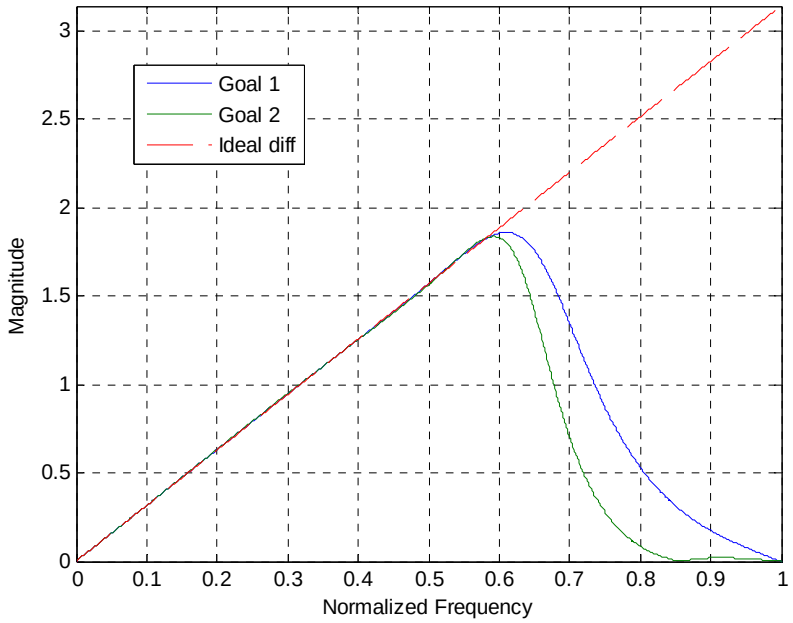

Figure 2.23 *Magnitude response of proposed low-pass differentiator using Goal 1 and Goal 2, for* $\omega_c = 0.6$.

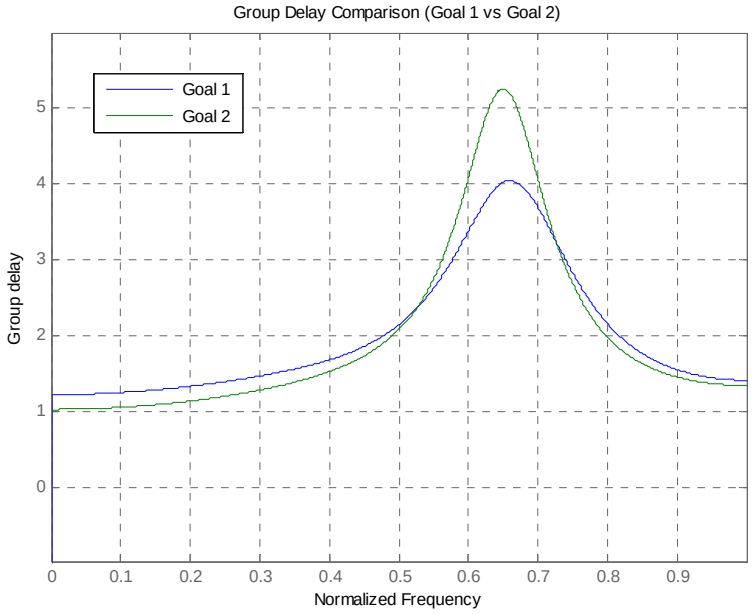

Figure 2.24 *Group delay of proposed low-pass differentiator using goal 1 and goal 2, for* $\omega_c = 0.6$.

2.4 Design of the FIR low-pass differentiator

The method of designing FIR low-pass differentiators is similar to that of IIR differentiators. As with the IIR differentiator the coefficients of the FIR filter are computed by the constraint optimization technique. As already stated, if an FIR differentiator is to have linear-phase, it will have either a Type III or a Type IV form [8]. Therefore, only the square error of the magnitude response and the variance of the filter are the components of the cost function.

2.4.1 FIR digital differentiator

The proposed FIR low-pass differentiators meet the equations (2.3) and (2.4), and the filter coefficients are antisymmetric. In Sections 2.2.1, only one solution exists, because the filter coefficients are computed using the Moore-Penrose pseudoinverse matrix, which yields resulting differentiators with optimum noise attenuation. However, in this section, the proposed differentiators are designed to not only have high accuracy low-frequency magnitude response, but also have steep roll-off and good stop band attenuation. To achieve this, the filter coefficients are computed using optimization techniques.

2.4.2 Design example 1

In this example, a twenty-first order FIR linear low-pass differentiator will be designed. The filter coefficients have to satisfy the equations (2.3) and (2.4), and the filter coefficients are antisymmetric. The filter coefficients can be expressed as:

$$h = \begin{bmatrix} h_0 & h_1 & \cdots & h_9 & h_{10} & -h_{10} & -h_9 & \cdots & -h_1 & -h_0 \end{bmatrix} \qquad (2.53)$$

where $h_0 = \frac{1}{21}\left(1 - 19h_1 - 17h_2 - 15h_3 - 13h_4 - 11h_5 - 9h_6 - 7h_7 - 5h_8 - 3h_9 - h_{10}\right)$

The proposed differentiators, with different cut-off frequencies, have been designed using the SQP technique, as described in Section 1.1.4. The optimal constraints include the square error of the magnitude response in the pass-band and the variance of the filter.

The cost function of the optimization is:

$$\varepsilon = w_1 F_1 + w_3 F_3 \qquad (2.54)$$

Table 2.5 lists the coefficients of the proposed differentiators. Figure 2.25 shows the corresponding magnitude responses, illustrating that the proposed differentiators have good pass-band magnitude response and steep roll-off. Because the proposed differentiators are Type IV filters, the group delays are constant.

Table 2.5 Coefficients and optimization parameters of the proposed twenty-first order, low-pass FIR differentiators

$\omega_c(rad/s)$	0.2	0.3	0.4	0.5	0.6	0.7
h_0	-0.0222	0.0177	-0.0081	0.0048	-0.0039	0.0083
h_1	0.0343	-0.0370	0.0150	-0.0089	0.0096	-0.0271
h_2	0.0241	-0.0073	0.0143	-0.0102	-0.0047	0.0523
h_3	-0.0182	0.0485	-0.0586	0.0579	-0.0250	-0.0748
h_4	-0.0470	0.0275	0.0239	-0.0864	0.0800	0.0750
h_5	-0.0338	-0.0519	0.0779	0.0249	-0.1269	-0.0359
h_6	0.0184	-0.0768	-0.0558	0.1058	0.1080	-0.0530
h_7	0.0810	0.0178	-0.1217	-0.1459	0.0230	0.1810
h_8	0.1166	0.1601	0.1006	-0.0642	-0.2480	-0.3140
h_9	0.1021	0.2066	0.3363	0.4260	0.4340	0.3620
h_{10}	0.0404	0.0899	0.1953	0.3328	0.5152	0.6884
F_1	0.0001	0.0001	0.0001	0.0001	0.0001	0.0001
F_3	0.077	0.18	0.38	0.68	1.1	1.5
Weight vector	[1 1]	[1 1]	[1 1]	[1 1]	[1 1]	[1 1]

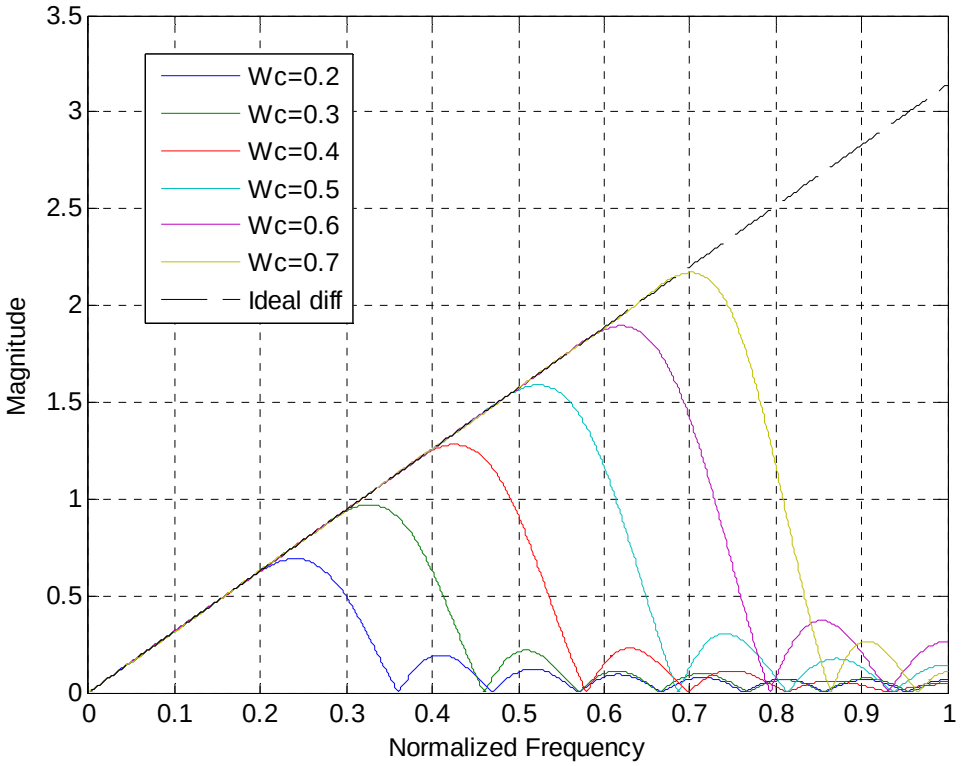

Figure 2.25 *Magnitude response of proposed FIR low-pass differentiators with different cut-off frequencies.*

2.4.3 Design example 2

In this example, the proposed FIR low-pass differentiators will be compared with the maximally flat low-pass digital differentiators. A differentiator design using a window function is not included in the comparison because the cut-off frequency cannot be chosen freely for such a filter. The design is based on the design of twenty-first order FIR differentiators with a cut-off frequency of $\omega_c = 0.4$. For the maximally flat low-pass digital differentiator, the parameter $C = 6$ is used (The filter coefficients can be obtained from (2.17) and (2.18)).

Note that C is the number of zeros at $z=-1$, as before; (Lower values of cut-off frequency require larger C values). The filter coefficients of the maximally flat differentiator are quantized to either four or fifteen digits.

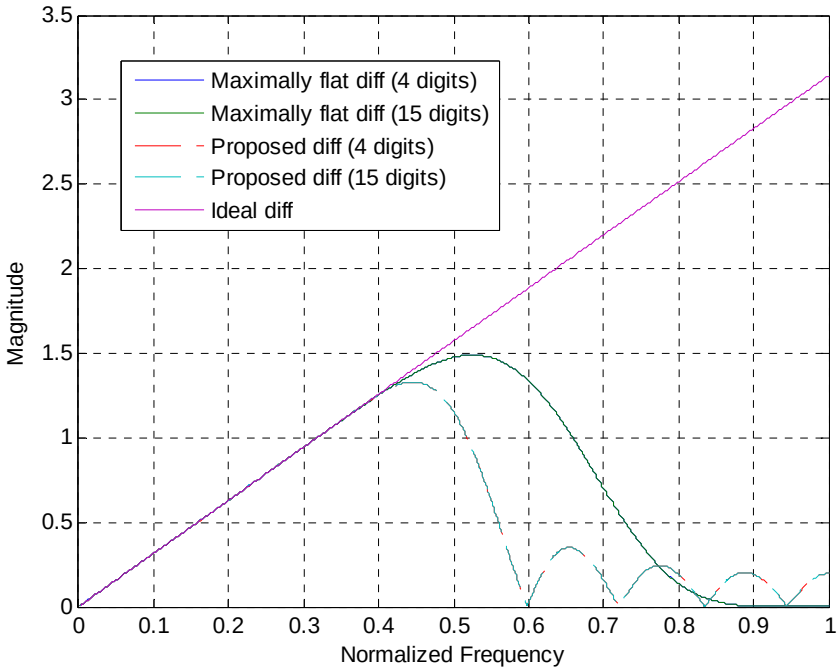

Figure 2.26 *Comparison of the magnitude response of proposed FIR low-pass differentiators and maximally flat FIR differentiator,* $\omega_c = 0.4$.

Based on Figure 2.26 and Figure 2.27, one can draw a conclusion that the maximally flat differentiator has better magnitude response in the pass-band, while the proposed FIR differentiator has steeper roll-off and better stop-band attenuation. Comparing the cases of the filter for which the coefficients are quantized to four significant digits and the filter for which quantization is not an issue (when 15 digits used), the magnitude responses in the pass-band are shown to be similar. It can be found from Figure 2.27, that the maximally flat differentiator with 15 digits exhibits almost zero percentage error in the low frequency range. However, when the coefficients limited to four digits, the maximally flat differentiator shows obvious error, but it is still better in this

regard than the proposed FIR differentiator. It can be concluded that, in the case of very small error (less than 0. 01%), the limit of the differentiator accuracy is due to the quantization of filter coefficients.

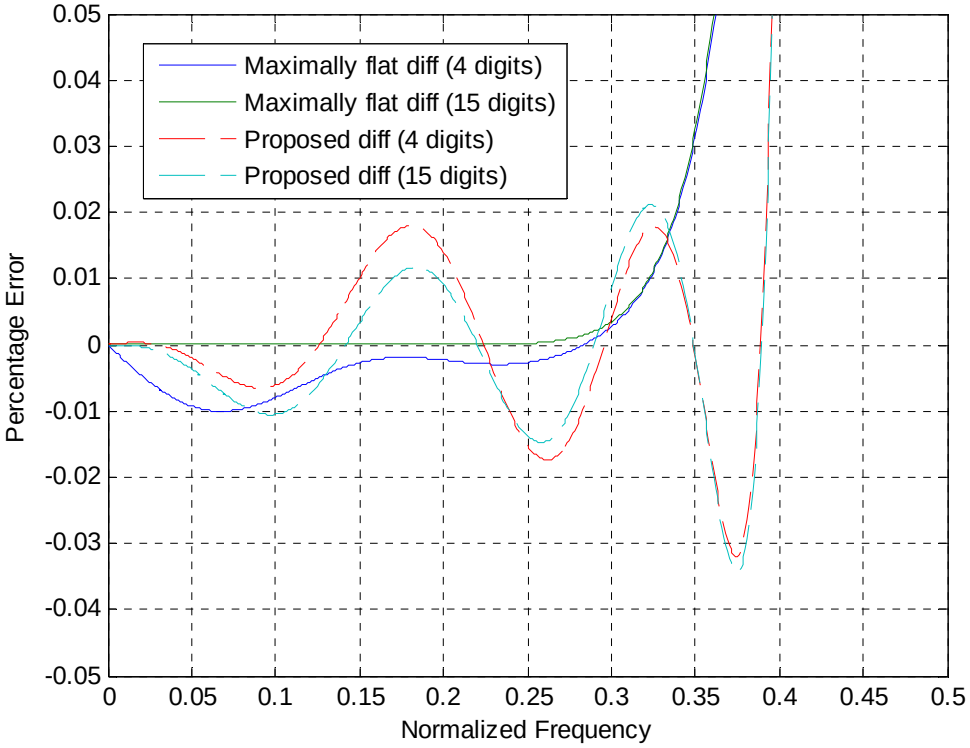

Figure 2.27 *Comparison of the magnitude response percentage error of the proposed FIR low-pass differentiators and maximally flat FIR differentiators,* $\omega_c = 0.4$

2.5 Discussion

In this section, a table is given to shown the advantage and disadvantages of the proposed differentiators and some previous works.

Table 2.6 Coefficients and optimization parameters of the proposed twenty-first order, low-pass FIR differentiators

	Magnitude (passband)	Roll-off	Cut-off frequency	Group delay	Filter order
Optimum noise diff	Good (at very low frequency)	Fast	Very low cut-off frequency	Constant (FIR)	Variable
Maximally flat diff	Excellent	Fast	Variable (not an accurately known frequency)	Constant (FIR)	Variable
Chebyshev diff	Very good	Adjustable	Variable	Constant (FIR)	Variable
Al-Alaoui diff 1	Good	Fast	Variable	Almost constant	Variable
Optimized Al-Alaoui	Good	Adjustable	Variable	Almost constant	4^{th} or 5^{th} order
Proposed diff	Very good	Adjustable	Variable	Almost constant	Variable

2.6 Performance of Proposed Differentiators in the Time-Domain

The performance of the proposed differentiators has been analyzed in the frequency-domain. In time-domain analysis, the desired output signal should be the derivative of input signal. However, the proposed differentiators have almost constant group delay, or linear phase, in the pass-band, which should cause a delay in the time domain when signals are processed by the differentiator. In addition, the input signal is typically subject to noise interference. Often, it can be assumed that quantization effects in digital filters are stochastic in nature [24][25], so it is important to consider the effects of quantization of the input signal. The fourth order IIR differentiator under test is shown in Table 2.3, with a normalized cut-off frequency of $\omega_c = 0.35$, and the twenty-first order FIR differentiator under test is shown in Table 2.5, with a normalized cut-off frequency of $\omega_c = 0.4$.

The test signals used in this section include:

- Basic noise-free quadratic function.

The input signal function is: $x(t) = 2t^2 + 4t + 1$, so the ideal output, the derivative of the input signal, is: $y(t) = x'(t) = 4x + 4$. The sample time is $T = 0.001s$. Figure 2.28 show that the outputs of the proposed differentiators are the derivatives of the input signals in the time-domain. The proposed differentiator shows initial transient oscillations, which is acceptable for an IIR filter, as the effect is transitory. However, the FIR differentiator shows a much longer delay because of the higher filter order.

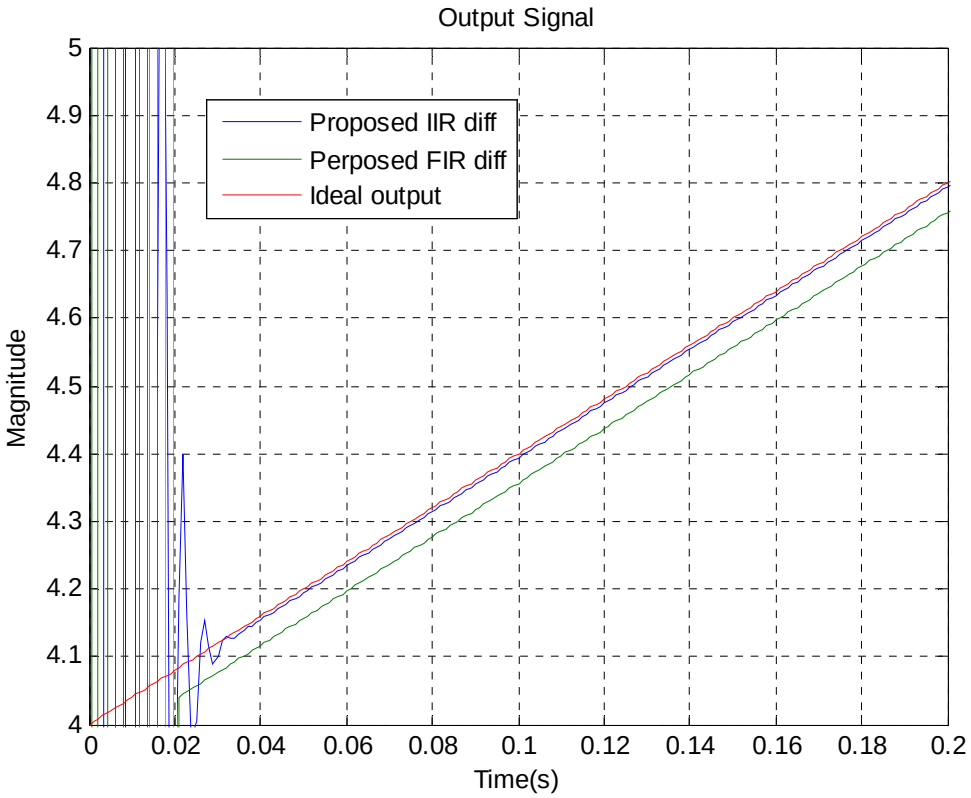

Figure 2.28 *Output signal of quadratic test signal.*

- Basic, noise-free triangular wave.

The proposed IIR and FIR differentiators considered above are used as test differentiators for other inputs. In Figure 2.29, the resulting output with sample time $T_s = 0.001s$ of the proposed IIR differentiator output signal shows very good performance in the time-domain, with small overshoot. However, the proposed FIR differentiator exhibits significant delay, of about 0.01 second, or 11 samples, as expected, and acceptable overshoot.

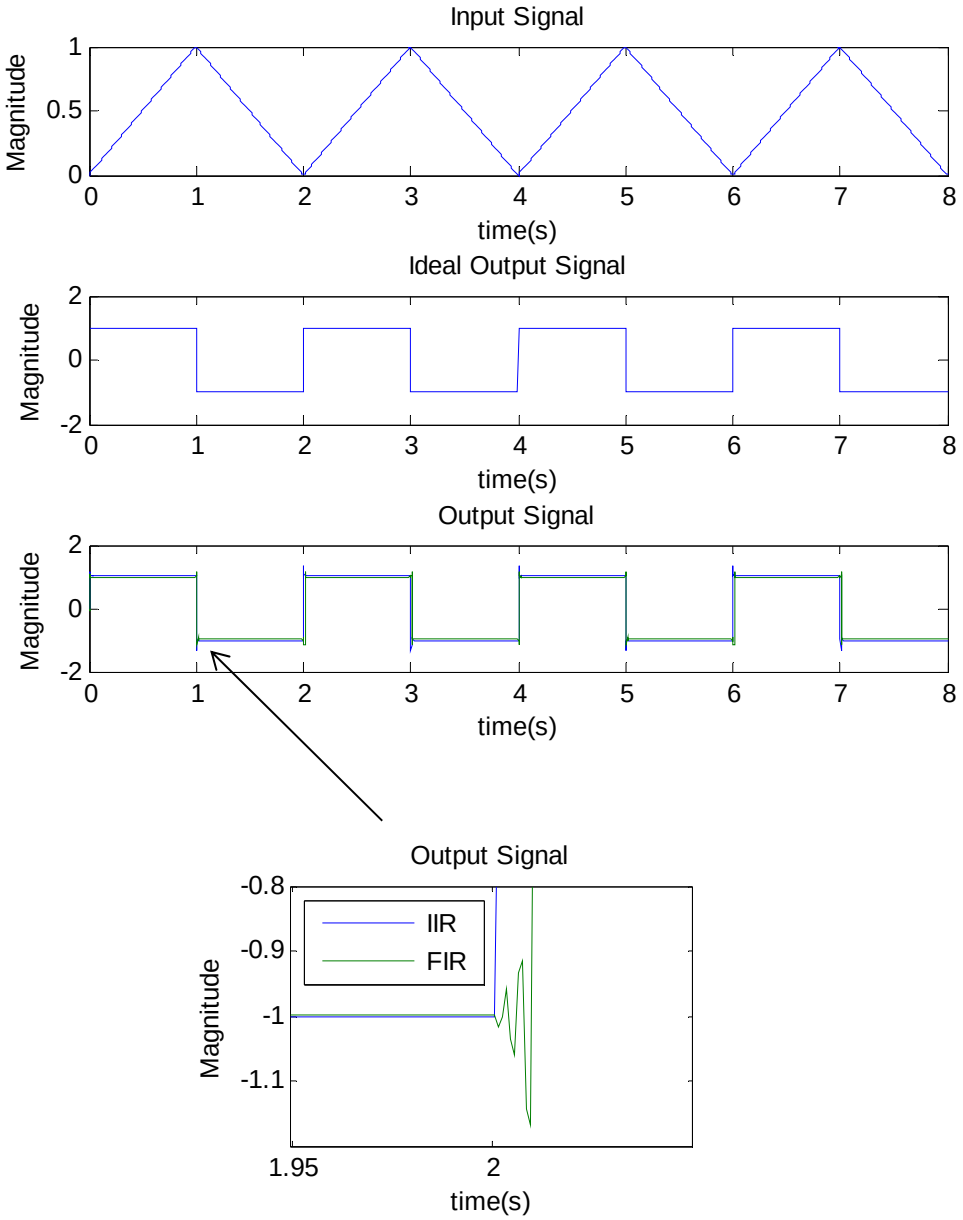

Figure 2.29 *Time-domain response of triangular wave input signal for the proposed IIR and FIR differentiators.*

- Quantized composite signal.

To analyze the time domain performance of a quantized signal, the proposed differentiators, with different cut-off frequencies, (for which the coefficients are as given in Table 2.3 and Table 2.5) are tested. The derivative of the stationary input signal is defined as:

$$f(x)=\begin{cases} 20+250(x-17) & x<517 \\ 22+2\sin\left(\dfrac{2\pi(x-517)}{40-(x-517)/20}\right) & x\geq 517 \end{cases} \tag{2.55}$$

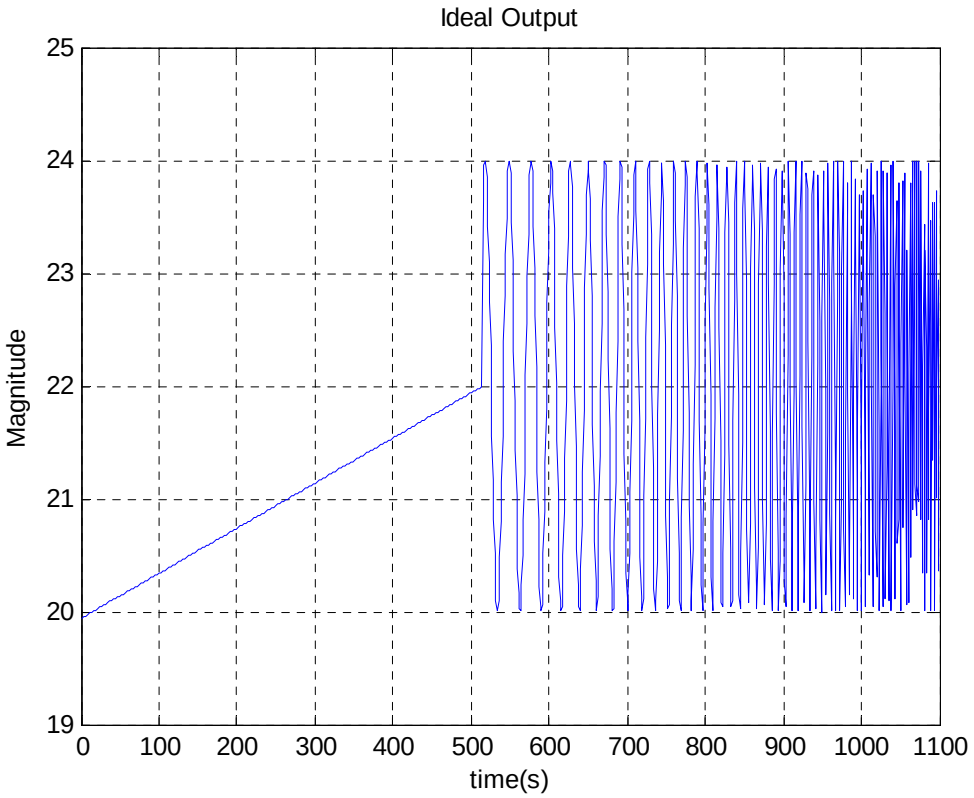

Figure 2.30 *Ideal output of input signal without quantized noise.*

The input signal can be obtained by numerically integrating this discrete derivative function (2.55), because a continuous function form of the input is not easily generated. The derivative of the stationary input signal without quantized noise is shown in Figure 2.30. The quantization noise can be added by

simply utilizing the ’ *floor*’ function in Matlab. Figure 2.31 and Figure 2.32 show the output for differentiators with different cut-off frequencies. It can be concluded that (1) the output of a differentiator of higher cut-off frequency exhibits more interference due to quantized noise, and (2) the proposed differentiator with lower cut-off frequency can substantially filter the quantized noise, but with significant attenuation of high-frequency inputs.

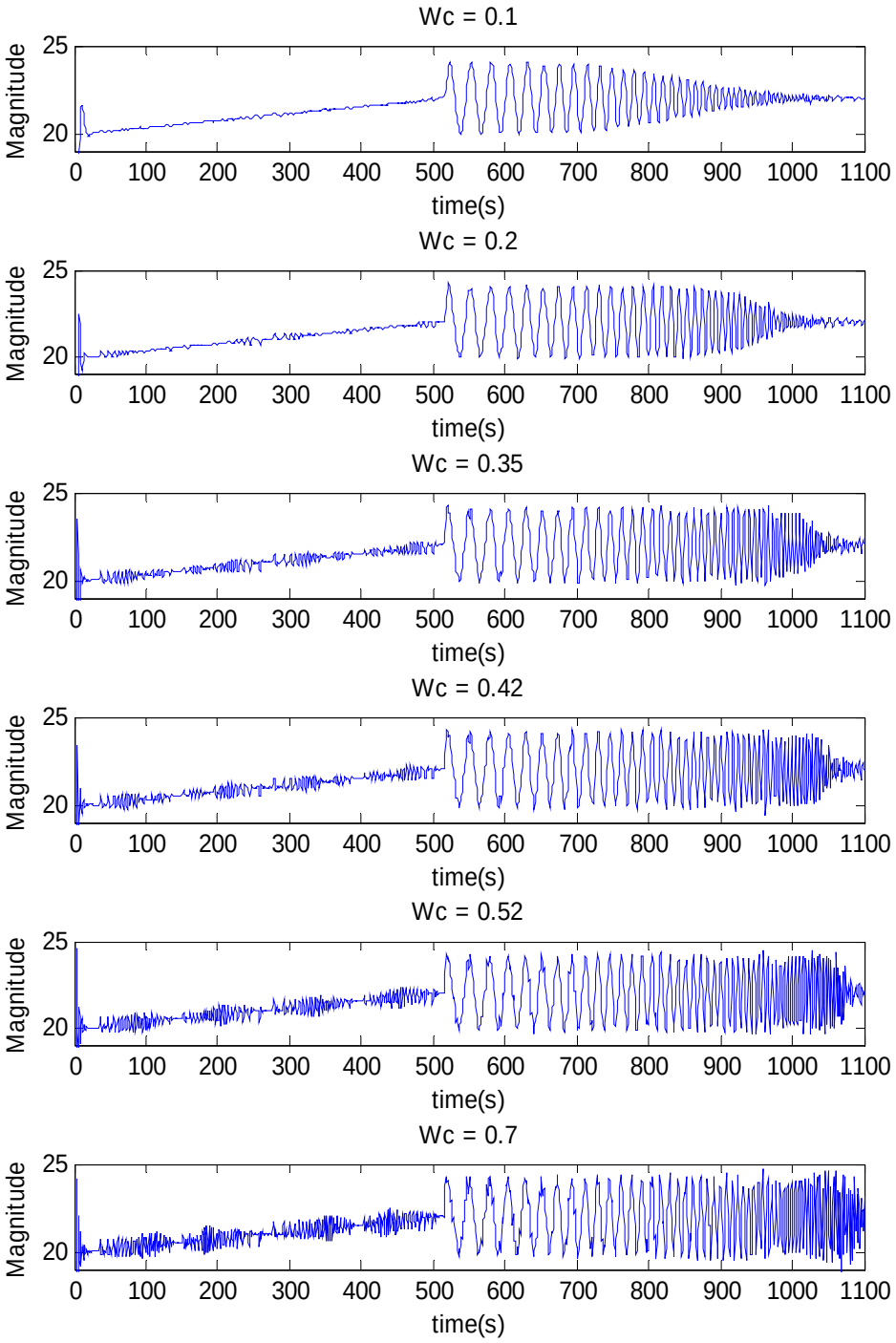

Figure 2.31 *Output of quantized inputs for IIR differentiators of different cut-off frequencies.*

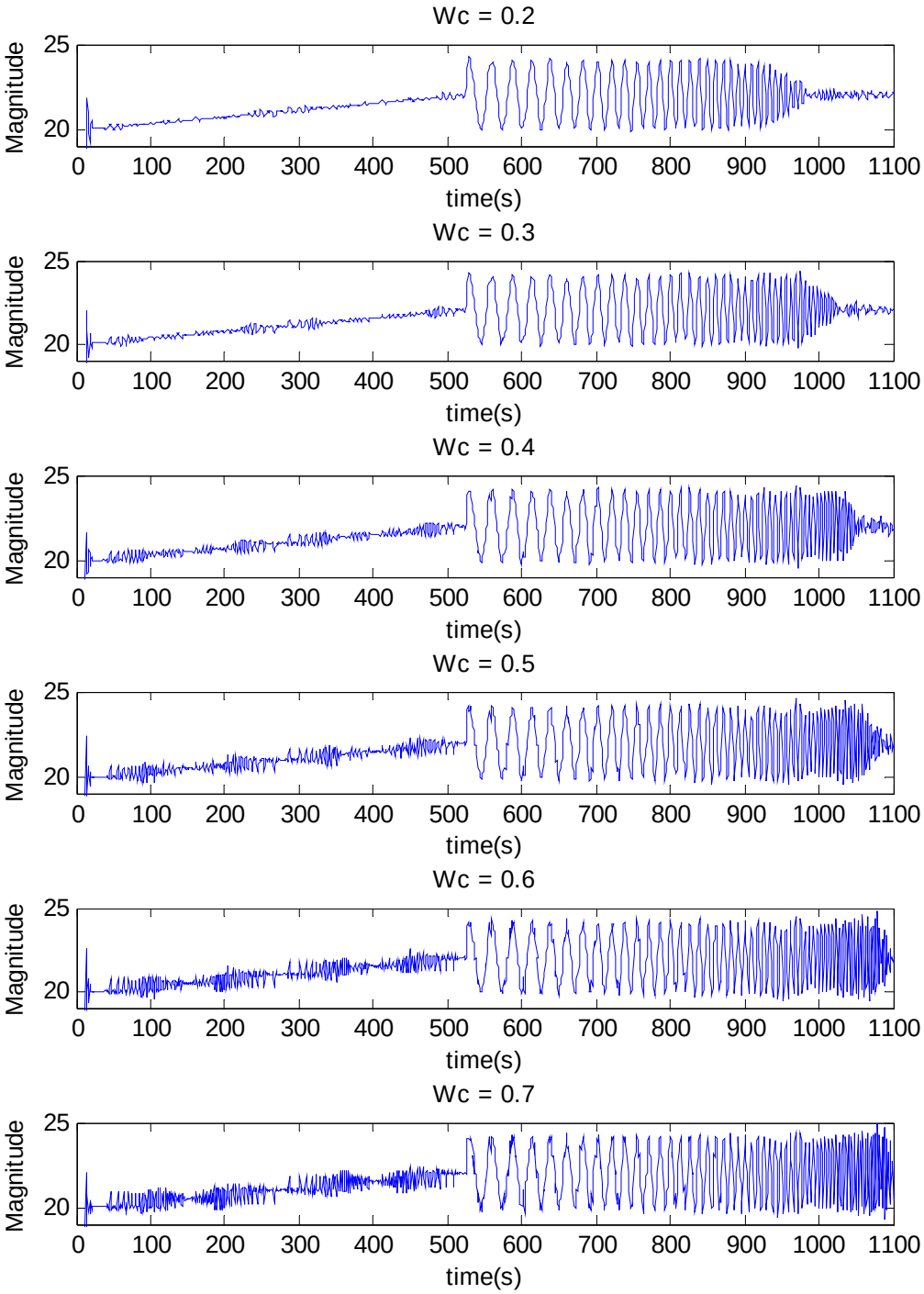

Figure 2.32 *Comparison of output of quantized inputs for FIR differentiators of different cut-off frequencies.*

Another example is shown in Figure 2.33 and Figure 2.34. The FIR differentiators are both twenty-first order, and the IIR differentiators are both fourth order. For the maximally flat differentiators, it has been chosen that $C = 6$ so that the cut-off frequency is close to $\omega_c = 0.42$. It can be concluded that (1) the FIR filters have more delay than the IIR filters; (2) the output of the maximally flat differentiator has more quantized noise interference at both the low-frequency and high-frequency ranges, due to its smooth roll-off of magnitude response; and (3) in Figure 2.34, the proposed IIR differentiator is shown to have faster attenuation at high frequency than Al-Alaoui's differentiator, because the proposed IIR differentiator has steeper roll-off of the magnitude response.

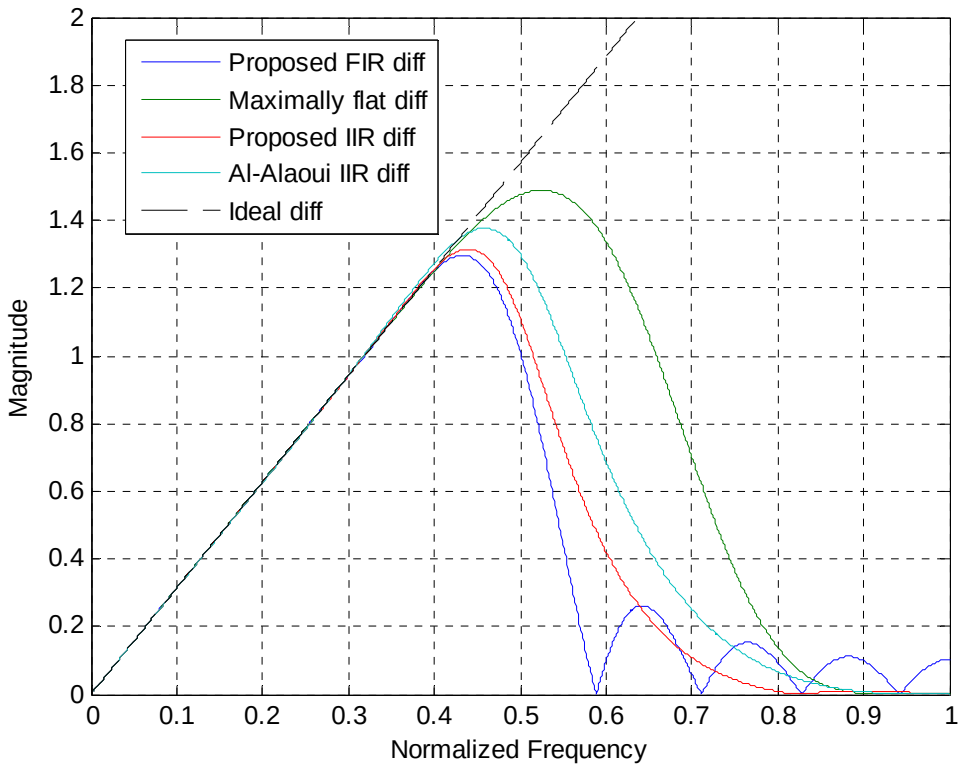

Figure 2.33 *Magnitude response of the FIR and IIR differentiators with cut-off frequency* $\omega_c = 0.42$.

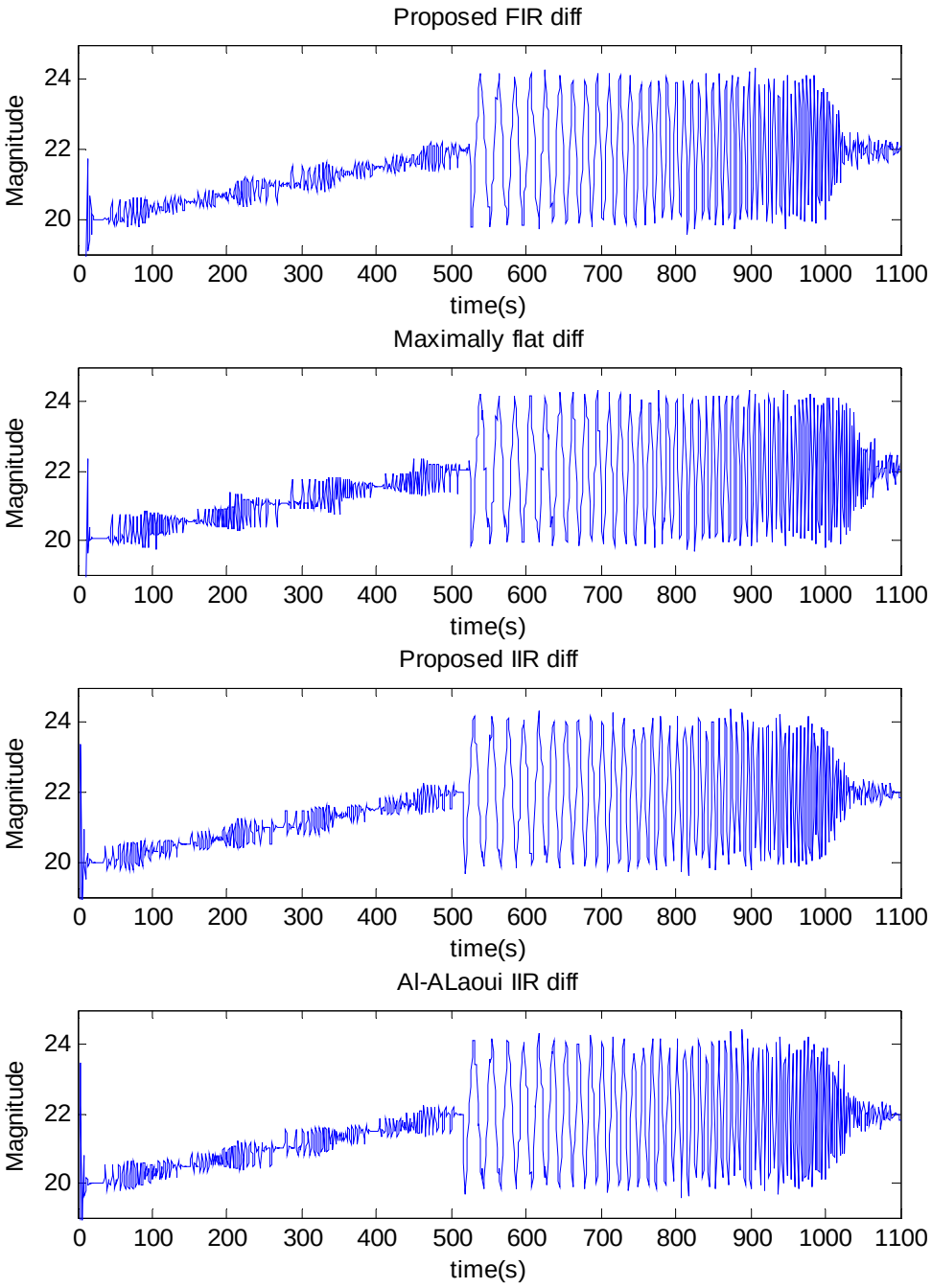

Figure 2.34 *Time-domain outputs of quantized inputs for FIR and IIR differentiators with cut-off frequency* $\omega_c = 0.42$.

To test the noise reduction in performance of each differentiator, the error of the outputs between 50 seconds to 400 seconds is shown on Figure 2.35. To reduce the effect by the delay of the differentiators, a constant was added to each output to ensure the mean of the error is zero. The maximum absolute errors of each output are listed on the Figure. Though the Proposed FIR differentiator has the steepest roll-off within of the differentiators, its maximum absolute error is not the smallest because the ripples at the stop-band can be found in the magnitude response. These ripples for the FIR differentiator are a direct result of the optimization goals chosen. Basically, the differentiator is a Vainio-type differentiator, but with a variable cut-off frequency. Clearly, an optimization that focused more on reduced stop-band ripple, could be designed, at the expense of increased variance. Hence, the noise reductions in performance of the differentiators are dependent on both the cut-off frequency and stop-band performance of the magnitude response.

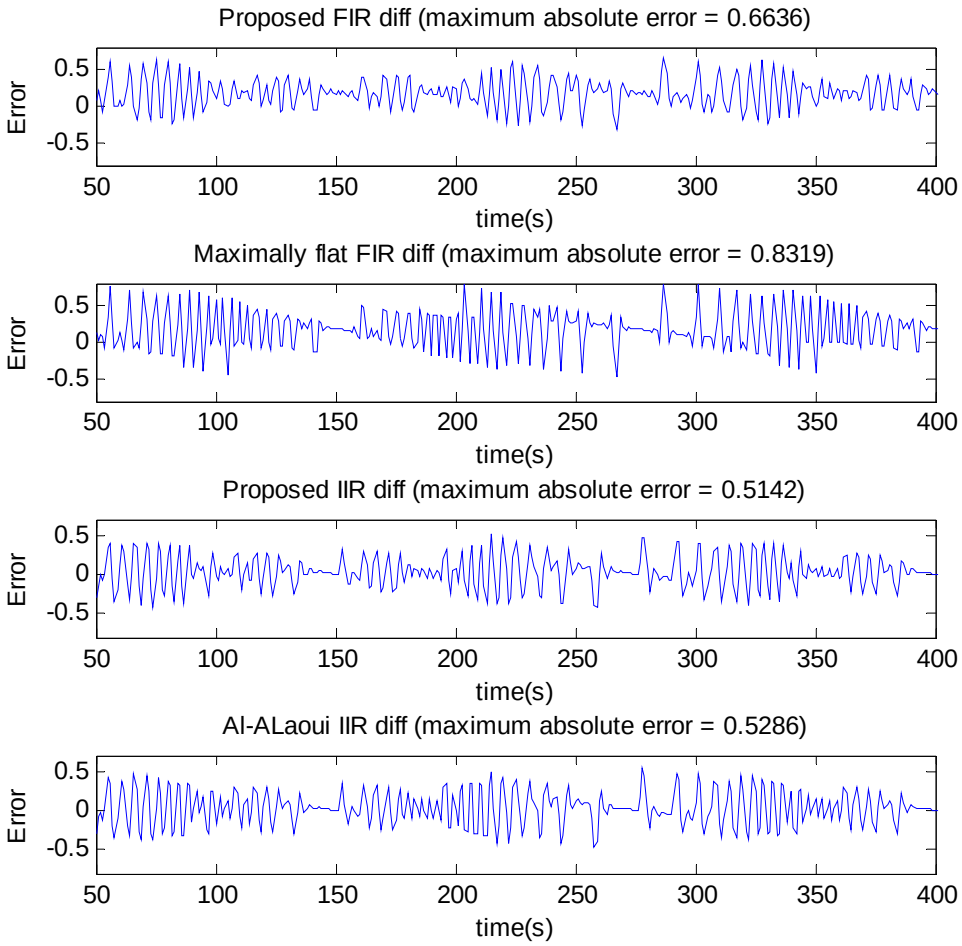

Figure 2.35 *Error between the outputs of the proposed FIR differentiators, and ideal output between 50 seconds to 400 seconds*

2.7 Conclusion

This Chapter introduces the concept of first-degree digital differentiator. Some papers have been reviewed on the design of both first-degree FIR and IIR differentiators.

Then, new methods for the design of low-pass digital differentiators are presented in this chapter. The transfer functions of the proposed IIR and FIR differentiators are introduced. The filter coefficients are obtained through utilization of the optimization technique. For the proposed low-pass IIR differentiator, the optimization goals include the magnitude response, variance and group delay of the filter. The low-pass characteristics of the proposed differentiators are obtained by minimizing the variance of the filter, which is the measure of the average power output for a white-noise input. The method to design low-pass FIR differentiators is shown to be to be similar to that of IIR differentiators, but the optimization goals clearly do not include the group delay of the filter, because a linear phase FIR filter (Type III or Type IV) is typically utilized.

The comparison between the proposed low-pass differentiators and other differentiators previously presented in this field shows that both the proposed IIR and FIR low-pass differentiators have excellent magnitude response in the pass band, as well as a short transition band. Specifically, the proposed IIR differentiator yields almost linear phase in the pass-band. The designer can design the differentiator for a particular group delay or roll-off characteristics, by choosing the application-dependent weight vector when defining the goals.

The testing of the proposed differentiators in time-domain also shows good performance. The outputs of both the IIR and FIR low-pass differentiators give the derivative of the input signal as expected，for various inputs. The testing

of a quantized signal is included in this chapter. The noise reduction performance is improved (relative to previously proposed differentiators) for both the cut-off frequency and stop-band performance of the magnitude response. Compared with the proposed IIR differentiator, the proposed FIR differentiator exhibits steeper roll-off, but has high-frequency ripple at high frequencies, when both have the same cut-off frequency. This is as a direct consequence of the different constraints utilized for the design of the filters. The goal of variance minimization leads to the proposed IIR differentiator having the smallest maximum absolute error found when processing quantized signals.

Chapter 3 Design of a Second-Degree Digital Differentiator

Second-degree, or higher-degree, digital differentiators have a large range of applications. For example, in radar systems, acceleration can be computed from the position measurements using a second-degree differentiator [26]. An all-optical second-order temporal differentiator based on a mechanically-induced long-period fiber grating (MILPFG) with a single π -shift is demonstrated in [27]. In biomedical engineering applications, biomedical information, such as electroencephalogram (EEG) and electrocardiogram (EKG) data, is often evaluated using the second-degree derivative of the signals [28]. The ideal differentiator of a second degree integer order has the following frequency response:

$$H\left(e^{j\omega}\right)=(j\omega)^2, \quad |\omega \le \pi| \tag{3.1}$$

3.1 Introduction and Literature review

3.1.1 The FIR second- degree differentiator

The FIR second-degree differentiator (also termed the double differentiator) should have similar constraints to that of first-degree differentiators, as described using (2.3) and (2.4). This differentiator, it should meet the following equations:

$$\sum_{n=0}^{N} h_n = 0 \tag{3.2}$$

$$\sum_{n=0}^{N} n\,h_n = 0 \tag{3.3}$$

$$\sum_{n=0}^{N} n^2 h_n = 2! \tag{3.4}$$

Equation (3.4) corresponds to $\frac{d}{d^2 x}\left(x^2\right) = 2 \times \left(x\right)' = 2 \times 1 = 2!$.

The filter can be computed from the above equations (3.2) (3.3) and (3.4) using the Moore-Penrose pseudoinverse, as previously presented in Sections 2.2.1 for first-degree differentiators. The magnitude responses of some corresponding double differentiators are shown in Figure 3.1:

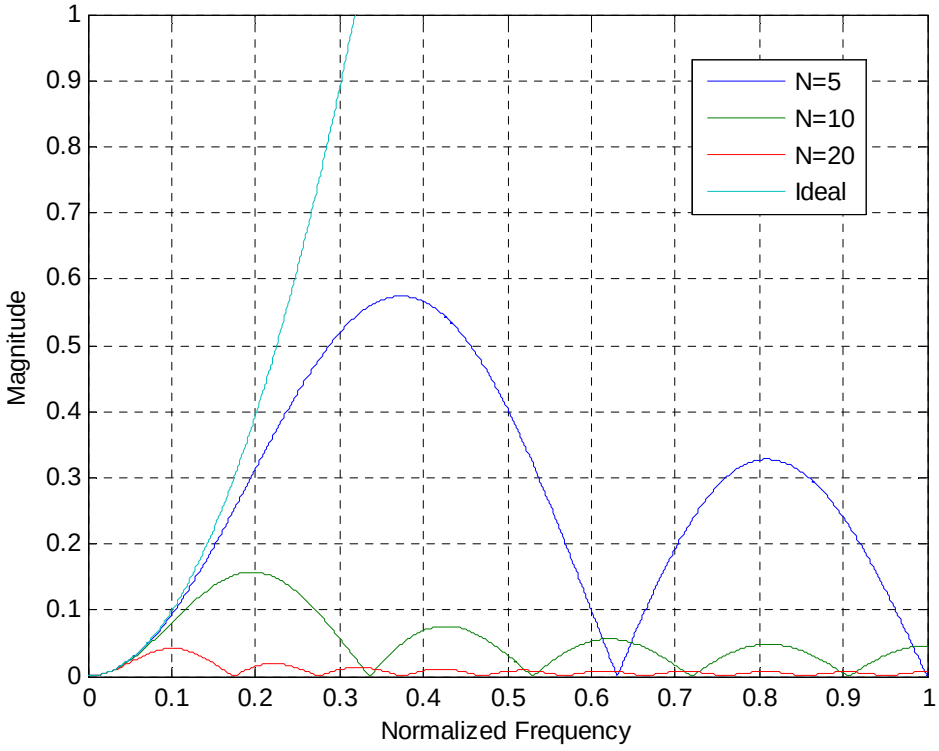

Figure 3.1 *Magnitude responses of the second-degree differentiator with* $N = 5$, $N = 10$, $N = 20$, *and the ideal digital double differentiator.*

In [28], an FIR differentiator is designed for estimation of signal derivatives and of sharpness at extremes. The filtering method is described as follows:

If $\{(x_i, y_i), i = 1, \ldots, p\}$ are data points to be interpolated by the parabola, $P(x) = v_2 x^2 + v_1 x + v_0$, then the optimal coefficients v_2, v_1 and v_0 which minimize the mean square error, are given by:

$$\sum_{i=1}^{p} (y_i - P(x_i))^2 \tag{3.5}$$

over all choices of such coefficients. These are obtained by solving the equation [28]:

$$\begin{bmatrix} v_2 & v_1 & v_0 \end{bmatrix}' = (X'X) + X'Y \tag{3.6}$$

where $X_{ij} = x_i^{3-j}$, for $1 \le i \le p$, $1 \le j \le 3$, $Y = \begin{bmatrix} y_1, \ldots, y_p \end{bmatrix}'$, X' denotes the transpose of X, and $(X'X)^+$ denotes the Moore-Penrose pseudoinverse of the symmetric matrix $X'X$. Letting $A = X'X$, the elements of the matrix A are given by:

$$A_{ij} = \sum_{k=1}^{p} x_k^{6-i-j}, \quad 1 \le i \le p, \quad 1 \le j \le 3. \tag{3.7}$$

Because the formula for v_2 is linear in Y, these estimates may be obtained from the output of an FIR filter which can be applied to the time series. This sequence of acceleration estimates are given by:

$$v_2\left(k - \left[\frac{p-1}{2}\right]\right) = F_p y_k + F_{p-1} y_{k-1} + \ldots + F_2 y_{k-p+2} + F_1 y_{k-p+1} \tag{3.8}$$

where $\{y_k, k = 1, 2 \ldots,\}$ is the signal being analyzed, and p is the number of

points used in the parabolic fit. The number of points used in the parabolic curve fitting is equivalent to that of an FIR filter with p coefficients (of identical values). Using $n \equiv j-1$ and $N \equiv p-1$ when equating the derivations of [28] (from which the above description is excerpted) with the standard nomenclature employed in this thesis, the following FIR filter can be explicitly computed for a system of order N [28]:

$$h(n) = 60\frac{6n^2 - 6nN + N^2 - N}{(N-1)N(N+1)(N+2)(N+3)} \quad n = 0,\ldots,N \qquad (3.9)$$

Equation (3.9) here, gives the same results as the coefficients obtained through use of equations (3.2), (3.3) and (3.4). As for the differentiator, it should be noted that the filter coefficients of the second-degree differentiator obtained using Lagrange multipliers, or using the Moore-Penrose pseudoinverse to compute the filter coefficients, or equivalent least-squares-based curve fitting techniques, produce exactly the same coefficients. Therefore, the same transfer function is computed from seemingly different, but equivalent methods.

3.1.2 Design using Richardson extrapolation and fractional delay

A method to design the second-degree differentiator, using Richardson extrapolation and fractional delay, is introduced in [29]. Richardson extrapolation is used to generate a highly accurate response (i.e. closely following the ideal curve in the pass-band). Then, a conventional Lagrange FIR fractional delay filter is directly applied to implement the second-degree differentiator. From [29], the backward difference formula to estimate the

second derivative is given, for a given signal $x(n)$, by:

$$x''(n) = \frac{x(n) - 2x(n-\alpha) + x(n-2\alpha)}{\alpha^2} \tag{3.10}$$

Taking the *z*-transform at both sides, the transfer function of the differentiator is:

$$A_0(z,\alpha) = \frac{X''(z)}{X(z)} = \frac{1 - 2z^{-\alpha} + z^{-2\alpha}}{\alpha^2} \tag{3.11}$$

where α is the fractional delay. Replacing z by $e^{j\omega}$ in steady-state,

$$A_0(e^{j\omega},\alpha) = D(\omega) + O(\alpha) \tag{3.12}$$

where $O(\alpha)$ denotes that the error term decays as fast as α, and $H_d(\omega)$ is the ideal full-band second-degree differentiator. If parameter α approaches zero:

$$\lim_{\alpha \to 0} A_0(e^{j\omega},\alpha) = H_d(\omega) \tag{3.13}$$

From [29] an improved discrete estimate of the differentiator is obtained using Richardson's iterative improvement process, which yields the first improved differentiator estimate, A_1, as follows:

$$\begin{aligned} A_1(e^{j\omega},\alpha) &= 2A_0(e^{j\omega},\alpha) - A_0(e^{j\omega},2\alpha) \\ &= H_d(\omega) + O(\alpha^2) \end{aligned} \tag{3.14}$$

The order of the error term of $A_1(e^{j\omega},\alpha)$ is $O(\alpha^2)$, which produces faster convergence speed than $A_0(e^{j\omega},2\alpha)$ when α approaches zero. A simple recurrence formula can be used:

$$A_k(e^{j\omega},\alpha)=\frac{2^k A_{k-1}(e^{j\omega},\alpha)-A_{k-1}(e^{j\omega},2\alpha)}{2^k-1}$$
$$=H_d(\omega)+O(\alpha^{k+1}) \tag{3.15}$$

Therefore, it can be concluded that the error can be reduced by increasing k or decreasing α. The implementation of differentiator $A_k(z,\alpha)$ involves a fractional delay. Chien-Cheng Tseng and Su-Ling Lee solved this problem by using the Lagrange FIR fractional delay filter. In this method, a pure integer delay z^{-I} is cascaded with $A_k(z,\alpha)$.

The filter coefficients are given in [29] for the cases $k=0,1$:

$$h_0(n)=\frac{1}{\alpha^2}\delta(n-1)-\frac{2}{\alpha^2}\prod_{k=0,k\neq n}^{N}\frac{I+\alpha-k}{n-k}+\frac{2}{\alpha^2}\prod_{k=0,k\neq n}^{N}\frac{I+2\alpha-k}{n-k} \tag{3.16}$$

$$h_1(n)=\frac{1}{4\alpha^2}\delta(n-1)-\frac{16}{4\alpha^2}\prod_{k=0,k\neq n}^{N}\frac{I+\alpha-k}{n-k}$$
$$+\frac{10}{4\alpha^2}\prod_{k=0,k\neq n}^{N}\frac{I+2\alpha-k}{n-k}-\frac{1}{4\alpha^2}\prod_{k=0,k\neq n}^{N}\frac{I+4\alpha-k}{n-k} \tag{3.17}$$

where $n=0,\ldots,N$, N is the order of the differentiator and $\delta(\cdot)$ is the delta function .

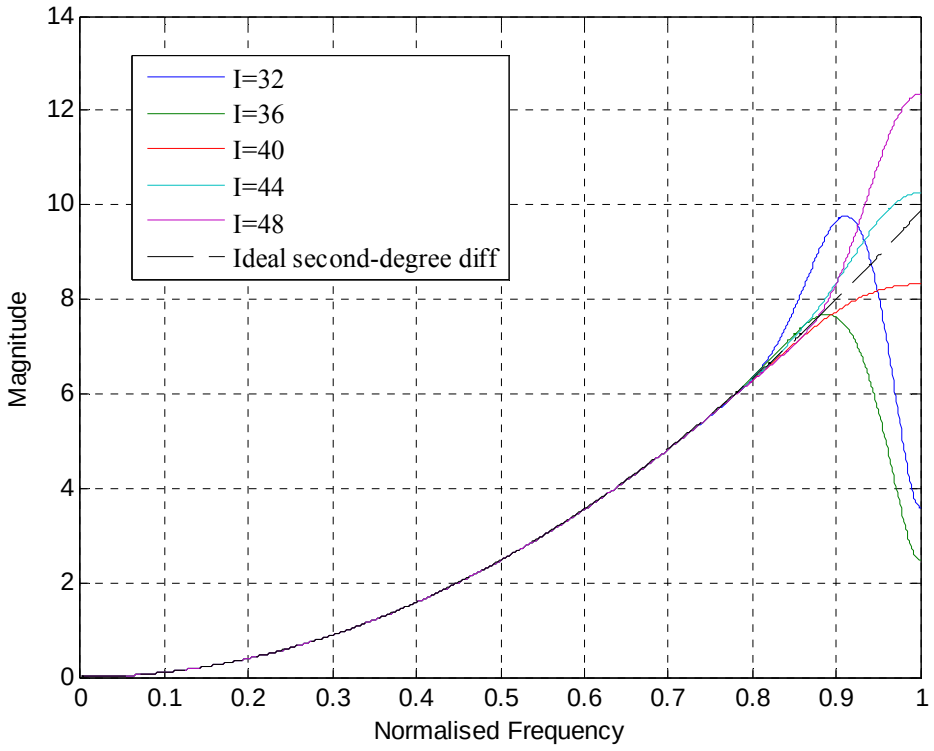

Figure 3.2 *Comparison of the magnitude responses of the second-degree differentiator designed using Richardson extrapolation and fractional delay, with a differentiator of purely integer delay.*

An example of this technique, an second-degree with order $N = 80$, fractional delay $\alpha = 0.1$, integer delay $I = 32,\ 36,\ 40,\ 44, \text{or } 48$, using (3.16) (for the case of $k = 0$), is considered. The magnitude response of the second-degree differentiator is shown in Figure 3.2. The resulting differentiators almost overlap with the ideal response in the frequency range of up to 0.8 of the normalized frequency. For the high-frequency range, the magnitude response of the differentiators is close to the ideal response when the value of I is close to the value of half of the filter order ($N/2 = 40$ in this example). This is because the fractional delay filter is obtained using a Lagrange interpolator. One characteristic of Lagrange interpolation is that the maximum

of the magnitude response never exceeds unity when the delay is near to half the filter length .Although the filter coefficients are not symmetrical, the resulting second-degree differentiators exhibits constant group delay performance in the frequency range of up to approximately 0.8 of the normalized Nyquist frequency.

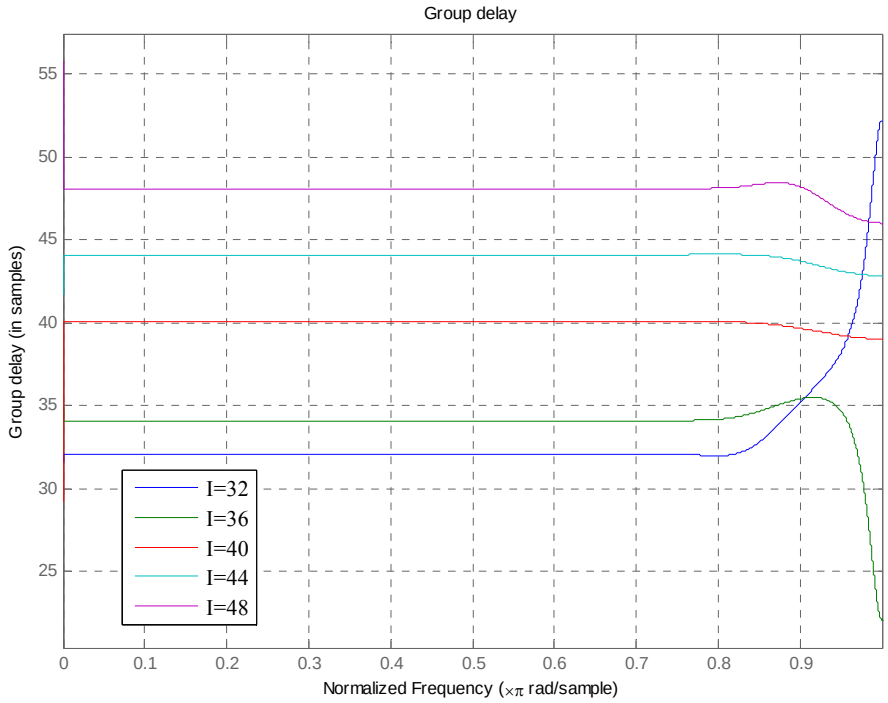

Figure 3.3 *Comparison of the group delay of the second-degree differentiator designed using Richardson extrapolation and fractional delay, with differentiator of purely integer delay.*

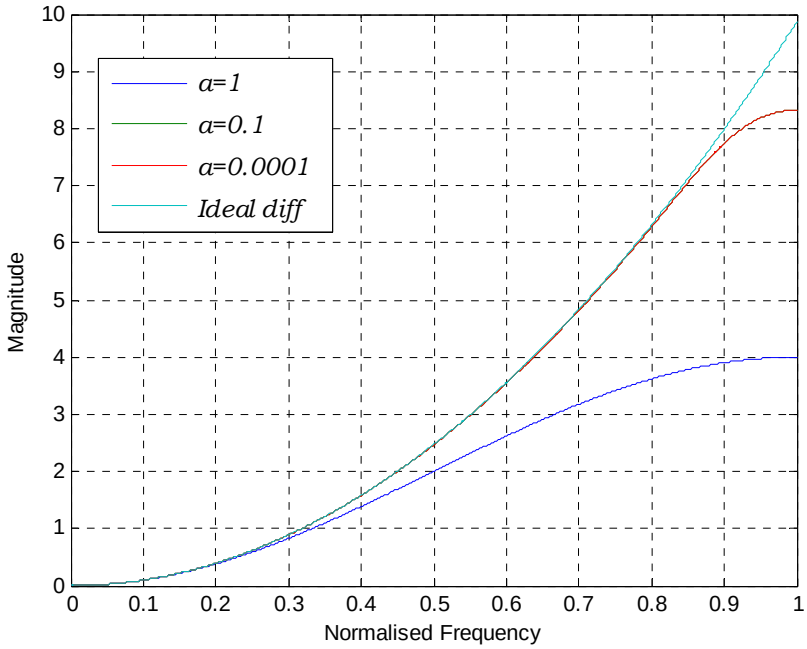

Figure 3.4 *Comparison of magnitude response of the second-degree differentiator with different fractional delays.*

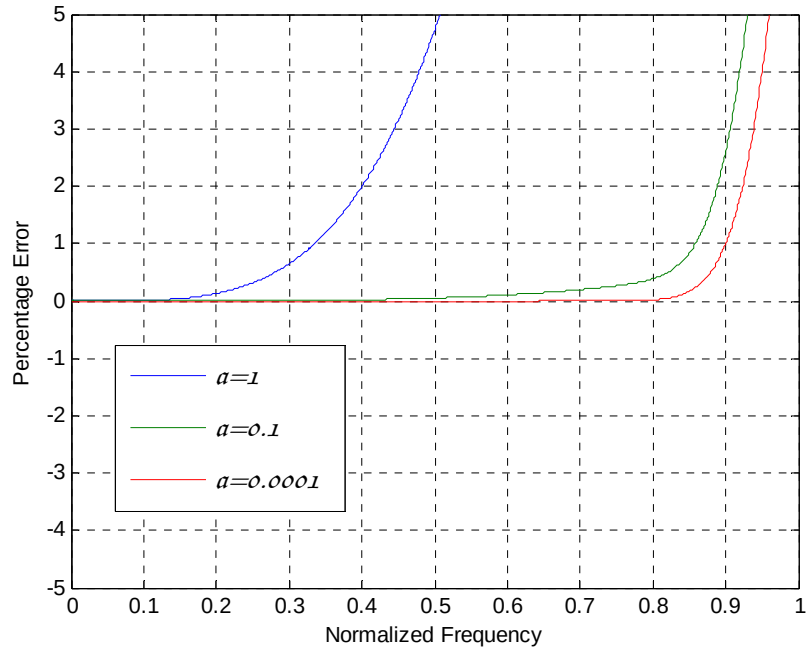

Figure 3.5 *Comparison of percentage error of the second-degree differentiator with different fractional delays.*

Another example is used to test the performance when the delay $\alpha = 1, 0.1, \text{or } 0.0001$. As shown in in Figure 3.4 and Figure 3.5. it is clear that the smaller the value of α, the smaller the percentage error in the pass-band.

3.2 Design of second-degree IIR low-pass differentiator

The high-order IIR Low-Pass differentiator is designed using the optimization method presented in Chapter 2.

In this section, the second-degree IIR low-pass differentiator is designed. The coefficients of the numerator and denominator are denoted by b_n and a_n, where $0 \le n \le N$, yielding the following equations:

$$\sum_{n=0}^{N} b_n = 0 \tag{3.18}$$

$$\sum_{n=0}^{N} n b_n = 0 \tag{3.19}$$

$$\sum_{n=0}^{N} n^2 b_n = (2!) \sum_{n=0}^{N} a_n \tag{3.20}$$

These equations arise from a second-degree differentiator that produces no output (in steady-state) for a constant input or an input with constant slope, while a parabola will produce an output that is equal to the (constant) second derivative of the parabolic input. The cost functions are the same as for the standard differentiator in (2.48), (2.49) and (2.50), so the optimization function

is given by (2.51). For example, the transfer function of a fourth-order IIR second-degree differentiator can be written as:

$$H_4(z)=\frac{2(1+a_1+a_2+a_3+a_4)}{4+d_1}\frac{1+d_1z^{-1}-2(1+d_1)z^{-2}+d_1z^{-3}+z^{-4}}{1+a_1z^{-1}+a_2z^{-2}+a_3z^{-3}+a_4z^{-4}} \quad (3.21)$$

It should be noted that, for a second-degree differentiator, the coefficient of the numerator is even symmetrical, which means that two zeros lie at $z=1$. The resultant coefficients of the sample differentiators are given in Table 3.1. The magnitude response and group delay of the proposed differentiators are shown in Figure 3.6 , Figure 3.7 and Figure 3.8. The proposed differentiators exhibit high accuracy in the pass-band, for which the maximum percentage errors are less than 0.003%, and they show good attenuation in the stop-band, as well as a steep transition band. Additionally, the proposed differentiators also show almost constant group delay over the pass-band.

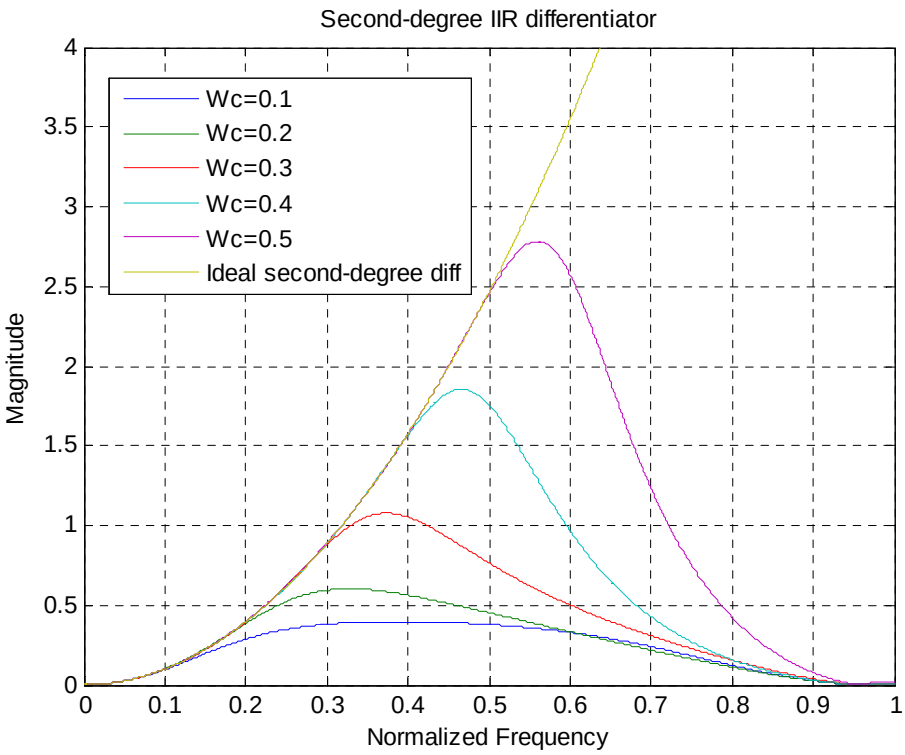

Figure 3.6 *Magnitude response of proposed second-degree IIR differentiators.*

Table 3.1 Coefficients of the proposed second-degree low-pass IIR differentiators

$\omega_c(rad/s)$	0.1	0.2	0.3	0.4	0.5
$b(0)$	0.1248	0.1395	0.1916	0.2307	0.3716
$b(1)$	-0.0025	-0.0028	-0.0038	-0.0046	-0.0074
$b(2)$	-0.2446	-0.2735	-0.3756	-0.4522	-0.7284
$b(3)$	-0.0025	-0.0028	-0.0038	-0.0046	-0.0074
$b(4)$	0.1248	0.1395	0.1916	0.2307	0.3716
$a(0)$	1.0000	1.0000	1.0000	1.0000	1.0000
$a(1)$	-0.4862	-0.6462	-0.5050	-0.5277	0.0848
$a(2)$	-0.1247	0.0637	0.1868	0.6239	0.4742
$a(3)$	0.0384	0.1642	0.1709	-0.2226	-0.1179
$a(4)$	0.0691	-0.0263	-0.0900	0.0447	0.0380
F_1	0.0001	0.001	0.001	0.001	0.001
F_2	0.28	0.36	0.4	0.76	0.7
F_3	0.07	0.12	0.3	0.76	1.8
Weight vector	[1 1 1]	[1 1 1]	[1 1 1]	[1 1 1]	[1 1 1]

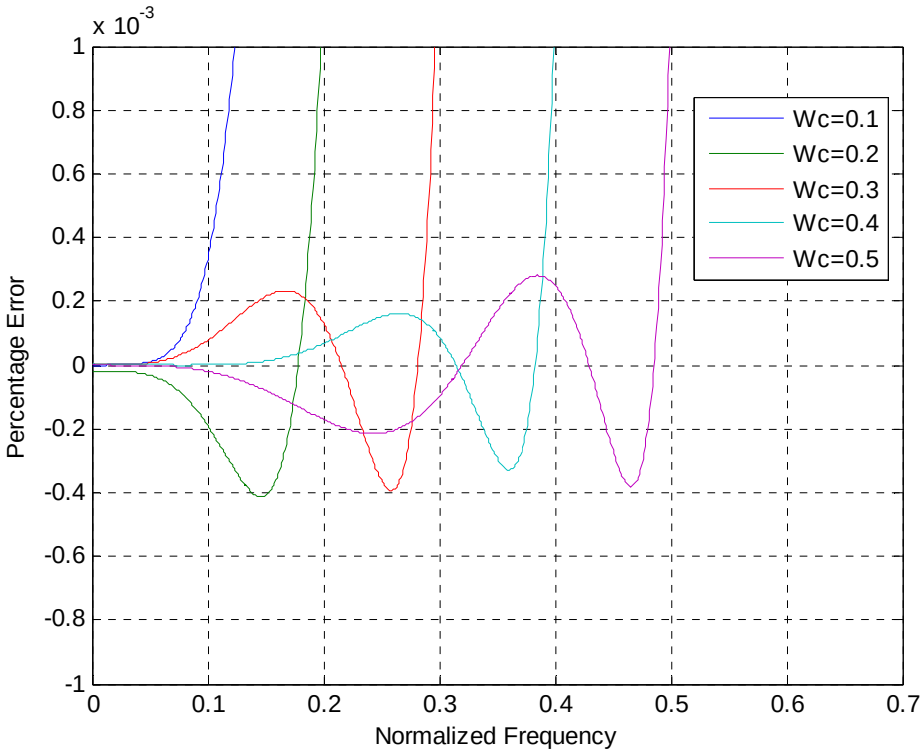

Figure 3.7 *Percentage Error of fourth-order second-degree IIR differentiators.*

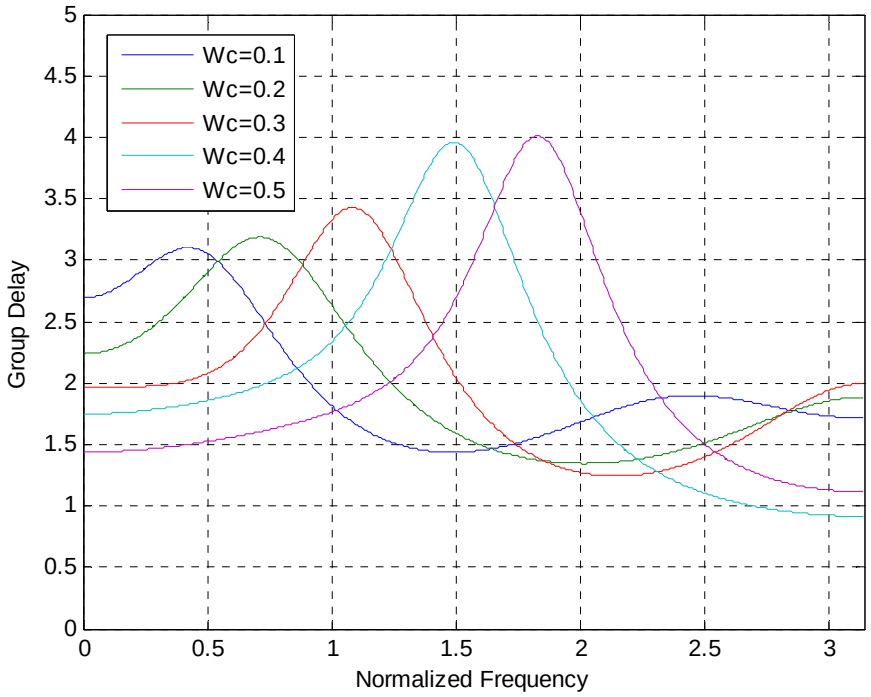

Figure 3.8 *Group delay of fourth-order second-degree IIR differentiators.*

3.3 Design of Second-degree FIR low-pass differentiator

The method of designing FIR second-degree differentiators was discussed in Section 3.1. The filter coefficients are computed using the Moore-Penrose pseudoinverse, to minimize the variance (the square sum of filter coefficients of the FIR filter). However, the choice of the cut-off frequency is not controllable when designing using the Moore-Penrose pseudoinverse. A method of designing the FIR low-pass second-degree differentiators is introduced in this section to rectify this deficiency.

The constraints used for this method is the same as those of (3.2) (3.3) and (3.4), and the filter coefficients are desired to be even symmetrical for second-degree differentiator, to ensure that the proposed differentiator have linear phase, or constant group delay.

The remaining filter coefficients are computed using the optimization techniques discussed in Chapter 2. Therefore, the optimization goals of a second-degree FIR differentiator include the magnitude response in the pass-band and the filter variance, which are represented by F_1 and F_3, respectively, as (defined in (2.48) and (2.50)). The filter coefficients of the transfer function can be computed using an optimization technique. The cost function of the optimization is the same as for (2.54). In addition, this method could also be used for differentiators of higher degree. An example is given (in Figure 3.9 and Figure 3.10) to show the magnitude response and percentage error of twenty-first order FIR second-degree differentiators of different cut-off frequencies. The filter coefficients can be expressed as:

$$h = \begin{bmatrix} h_0 & h_1 & \cdots & h_9 & h_{10} & h_{10} & h_9 & \cdots & h_1 & h_0 \end{bmatrix} \qquad (3.22)$$

where $h_0 = \frac{1}{10}\left(\frac{1}{2} + 9h_2 + 17h_3 + 24h_4 + 30h_5 + 35h_6 + 39h_7 + 42h_8 + 44h_9 + 45h_{10}\right)$

$$h_1 = -\frac{1}{10}\left(\frac{1}{2} + 19h_2 + 27h_3 + 34h_4 + 40h_5 + 45h_6 + 49h_7 + 52h_8 + 54h_9 + 55h_{10}\right)$$

The filter coefficients of the proposed differentiator are given in Table 3.2. The proposed differentiators exhibit high accuracy in the pass-band, and fast attenuation in the stop-band. A Comparison of Figure 3.6 and Figure 3.9, shows that the proposed second-degree differentiators exhibit high accuracy in the pass-band. The FIR differentiators show steeper roll-off but large ripple in the stop-band, when compared with the proposed IIR filter. Additionally, the proposed FIR second-degree differentiators have linear phase because the filter coefficients are even symmetrical.

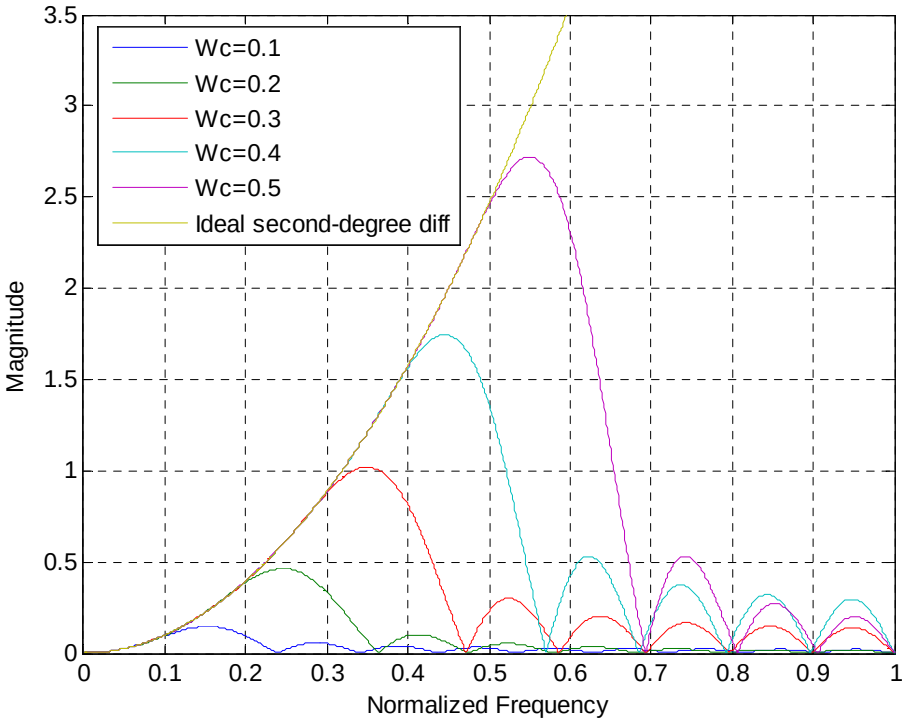

Figure 3.9 *Magnitude response of twenty first-order FIR second-degree differentiators.*

Table 3.2 Coefficients of the proposed second-degree twenty-first order, low-pass FIR differentiators

$\omega_c\left(rad/s\right)$	0.1	0.2	0.3	0.4	0.5
h_0	-0.0125	0.0052	0.0105	-0.0164	0.0128
h_1	0.0011	0.0099	-0.0490	0.0724	-0.0550
h_2	0.0096	-0.0186	0.0541	-0.1129	0.1002
h_3	0.0135	-0.0273	0.0381	0.0268	-0.0717
h_4	0.0132	-0.0047	-0.0576	0.1186	-0.0685
h_5	0.0097	0.0318	-0.0756	-0.0664	0.1993
h_6	0.0042	0.0549	0.0284	-0.1569	-0.1034
h_7	-0.0022	0.0470	0.1399	0.0921	-0.2381
h_8	-0.0083	0.0097	0.1210	0.3026	0.4009
h_9	-0.0129	-0.0377	-0.0313	0.0703	0.3796
h_{10}	-0.0154	-0.0702	-0.1785	-0.3302	-0.5561
F_1	0.0001	0.001	0.001	0.001	0.001
F_3	0.0023	0.028	0.17	0.55	1.5
Weight vecetor	[1 1]	[1 1]	[1 1]	[1 1]	[1 1]

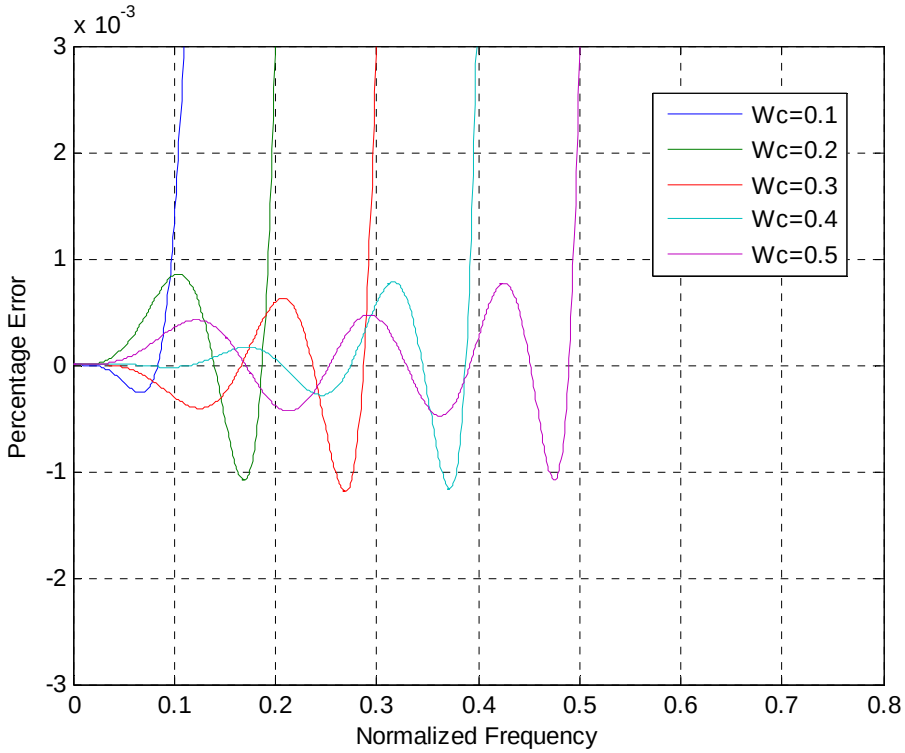

Figure 3.10 *Percentage error of fourth-order second-degree FIR differentiators.*

3.4 Performance of Proposed Second-degree Differentiators in the Time-Domain

Some similar tests to those considered in the previous chapter are used in this section to test the performance of some proposed second-degree differentiators in the time-domain. In time-domain analysis, the desired output signal should be the double derivative of the input signal. The proposed second-degree differentiators being tested include IIR and FIR differentiators with a cut-off frequency of $\omega_c = 0.3$, for which the filter coefficients can be found in Table 3.1 and Table 3.2.

- Basic noise-free Cubic function.

The input signal function chosen is: $f(t) = 3t^3 + 4t^2 + 2t + 1$, for a sample time $T_s = 0.001s$, so the ideal output, the double derivative of input signal is: $f''(t) = 18t + 8$. Figure 3.11 show the filter output to this test signal that results from the polynomial signal described in this section. The ideal output is simply the double derivative of the input However, the proposed second-degree differentiators shows more extreme intial transients than the first-degree differentiator designed in Section 2.6. In addition, the output of the FIR differerentiator shows obvious delay in comparsion with the output of the corresponding IIR filter.

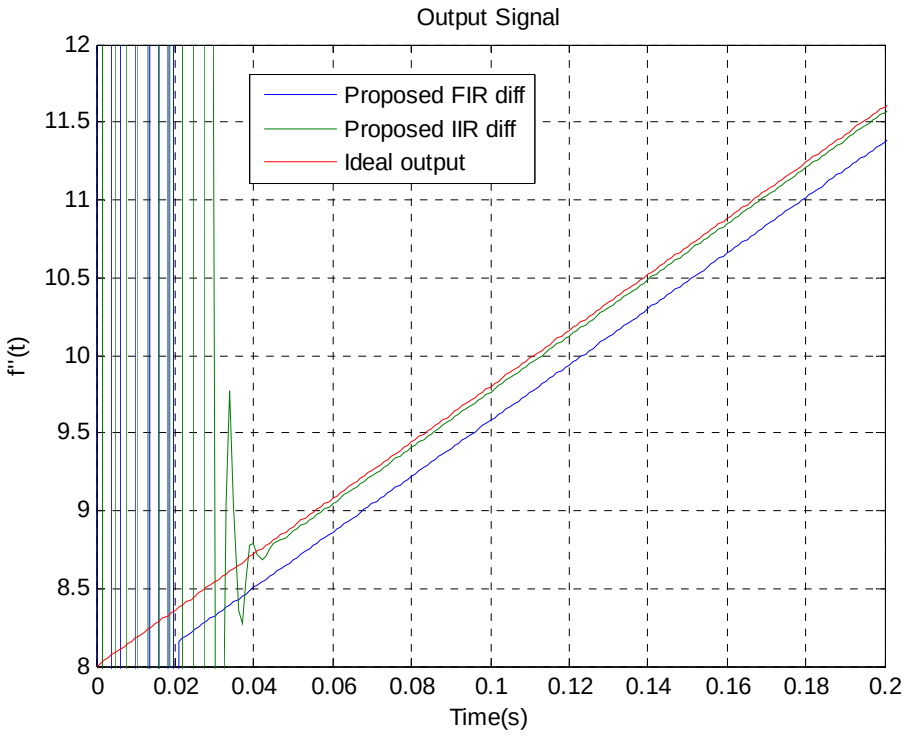

Figure 3.11 *Output signals for the cubic test signal input.*

- Basic, noise-free sinusoidal wave.

The input signal is the sinusoidal wave is $f(t) = \sin t$, so that the ideal output is: $f''(t) = -\sin t$. In Figure 3.12, the resulting output signal of the proposed IIR differentiator shows very good performance in the time-domain, with almost no delay, for a sample time $T_s = 0.01s$. The delay by the FIR filter is evident, causing an obvious error.

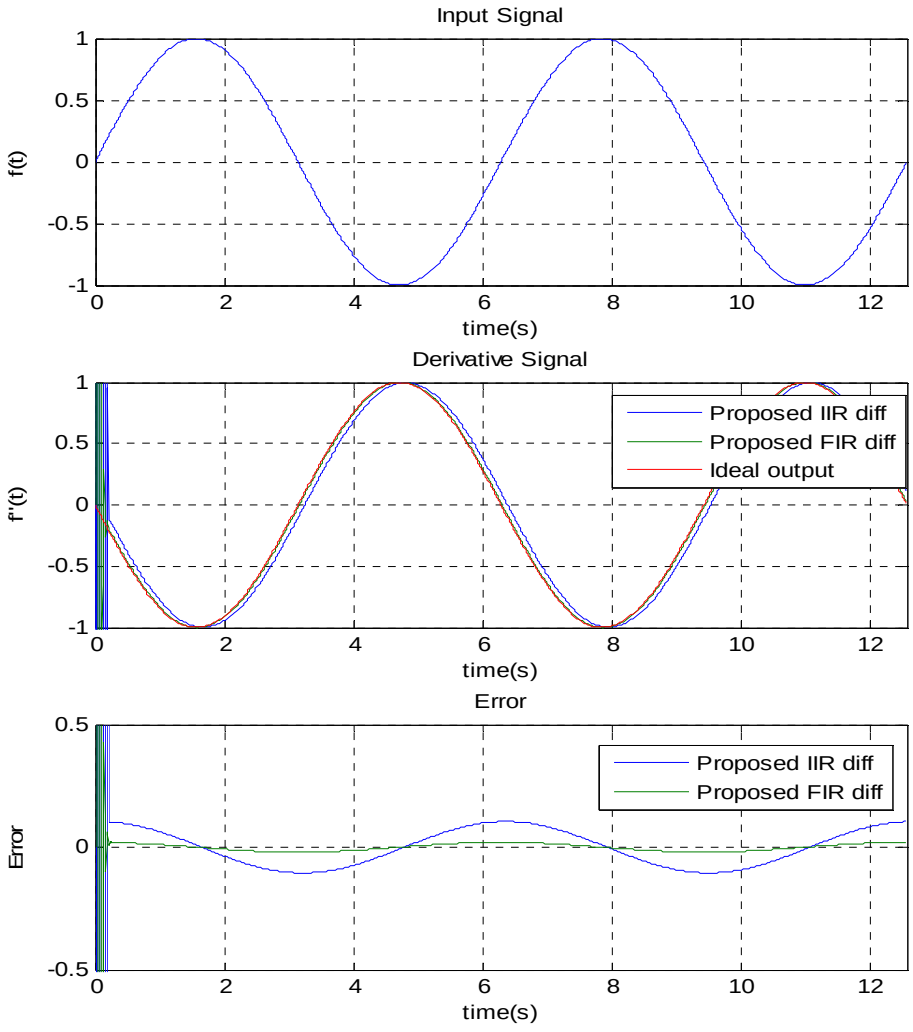

Figure 3.12 *Time domain analysis of sinusoidal wave signal with proposed second-degree differentiators.*

- Quantized composite signal.

The ideal output signal is the same as that used for testing the differentiators discussed in Section Chapter 1 (with an appropriate input signal). Figure 3.13 and Figure 3.14 provide the double derivative of the quantized input, which shows that it has similar characteristics to those of the first-degree differentiator: (1) the higher the cut-off frequency of the proposed differentiator, the more quantized noise interference ensues; (2) with very low cut-off frequency ,the proposed differentiator can substantially filter the quantized noise, with significant attenuation for high-frequency inputs.

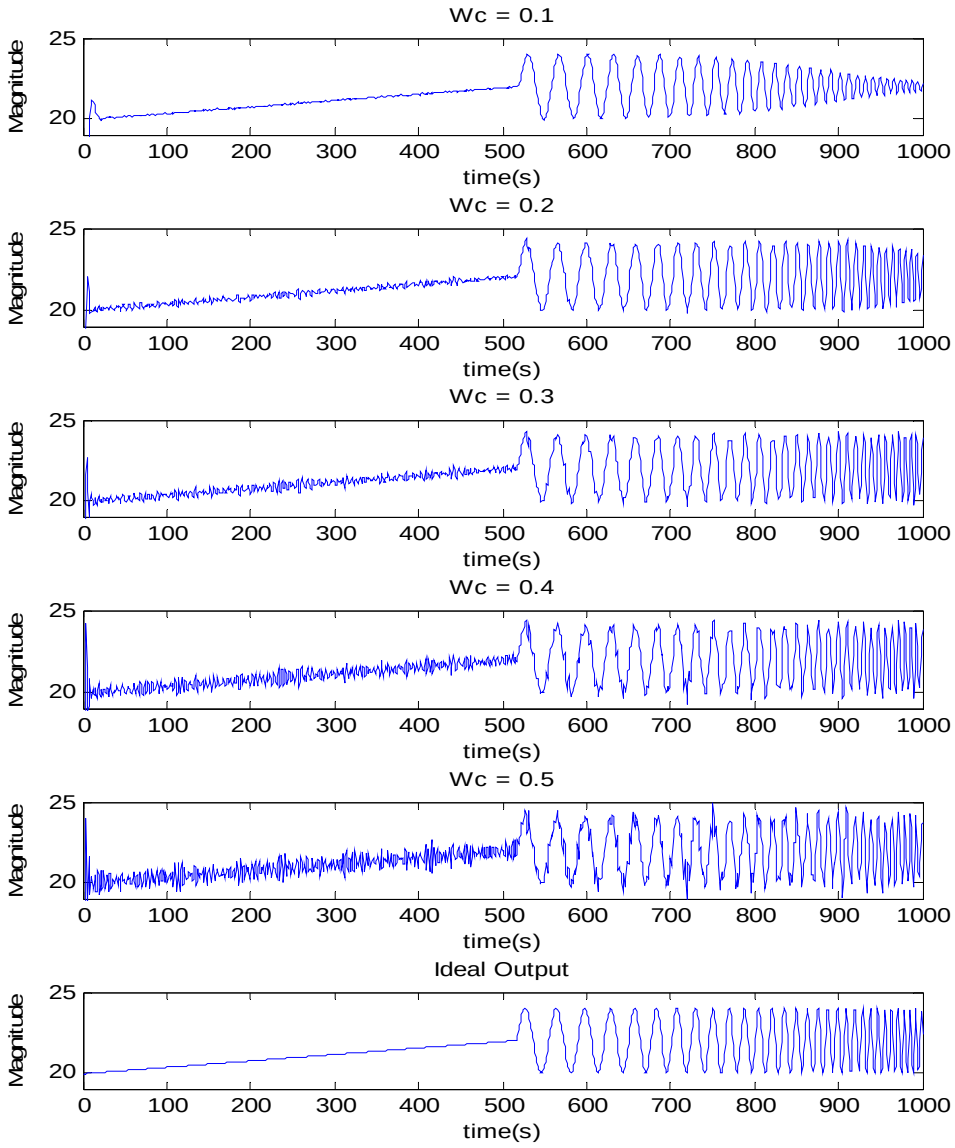

Figure 3.13 *Time domain analysis of constant acceleration and sinusoidal wave signal (of ideally constant output magnitude for varying input frequencies) for proposed second-degree IIR differentiators.*

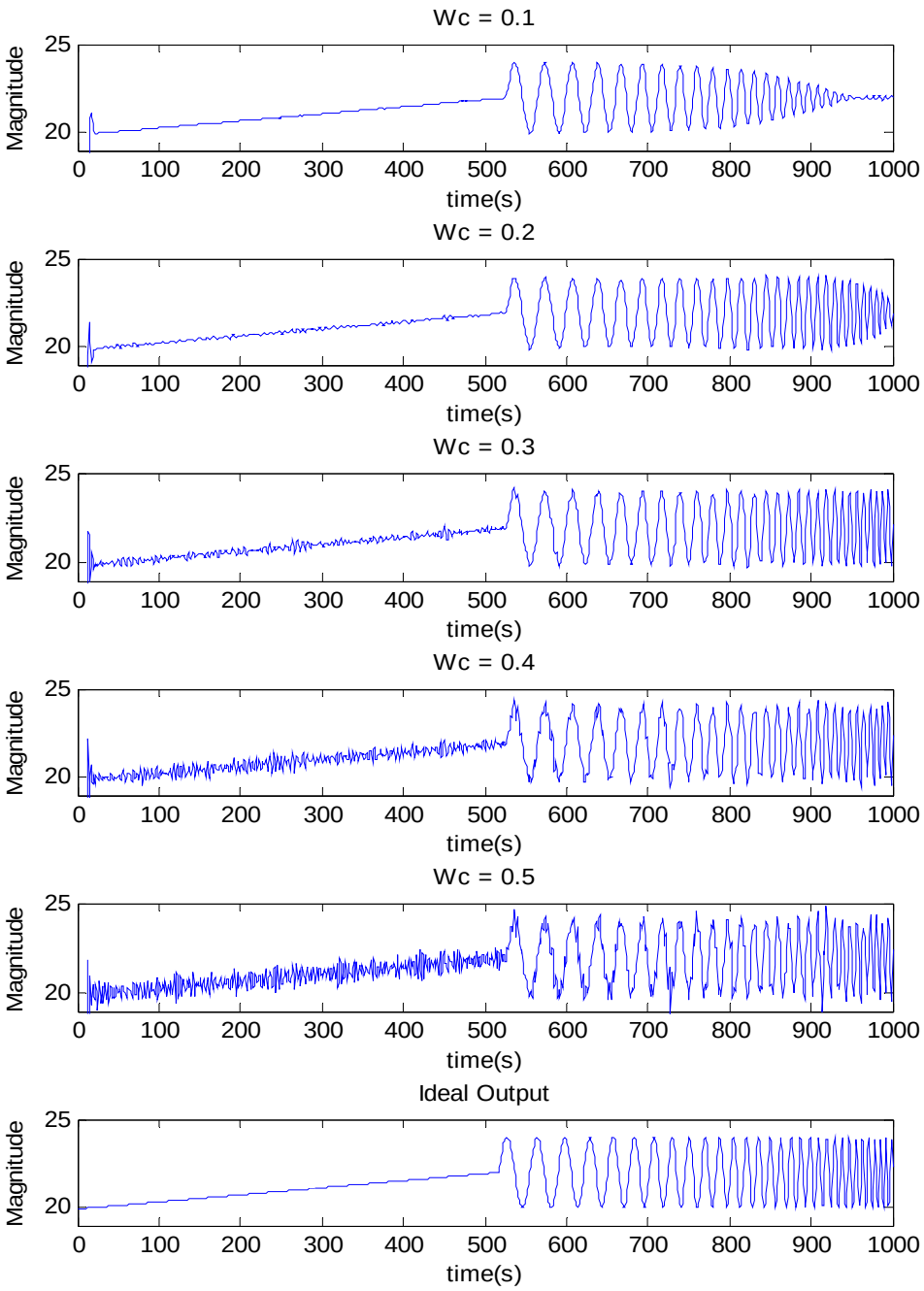

Figure 3.14 *Time-domain analysis of constant acceleration and sinusoidal signals (of ideally constant output magnitude for varying input frequencies) for proposed second-degree FIR differentiators.*

Another test is given to compare the performance in the time-domain of different second-degree differentiators. The second-degree differentiators to be tested include the fourth order proposed IIR differentiator, twenty-first order proposed FIR differentiator with cut-off frequency $\omega_c = 0.3$, for which filter coefficients can be found in Table 3.1 and Table 3.2; Vainio's FIR differentiator the coefficients of which can be computed from (3.9), and the differentiator designed by Chien-Cheng Tseng and Su-Ling Lee [29], for which the filter coefficients are as given in (3.16), ($\alpha = 0.1$, $N = 20$ and $I = 8$). The magnitude responses of the above second-degree differentiators are shown in Figure 3.15. Vainio's FIR differentiator exhibits the smallest cut-off frequency by minimizing the filter variance (with no choice available to the designer); the cut-off frequency of the proposed FIR and IIR differentiators are at $\omega_c = 0.3$. The FIR differentiator shows faster roll-off, but bigger ripple at high frequency, than the IIR differentiator. The second-degree differentiator designed by Chien-Cheng Tseng and Su-Ling Lee exhibits high accuracy in the passband, with cut-off frequency $\omega_c = 0.6$.

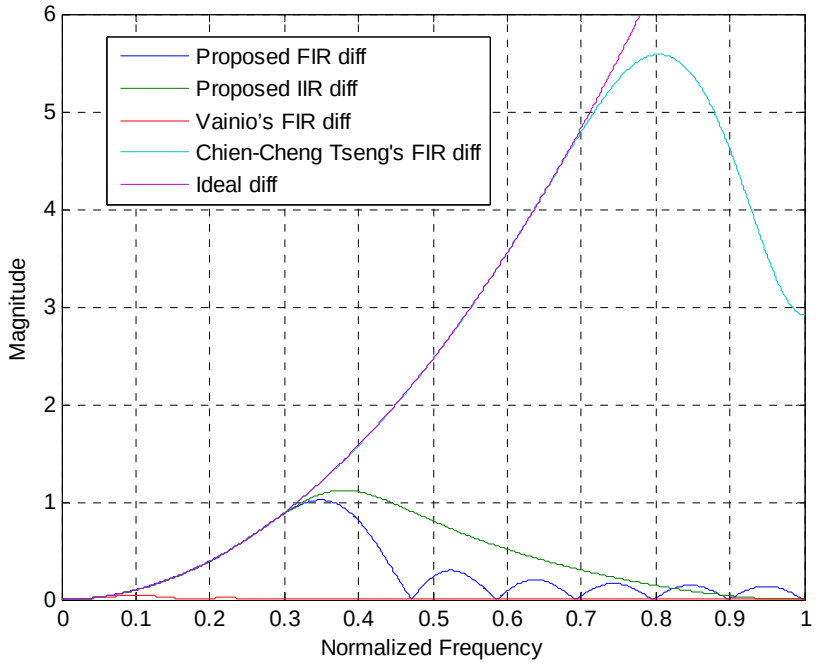

Figure 3.15 *The magnitude response of the second-degree differentiators to be tested.*

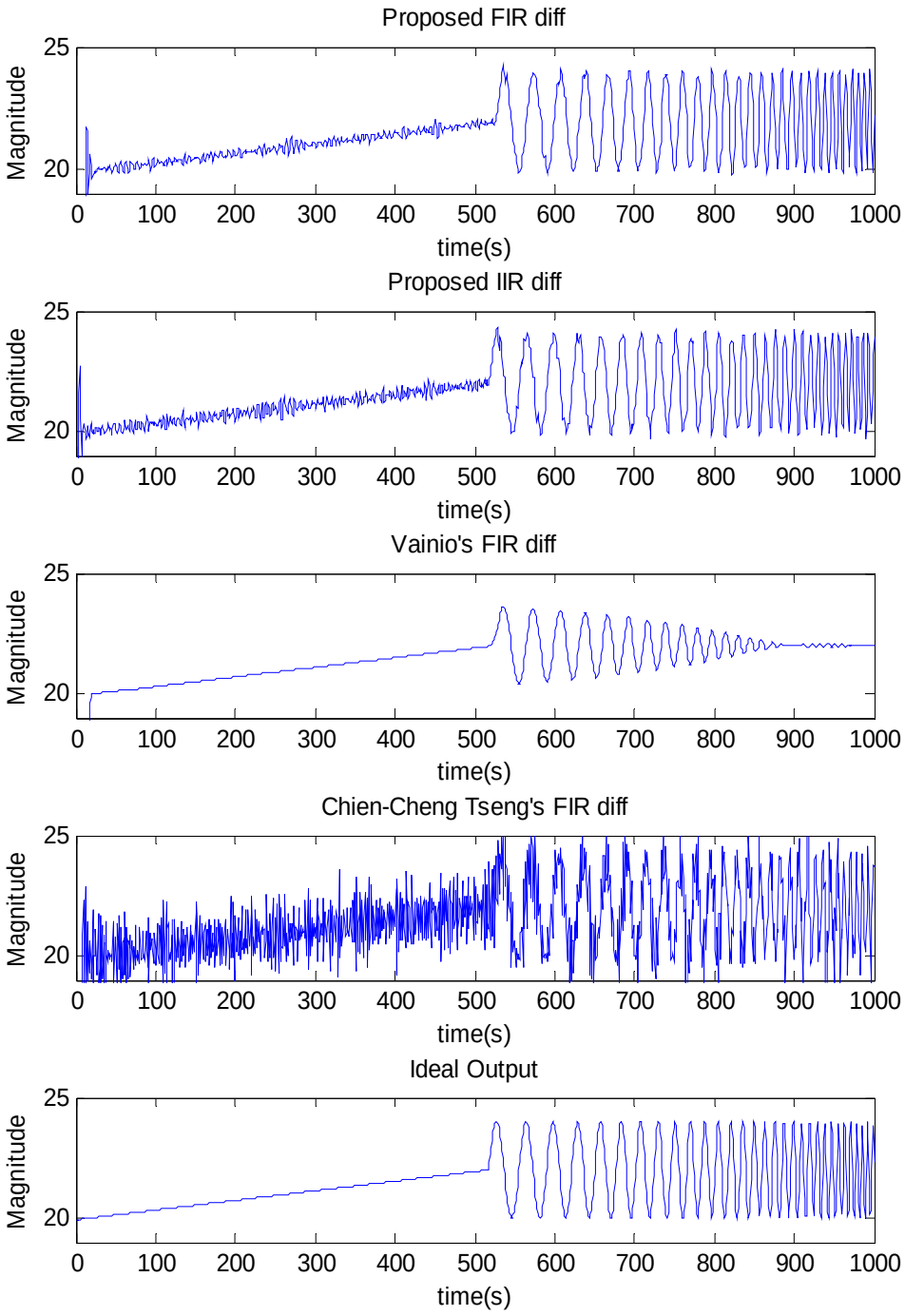

Figure 3.16 *Output of quantized inputs for FIR and IIR second-degree differentiators .*

The output of quantized inputs is shown on Figure 3.16. The proposed FIR

and IIR second-degree differentiators exhibit similar results, with good noise reduction performance and no attenuation in the high frequency range. In addition, the output of the proposed FIR second-degree differentiator has better noise reduction performance due to its faster roll-off. As expected from the magnitude response shown on Figure 3.15, Vainio's FIR second-degree differentiator shows almost perfect noise reduction performance but big attenuation at high frequencies. It can be found easily that there is obvious noise interference of the output when using Chien-Cheng Tseng's second-degree differentiator, because by its high cut-off frequency. It is evident that the second-degree differentiator is more sensitive to noise, because the noise is greatly amplified relative to the first-degree differentiator.

3.4 Conclusions

In this Chapter, some papers have been reviewed on the design of both second-degree FIR and IIR differentiators. A new method for the design of low-pass second-degree digital differentiators is presented in this chapter. The approach utilizes optimization techniques similar to those of Chapter 2, for which optimization goals include the magnitude response, variance and group delay of the filter.

In frequency-domain testing, both of the proposed FIR and IIR differentiators exhibit high accuracy in the pass-band. The FIR second-degree differentiator show faster roll-off than the second-degree IIR differentiator. While some small ripples it can be found in the transition band and stop band of the proposed FIR differentiators, its attenuation is still better than that of the proposed IIR differentiators. It should be noted that, for a second-degree differentiator, the coefficient of the numerator is even symmetrical, which means that two zeros lie at $z = 1$.

In time-domain testing, the proposed IIR and FIR low-pass second-degree differentiator also show good results. The outputs of both the IIR and FIR low-pass differentiators give the second derivative of input signal, as expected, for various inputs. The proposed differentiators show good performance for the testing of a quantized signal, in terms of the noise reduction performance and the fact there is no obvious unwanted attenuation at high frequencies. It should be noted that the second-degree differentiator is much sensitive to noise, so some all pass differentiators will not provide good results in many applications, due to the amplification of noise.

Chapter 4 Design of a Fractional-Degree Digital Differentiator

The history of the fractional calculus covers over three-hundred years, similar to that of classical differential calculus. Dated 30 September 1695, a letter on the meaning of the derivative of order one half is discussed between Leibniz and l'Hôpital. Nowadays, many scientists consider that day as the birthday of fractional calculus, with Leibniz as its father [30]. For three centuries, the theory of fractional derivatives developed mainly as a purely theoretical field of mathematics, useful only for mathematicians. However, in the last few decades, many authors have pointed out that these mathematical phenomena allow for the description of a real object more accurately than the classical integer-degree model [31].

As one example, the usefulness of fractional degree control has been illustrated for the improved control of dynamic systems described by the fractional model. The CRONE controller (French acronym for *Commande Robuste d'ordre Non Entier*) has been successfully implemented as a CAD toolbox: the CRONE Matlab toolbox [32]. In industrial control systems, a proportional integral derivative (PID) controller is probably the most commonly used feedback controller. A fractional degree $PI^{\rho_1}D^{\rho_2}$ controller (where the orders ρ_1 and ρ_2 assume real non-integer values) is proposed by Podlubny [33]. In [33], where an example is provided of the comparison between a classical PID controller and a fractional degree $PI^{\rho_1}D^{\rho_2}$ controller, the desirability of the latter structure for the more efficient control of fractional degree systems is demonstrated.

A further example of the application of a fractional differentiator (FD) has been proposed in the field of image processing, where the requirement is for edge detection of a noisy image. Tuning the degree of the differentiator allows optimum trade-off between noise reduction and sharp edge detection. In [34], an edge detector based on a FD was shown to improve the criteria of 'thin detection', and the immunity to noise. In addition, Hilfer [35] gives many other applications of fractional calculus, including medical science [36], signal processing [37], fluid flow [38], and the theory of viscoelasticity [39], etc.

In the fractional degree controller, the discretization of the fractional differentiator or integrator is the key step of the realization techniques. In this chapter, some existing open-loop methods for the design of FDs are introduced. Then, a feedback system is used to modify these previous fractional degree implementations, in order to ensure that the differentiator performs well in terms of both its time-domain and frequency-domain behavior. Frequency-domain plots are indicative of the steady-state performance of the system, while the time-domain characteristics give a better insight into its transient behavior.

4.1 Background of fractional calculus

In this section, some basic functions and concepts of fractional calculus will be introduced.

4.1.1 The Gamma function

One of the most basic functions of the fractional calculus is Euler's gamma function, $\Gamma(z)$, which generalizes the factorial $n!$, so that n is allowed to also take non-integer, and even complex, values.

The definition of the gamma function $\Gamma(z)$ is given by:

$$\Gamma(z)=\int_0^{\infty} e^{-t}t^{z-1}dt \quad z\in\mathbb{R} \tag{4.1}$$

One of the basic properties of the gamma function is that it satisfies the following equation:

$$\Gamma(z+1)=z\Gamma(z) \tag{4.2}$$

which can be proved as follows:

$$\Gamma(z+1)=\int_0^{\infty} e^{-t}t^{z}dt=\left[-e^{-t}t^{z}\right]_{t=0}^{t=\infty}+z\int_0^{\infty} e^{-t}t^{z-1}dt=z\Gamma(z) \tag{4.3}$$

Also, when $z\in\mathbb{N}_+$ using (4.2), it can be shown that:

$$\begin{aligned}
\Gamma(2)&=1\cdot\Gamma(1)=1=1!,\\
\Gamma(3)&=2\cdot\Gamma(2)=2\cdot1!=2!,\\
\Gamma(4)&=3\cdot\Gamma(3)=3\cdot2!=3!,\\
&\cdots\\
\Gamma(n+1)&=n\cdot\Gamma(n)=n\cdot(n-1)!=n!
\end{aligned} \tag{4.4}$$

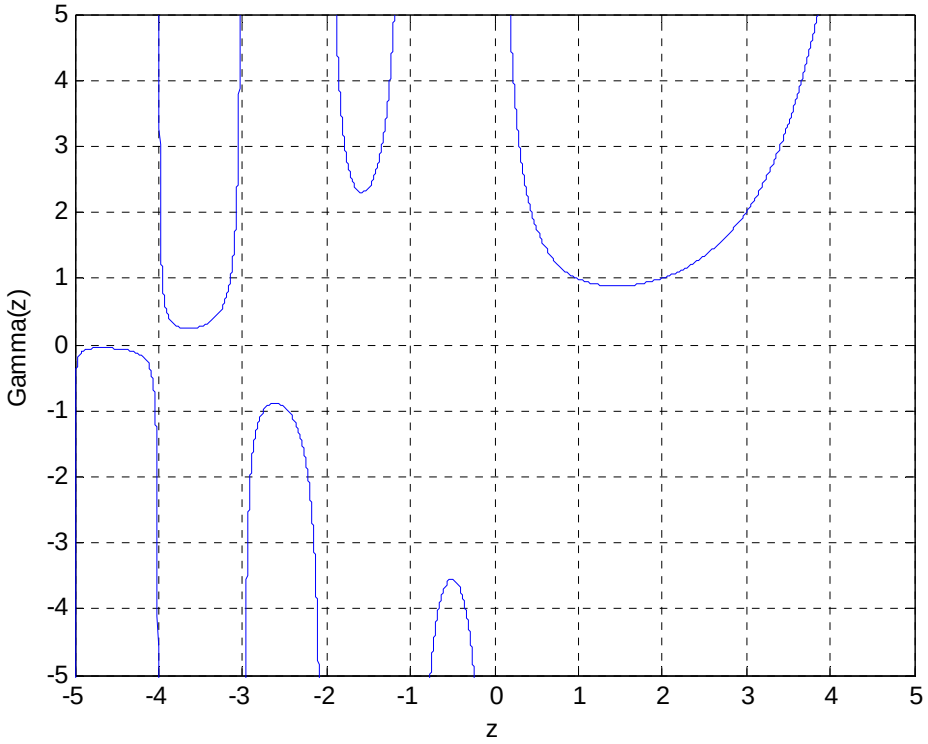

Figure 4.1 *The Gamma function.*

Figure 4.1 shows the Gamma function for small (positive and negative) inputs. Note that the gamma function has simple poles at negative integers.

4.1.2 Laplace transformation

The basic Laplace transform is defined by:

$$F(s) = L\{f(t)\} = \int_0^\infty e^{-st} f(t)dt \tag{4.5}$$

for a function $f(t)$. The convolution is:

$$f(t) * g(t) = \int_0^t f(t-\tau)g(\tau)d\tau = g(t) * f(t) \tag{4.6}$$

For the two functions $f(t)$ and $g(t)$, which are equal to zero for $t<0$. The Laplace transform also satisfies the following equation:

$$L\{f(t)*g(t)\}=F(s)G(s) \tag{4.7}$$

Another important property of the Laplace transform is that the derivative of an integer of degree n of the function $f(t)$ is defined by:

$$L\{f^{n}(t)\}=s^{n}F(s)-\sum_{k=0}^{n-1}s^{n-k-1}f^{(k)}(0)=s^{n}F(s)-\sum_{k=0}^{n-1}s^{k}f^{(n-k-1)}(0) \tag{4.8}$$

4.1.3 Definition of the fractional calculus

The following is the infinite sequence of *n*-fold integrals and *n*-fold integer derivatives:

$$\cdots,\quad \int_{a}^{t}d\tau_{2}\int_{a}^{\tau_{2}}f(\tau_{1})d\tau_{1},\quad \int_{a}^{t}f(\tau_{1})d\tau_{1},\quad f(t),\quad \frac{df(t)}{dt},\quad \frac{d^{2}f(t)}{dt^{2}},\quad \cdots$$

It is interesting that the derivative of the real degree v can be considered as an interpolation of this sequence of operators. The most comment notation used is ${}_{a}D_{t}^{v}f(t)$, where a and t are the two limits related to the operation of fractional differentiation [40].

4.1.3.1 Riemaan-Liouville fractional derivatives

The Riemann-Liouville derivative is the most widely used generalization of the fractional calculus. It is based on the Cauchy formula for n-fold integrals [41]. The first integral of a function is equivalent to differentiating it by degree -1:

$$D^{-1}f(t)=\int_0^t f(\tau)d\tau \tag{4.9}$$

Then, for the second derivative,

$$\begin{aligned} D^{-2}f(t)&=\int_0^t\int_0^{\tau_2} f(\tau_1)d\tau_1 d\tau_2=\int_0^t\int_{\tau_1}^t f(\tau_1)d\tau_2 d\tau_1=\int_0^t f(\tau_1)\int_{\tau_1}^t d\tau_2 d\tau_1\\ &=\int_0^t f(\tau)(t-\tau)d\tau \end{aligned} \tag{4.10}$$

Thus, in general,

$$D^{-n}f(t)=\frac{1}{(n-1)!}\int_0^t f(\tau)(t-\tau)^{n-1}d\tau \tag{4.11}$$

Formula (4.11) is Cauchy's formula. The Riemann-Liouville integral with lower limit a can be generalized as:

$${}_aJ_t^{\nu}f(t)=\frac{1}{\Gamma(\nu)}\int_a^t\frac{f(\tau)}{(t-\tau)^{1-\nu}}d\tau \tag{4.12}$$

where ${}_aJ_t^{\nu}$ represents the fractional integral operation of $\nu\in\mathbb{R}^+$, and the Riemann-Liouville derivative of degree $\nu>0$ can be obtained from (4.12):

$${}_aD_t^{\nu}f(t)=\frac{d^m}{dt^m}\frac{1}{\Gamma(m-\nu)}\int_a^t\frac{f(\tau)}{(t-\tau)^{\nu+1-m}}d\tau \tag{4.13}$$

where $m-1<\nu\le m$. It can be noted that the Riemann-Liouville derivative is defined as the left inverse of ${}_aJ_t^{\nu}$.

4.1.3.2 Grunwald-Letnikov fractional derivative

The fundamental definition of a continuous function $f(t)$ is defined as:

$$f'(t) = \lim_{\alpha \to 0} \frac{f(t+\alpha) - f(t)}{2} \tag{4.14}$$

Then, applying this definition twice, the second derivative can be found:

$$\begin{aligned} f''(t) &= \lim_{\alpha \to 0} \frac{f'(t) - f'(t-\alpha)}{\alpha} \\ &= \lim_{\alpha \to 0} \frac{1}{\alpha} \left(\frac{f(t) - f(t-\alpha)}{\alpha} - \frac{f(t-\alpha) - f(t-2\alpha)}{\alpha} \right) \\ &= \lim_{\alpha \to 0} \frac{f(t) - 2f(t-\alpha) + f(t-2\alpha)}{\alpha^2} \end{aligned} \tag{4.15}$$

The n^{th} degree derivative can be obtained by induction:

$$f^{(n)}(t) = \frac{d^n f}{dt^n} = \lim_{\alpha \to 0} \frac{1}{\alpha^n} \sum_{i=0}^{n} (-1)^i \binom{n}{i} f(t - i\alpha) \tag{4.16}$$

where

$$\binom{n}{i} = \frac{n(n-1)(n-2)\cdots(n-i+1)}{i!} \tag{4.17}$$

is the usual notation for the binomial coefficients.

To generate the formula for non-integer values of degree n, the standard factorial will be replaced by the Gamma function. In addition, when the upper limit t and lower limit a of differentiation are considered, the upper limit of the summation n will be replaced by $(t-a)/\alpha$. Thus, the Grunwald-Letnikov fractional derivative is:

$$ {}_aD_t^v f(t) = \lim_{\alpha \to 0} \frac{1}{\alpha^v} \sum_{i=0}^{\frac{t-a}{\alpha}} (-1)^i \frac{\Gamma(v+1)}{i!\Gamma(v-i+1)} f(t-i\alpha) \tag{4.18} $$

Next, the Grunwald-Letnikov derivative is considered for negative v. The notation $\binom{-n}{i}$ is defined as:

$$ \begin{aligned} \binom{-n}{i} &= \frac{-n(-n-1)(-n-2)(-n-3)\cdots(-n-i+1)}{i!} \\ &= (-1)^i \frac{n(n+1)(n+2)(n+3)\cdots(n+i-1)}{i!} \\ &= (-1)^i \frac{(n+i-1)!}{(n-1)!i!} \end{aligned} \tag{4.19} $$

Rewriting the formula (4.19) using v and the Gamma function:

$$ \binom{-v}{i} = (-1)^i \frac{\Gamma(v+i)}{\Gamma(v)i!} \tag{4.20} $$

Therefore, the Grunwald-Letnikov fractional integral is:

$$ {}_aD_t^{-v} f(t) = \lim_{\alpha \to 0} \alpha^v \sum_{i=0}^{\frac{t-a}{\alpha}} \frac{\Gamma(v+i)}{i!\Gamma(v)} f(t-i\alpha) \tag{4.21} $$

4.1.3.3 Caputo fractional derivative

Two formulations of fractional derivative have been introduced in the above sections. It can be shown that the two definitions are equivalent. The mathematical proof of this equivalence can be found on [40].

However, the analysis of some new applications that exhibit

fractional-degree characteristics requires a revision of the well-established purely mathematical approach. For this purpose, a further definition of the fractional derivative was introduced by Caputo in 1967. This can be written as:

$$ {}_{a}^{C}D_{t}^{v} f(t) = \frac{1}{\Gamma(m-v)} \int_{a}^{t} \frac{f^{(m)}(\tau)}{(t-\tau)^{v+1-m}} d\tau \tag{4.22} $$

where $m-1 < v \le m$, m is a integer number.

The Caputo differential operator is a linear operator [43]:

$$ {}^{C}D^{v}(C_1 y_1(t) + C_2 y_2(t)) = {}^{C}D^{v} C_1 y_1(t) + {}^{C}D^{v} C_2 y_2(t) \tag{4.23} $$

and

$$ {}^{C}D^{v_1}\,{}^{C}D^{v_2} y(t) = {}^{C}D^{v_1+v_2} y(t) \tag{4.24} $$

4.2 Some methods for the design of fractional differentiators/integrators

Recently, many methods have been proposed for implementing an approximation of the digital fractional differentiator as an FIR or IIR filter. Chien-Cheng Tseng [42] gives the specification of an ideal linear phase v^{th} degree differentiator:

$$ H(e^{j\omega}) = (j\omega)^{v} e^{-jv\omega/2} \tag{4.25} $$

where v is the degree of the differentiator. If v is a fractional number, it is called a fractional degree differentiator design problem.

4.2.1 Design of a fractional differentiator using the Grunwald-Letnikov definition

The simplest and most straightforward method of designing the fractional differentiator is to use the Grunwald-Letnikov definition directly. To obtain an FIR filter approximation of this operator (4.18) is truncated from an infinite series to a finite number of terms. Thus, the transfer function of the FD can be rewritten as:

$$H_{GL}(z) = \sum_{i=0}^{N} (-1)^i \frac{\Gamma(v+1)}{i!\Gamma(v-i+1)} z^{-i} \tag{4.26}$$

where N is the order of the FIR filter.

4.2.2 Design of fractional differentiator using the Riemann-Liouville definition

A numerical algorithm for computing Riemann-Liouville integrals is introduced in [43], [44]. This method is based on a product trapezoidal rule which was developed by Odibat in [45]. Rewriting the formula as a digital filter with finite memory length, for $0 < v < 2$, with T as the sample period, the transfer function is:

$$H_{RL} = \frac{T^v}{\Gamma(2+v)} \sum_{i=0}^{N} h(i) z^{-i} \tag{4.27}$$

where $h(i) = \begin{cases} (1+v)N^{v} - N^{1+v} + (N-1)^{1+v} & \text{if} \quad i = 0, \\ (N-i+1)^{1+v} - 2(N-i)^{1+v} + (N-i-1)^{1+v} & \text{if} \quad 0 < i < N, \\ 1 & \text{if} \quad i = N. \end{cases}$

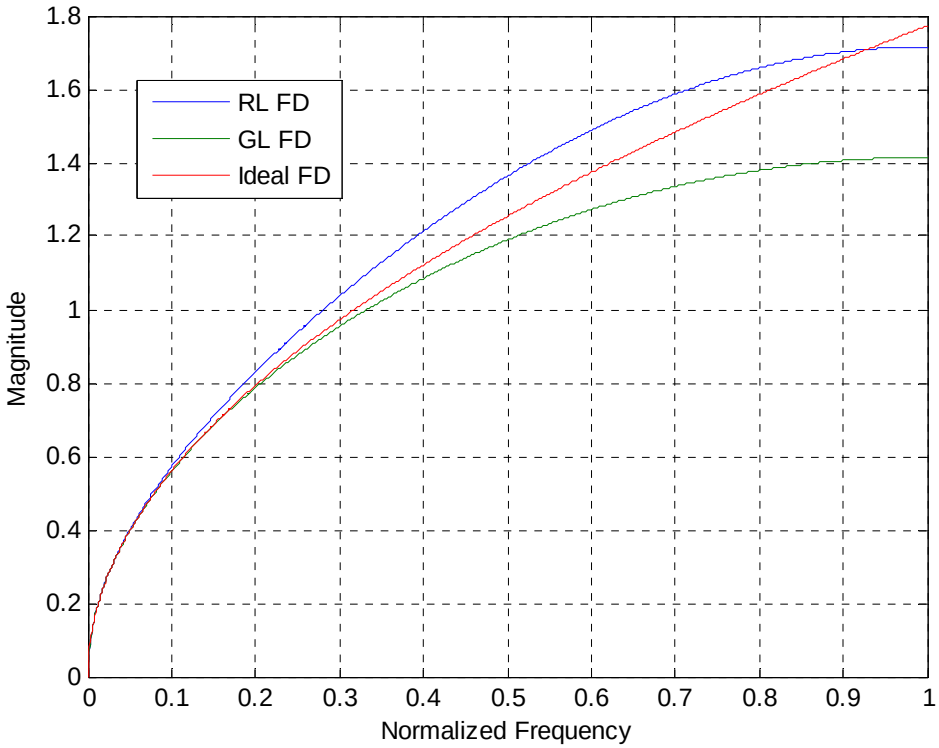

Figure 4.2 *Magnitude response of the Riemann-Liouville-based and Grunwald-Letnikov-based differentiators.*

Figure 4.2 shows the magnitude response of the fractional differentiators of degree $v = 0.5$, based on (4.26) and (4.27). The magnitude response of an ideal fractional degree differentiator is based on (4.25). The two differentiators under consideration have good magnitude response at very low frequency, but the performances at high frequency are not satisfactory, because these methods are based on the Newton-Cotes numerical integration rules. Thus, it is necessary to reduce the approximation error in the high frequency range.

4.2.3 Design of fractional differentiator using a discretization scheme

The Laplace transform of the Riemann-Liouville derivative for degree $0 \le v \le 1$, as given by [34]:

$$L\left\{ {}_0D_t^{\pm v}(t) \right\} = s^{\pm v}F(s) \tag{4.28}$$

The digital fractional differentiator is the discrete equivalent of the continuous operator s^v, which can be expressed by the generating function $s \equiv \omega(z^{-1})$. The most common methods of the discretization of the continuous operator s^v, are the Newton-Cotes integration rules (e.g. Euler rule, Trapezoid rule, or Al-Alaoui rule). A tunable generating function is given in [46][47]:

$$H(z) = \left(\frac{1}{\psi T} \frac{1 - z^{-1}}{\gamma + (1-\gamma)z^{-1}} \right)^v \tag{4.29}$$

where ψ and γ denote the gain and phase tuning parameters, respectively, and T is the sample period. In general, the Power Series Expansion (PSE) [48][49] are one of the most common ways to expand the generating function. For example, using the backward Euler rule, $H(z^{-1}) = (1 - z^{-1})/T$, and performing a PSE of $((1 - z^{-1})/T)^v$, the result is:

$$
\begin{aligned}
D^{\nu}(z) &= \left(\frac{1}{T}\right)^{\nu} \mathrm{PSE}\left\{\left(1-z^{-1}\right)^{\nu}\right\}_N \\
&= \left(\frac{1}{T}\right)^{\nu} P_N(z^{-1}) \\
&= \left(\frac{1}{T}\right)^{\nu} \left(h(0)+h(1)z^{-1}+\cdots h(N)z^{-N}\right),
\end{aligned}
\tag{4.30}
$$

where P is a polynomial of order N, $h(k)$, ($k=0,1\cdots$) are the coefficients of the FIR implementation, and

$$
h(k) = \begin{cases} 1 & \text{if} \quad k=0, \\ \left(1-\dfrac{1+\nu}{i}\right)h(k-1) & \text{if} \quad k=1,2,\cdots \end{cases}
\tag{4.31}
$$

The discretization formulae (4.30) and (4.31) correspond to the Grunwald-Letnikov definition (4.26).

In [50], a method is described for obtaining the impulse response of a digital fractional-degree differentiator. The discretized formula $H^{\nu}(z^{-1})$ can be written by taking the PSE of the function $(1-z^{-1})^{\nu}$ in (4.30) and (4.31) in the form:

$$
\begin{aligned}
H(z^{-1}) &= \left(\frac{1}{\psi T}\frac{1-z^{-1}}{\gamma+(1-\gamma)z^{-1}}\right)^{\nu} \\
&= \left(\frac{1}{\psi T}\right)^{\nu}\left(1-z^{-1}\right)^{\nu}\left(\gamma+(1-\gamma)z^{-1}\right)^{-\nu} \\
&= \sum_{k=0}^{\infty} h(k)z^{-k},
\end{aligned}
\tag{4.32}
$$

where the impulse response sequence $h^{\nu}(k)$ can be shown to be $(k \geq 0)$:

$$
h(k) = \left(\frac{1}{\psi T}\right)^{\nu} \sum_{i=0}^{k} \gamma^{-(\nu+k-i)}(1-\gamma)^{k-i} \times \binom{i-\nu-1}{i}\binom{-\nu}{k-i}
\tag{4.33}
$$

Table 4.1 shows the $s \to z$ transforms and impulse response sequences of

some of the most commonly used discretization schemes (i.e. the Euler, the Al-Alaoui and the Tustin operaters). These were computed from equation (4.32) (4.33), and by considering variations of the tuning parameter, i.e. when $\psi = 1$ and $\gamma \in [1, 7/8, 1/2]$,

Table 4.1. $s \to z$ transform and impulse response sequence of Euler, Al-Alaoui and Tustin operators

Method	$s \to z$	$h(k)$
Euler $(\gamma = 1)$	$s^{\nu} \approx \left(\frac{1}{T} \frac{1 - z^{-1}}{z^{-1}} \right)^{\nu}$	$\left(\frac{1}{T} \right)^{\nu} \binom{k - \nu - 1}{k}$
Al-Alaoui $(\gamma = \frac{7}{8})$	$s^{\nu} \approx \left(\frac{8}{7T} \frac{1 - z^{-1}}{1 - z^{-1}/7} \right)^{\nu}$	$\left(\frac{8}{7T} \right)^{\nu} \sum_{i=0}^{k} \left(\frac{1}{7} \right)^{k-i} \binom{i - \nu - 1}{i} \binom{-\nu}{k - i}$
Tustin $(\gamma = \frac{1}{2})$	$s^{\nu} \approx \left(\frac{2}{T} \frac{1 - z^{-1}}{1 + z^{-1}} \right)^{\nu}$	$\left(\frac{2}{T} \right)^{\nu} \sum_{i=0}^{k} \binom{i - \nu - 1}{i} \binom{-\nu}{k - i}$

Note that the fractional differentiators obtained using this method lead to an impulse response sequence of infinite length. Therefore, an N^{th} order FIR filter approximation implementation can be obtained by as $k = N$. For example, the filter coefficients of the fractional-degree differentiators of order $N = 150$ based on Euler, Al-Alaoui and Tustin methods can be obtained from Table 4.1. Figure 4.3 shows the magnitude response of the corresponding fractional differentiators. However, only Euler's method exhibits good results at low frequency; the other differentiators show large error in all frequency ranges. In

addition, the differentiators are not linear phase filters, as the filter coefficients are not symmetrical. Figure 4.4 illustrates the group delay of the fractional degree FIR differentiators designed by Euler's method, which shows big variations in steady-state at slightly differing input frequencies, in the low-frequency range.

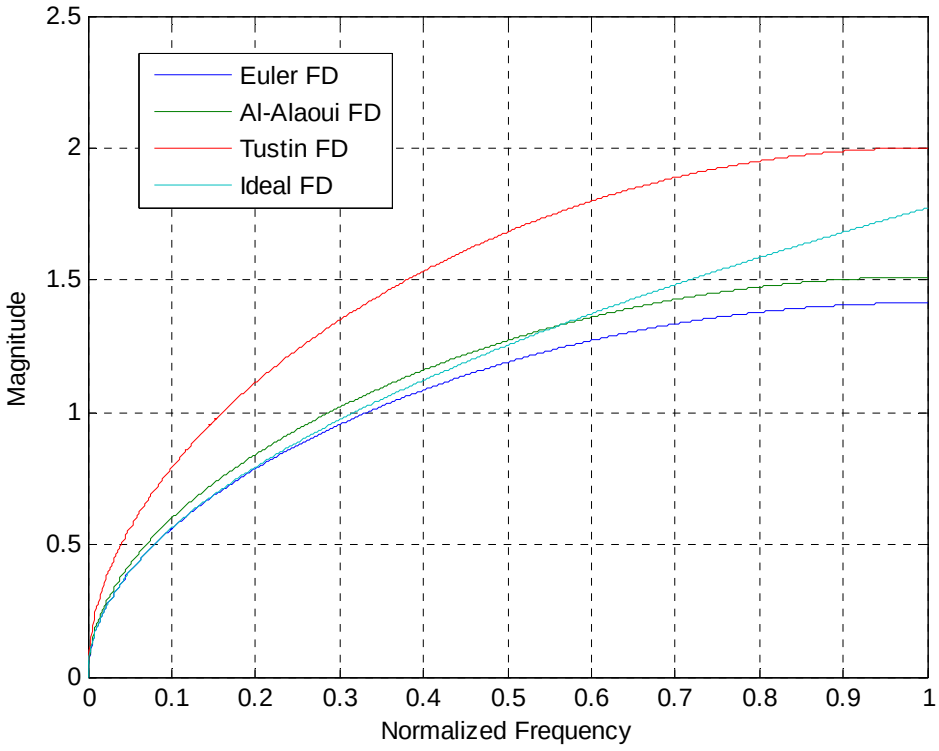

Figure 4.3 *Magnitude response of the fractional degree FIR differentiators designed by Euler's method, Al-Alaoui's method, and Tustin's method.*

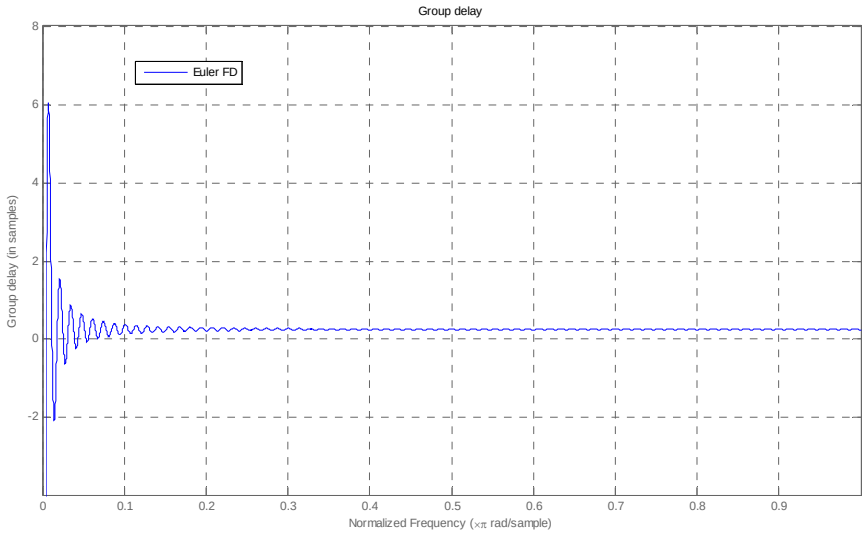

Figure 4.4 *Group delay of the fractional degree FIR differentiators designed by Euler's method.*

4.2.4 Design of IIR approximations to fractional differentiators

Some least-squares methods have been used to obtain an IIR fractional differentiator from a FIR filter. These methods, such as the Padé approximation, Prony's method, and Shanks' method, are introduced and described in [50] [53]. In this section, Prony's method is applied to design IIR fractional differentiators.

Assuming that the desired FIR filter coefficients $h(k)$ can be obtained from Table 4.1, the transfer function of an IIR filter $H(z)$, to be designed, has the form of an IIR filter, shows at (1.2), where m is the order of the nominator, and n the order of the denominator, $m \leq n$. The denominator coefficients vector $\mathbf{a}$ can be obtained by solving the following linear equation:

$$\begin{bmatrix} h^{\nu}(m) & h^{\nu}(m-1) & \cdots & h^{\nu}(m-n+1) \\ h^{\nu}(m+1) & h^{\nu}(m) & \cdots & h^{\nu}(m-n+2) \\ \vdots & \vdots & \ddots & \vdots \\ h^{\nu}(N-2) & h^{\nu}(N-3) & \cdots & h^{\nu}(N-n-1) \end{bmatrix} \times \begin{bmatrix} a_1 \\ a_2 \\ \vdots \\ a_n \end{bmatrix} = - \begin{bmatrix} h^{\nu}(m+1) \\ h^{\nu}(m+2) \\ \vdots \\ h^{\nu}(N-1) \end{bmatrix} \quad (4.34)$$

As described in [50], and elsewhere, (4.34) can be routinely solved using a pseudoinverse-based method to produce the optimum vector (in terms of least-squared error) of the denominator coefficients $\mathbf{a} = \left[a_1, a_2, \cdots, a_n\right]^T$. Then, the numerator coefficients, $\mathbf{b}$, can be found as [50]:

$$\mathbf{b} = h^{\nu}(k) + \sum_{i=1}^{n} a_l h^{\nu}(k-i) \quad 0 \le k \le m \quad (4.35)$$

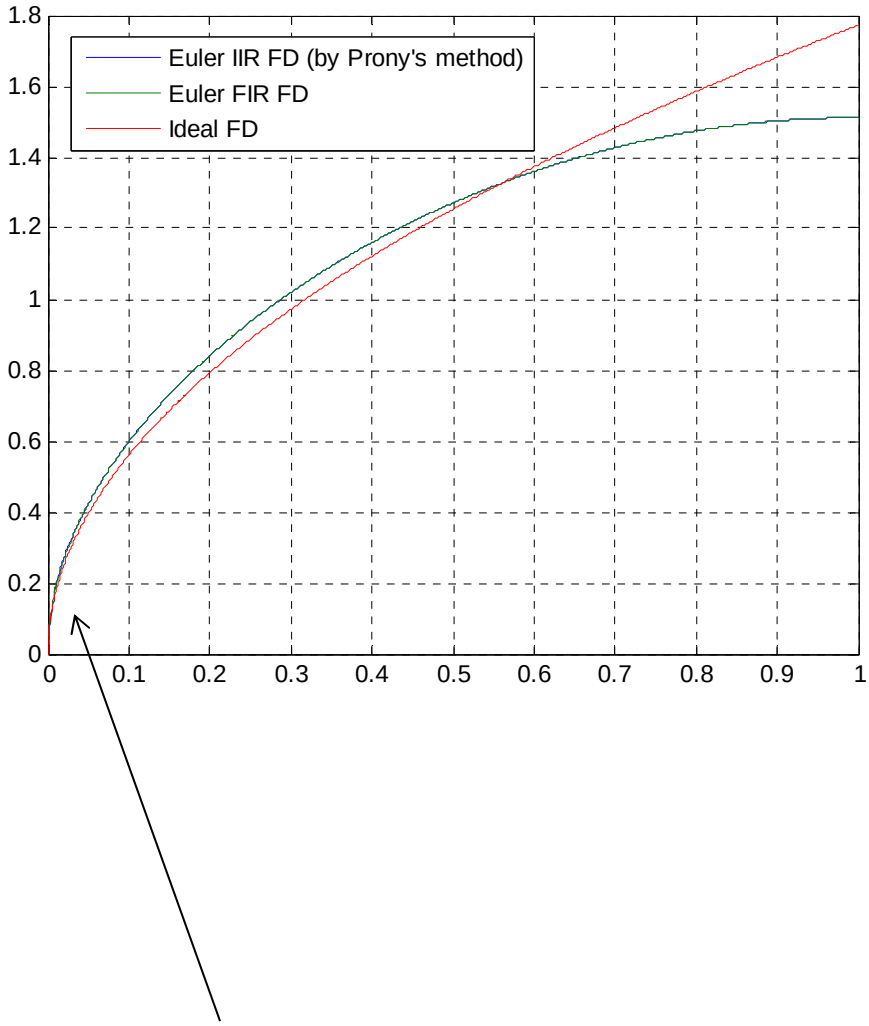

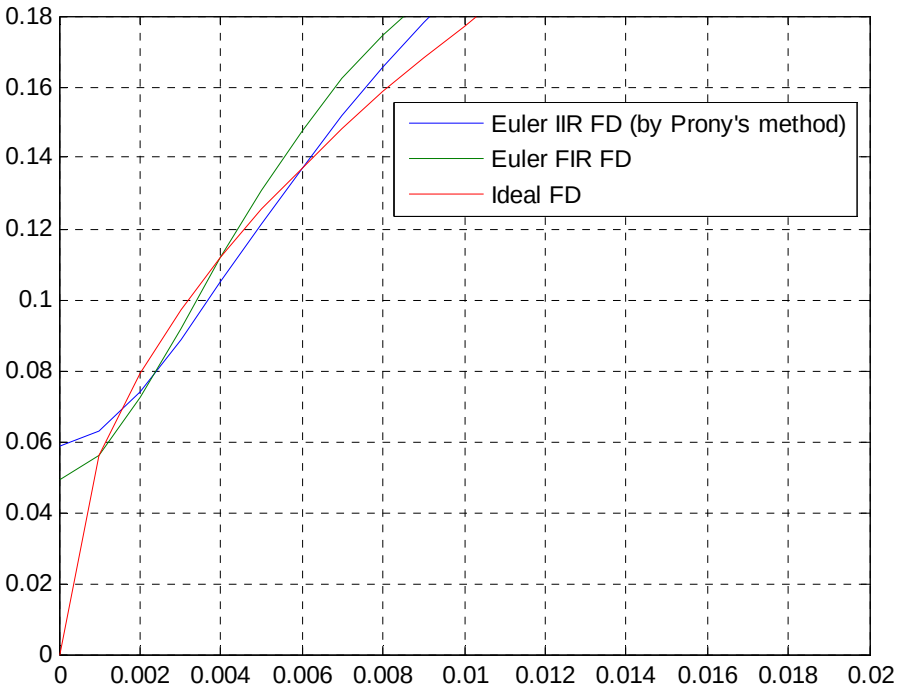

Figure 4.5 *Magnitude response of the fractional degree Euler IIR differentiator (FIR-to-IIR transformation using Prony's method) and Euler FIR differentiator.*

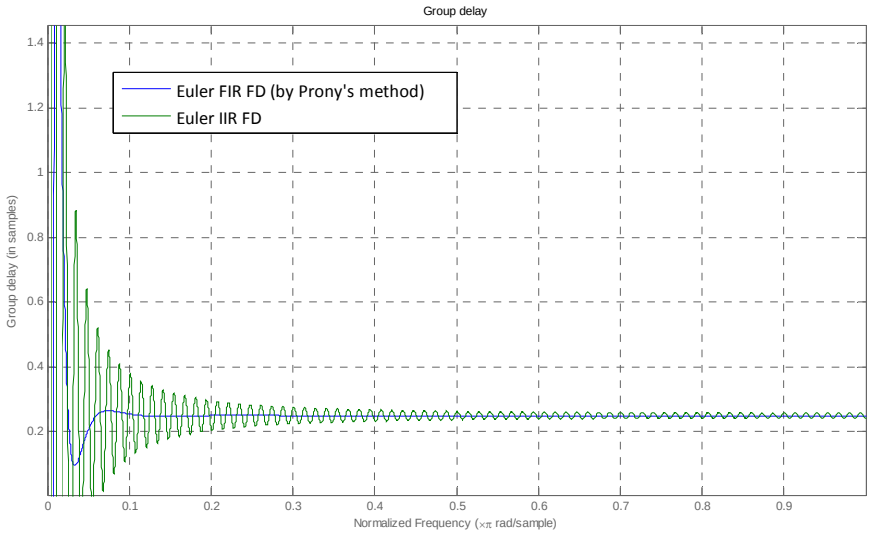

Figure 4.6 *Magnitude response of the fractional degree Euler IIR*

differentiators (FIR-to-IIR transformation using Prony's method) and Euler FIR differentiator.

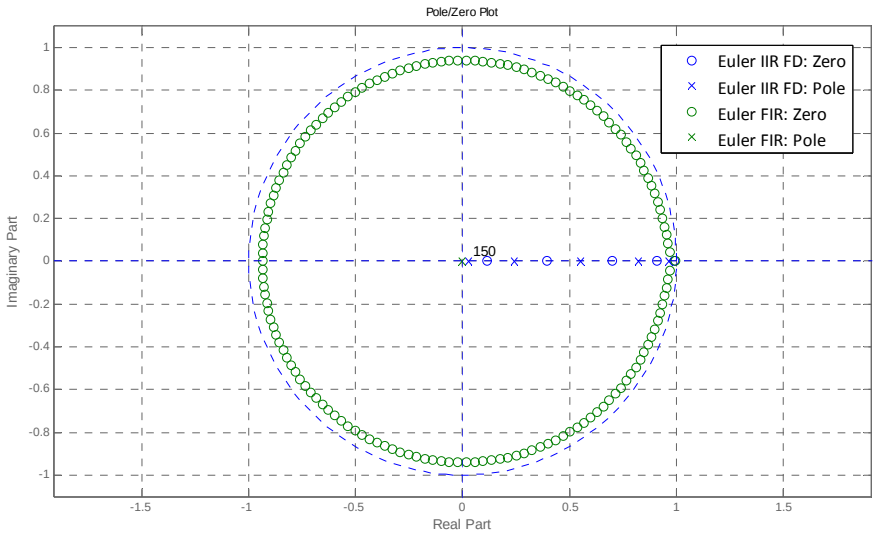

Figure 4.7 *Pole/zero Plot of the fractional degree Euler IIR differentiator (FIR-to-IIR transformation using Prony's method) and Euler FIR differentiator.*

Plots associated with two fractional-degree, Euler-based differentiators (one FIR and one IIR) is shown in Figure 4.5 to Figure 4.7. The IIR fractional differentiator has a very good match to the desired FIR fractional differentiator, and the tiny error in the very-low-frequency-range is acceptable. The group delay of the IIR fractional differentiator has less variation due to differing input frequencies and is more stable than that of the FIR implementation, as is illustrated by Figure 4.6. It is also clear from consideration of the pole/zero plot (Figure 4.7) that all the poles are located inside the unit circle to ensure the system's stability, though one pole is very close to the unit circle.

4.3 Modified design of fractional degree differentiators

In this section, a new fractional–degree differentiator is designed, based on a feedback system. In [54], the use is presented of a feedback-based structure which permits the implementation of an accurate, stable estimate of a Caputo fractional differentiator, with automatic initialization, due to the fact that the feedback drives the system error toward zero after a short transient, irrespective of initial conditions.

The fractional integrator operator J^{v} and the fractional differentiator operator D^{v} of order $v \in R^{+}$ are now considered. It should be noted that D^{v} is the left-inverse of the corresponding integral operator J^{v}, so that it satisfies the following ideal relationship:

$$D^{v} J^{v} = I \tag{4.36}$$

A fractional differentiator $H_D(z)$, with degree v, and an fractional integrator $H_J(z)$ are designed. It is assumed that the input is $X(z)$, the ideal fractional order derivative of the input is $Y(z)$, and that a feedback system is created as in Figure 4.8. (Note that the fractional differentiator and fractional integrator designed in Section 4.2, would be suitable examples for use as $H_D(z)$ and $H_J(z)$).

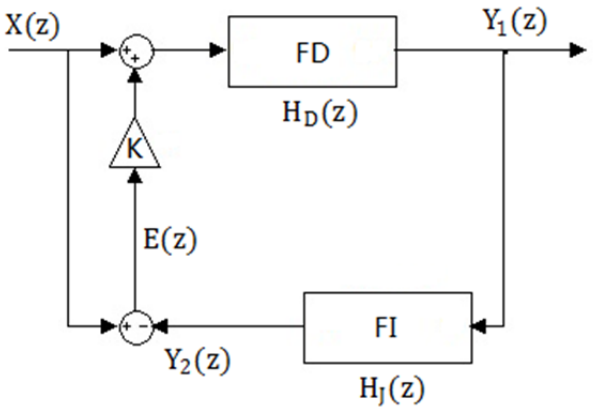

Figure 4.8 *Fractional order differentiator structure with added feedback.*

Because the fractional order differentiator and integrator are connected in cascade,

$$Y_1(z) \approx D^v(X(z)) \tag{4.37}$$

and

$$Y_2(z) \approx J^v(Y_1(z)) \approx J^v(D^v(X(z))) \approx X(z) \tag{4.38}$$

Therefore, $Y_1(z)$ is the approximation of the ideal fractional order derivative, and $Y_2(z)$ should approximate the input $X(z)$. The feedback system is designed to reduce the error, $E(z)$. Assuming that the transfer function of the fractional differentiator and fractional integrator, respectively, are:

$$H_D(z) = \frac{N_1(z)}{D_1(z)} \tag{4.39}$$

and

$$H_J(z) = \frac{N_2(z)}{D_2(z)} \tag{4.40}$$

The output of the system is:

$$\begin{aligned} Y_1 &= (1+K)\frac{H_D(z)}{1+KH_D(z)H_J(z)} \\ &= (1+K)\frac{N_1(z)D_2(z)}{D_1(z)D_2(z)+KN_1(z)N_2(z)} \end{aligned} \tag{4.41}$$

The speed of convergence clearly depends on the proportional gain K. The limiting characteristics of the closed-loop system correspond to those of standard feedback systems:

$$Y_1(z) = \frac{N_1(z)}{D_1(z)} = H_d(z), \quad K \to 0 \tag{4.42}$$

$$Y_2(z) = \frac{N_2(z)}{D_2(z)} = H_j(z), \quad K \to \infty \tag{4.43}$$

so that when $K \to 0$, the system corresponds to an open-loop system with the same performance as the fractional differentiator $H_d(z)$. Clearly, the type of differentiator/ integrator and the feedback gain, K, must be selected according to both desired frequency-domain and time-domain performances.

The design method can be described by the following sequence of steps:

1) Design FIR fractional-degree differentiators and integrators. Some methods are described in Section 4.2.1, 4.2.2 and 4.2.3.

2) Transform the resulting FIR fractional-degree differentiators and integrators to IIR filters.

3) Implement the feedback system using equation (4.41).

Two examples are given to shown the performance of the closed-loop system. Three fractional differentiators of degree $v = 0.5$ were designed using the feedback system of (4.41), and sample period $T = 1\,s$, with the order of the FIR filter being $N = 150$, and the order of IIR filter being defined by $m = n = 5$. The coefficients of the FIR fractional-degree differentiators are obtained from (4.33), Table 4.1 and (4.27), then transform from FIR filter to an IIR filter using Prony's method (4.35).

The first examples are constructed by an IIR Euler fractional differentiator and IIR Riemann-Liouville fractional integrator with different values of proportional gain K. For cases (a) $K = 0.1$, (b) $K = 0.3$, and (c) $K = 2$. The corresponding magnitude responses are shown in Figure 4.9.

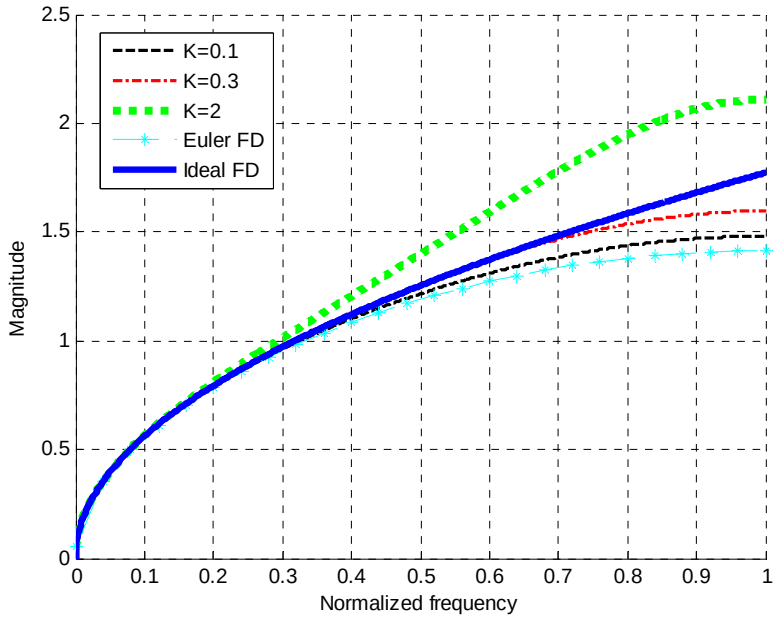

Figure 4.9 *Magnitude response of the feedback systems constructed by an Euler FD and RL FI with different proportional gains,* K.

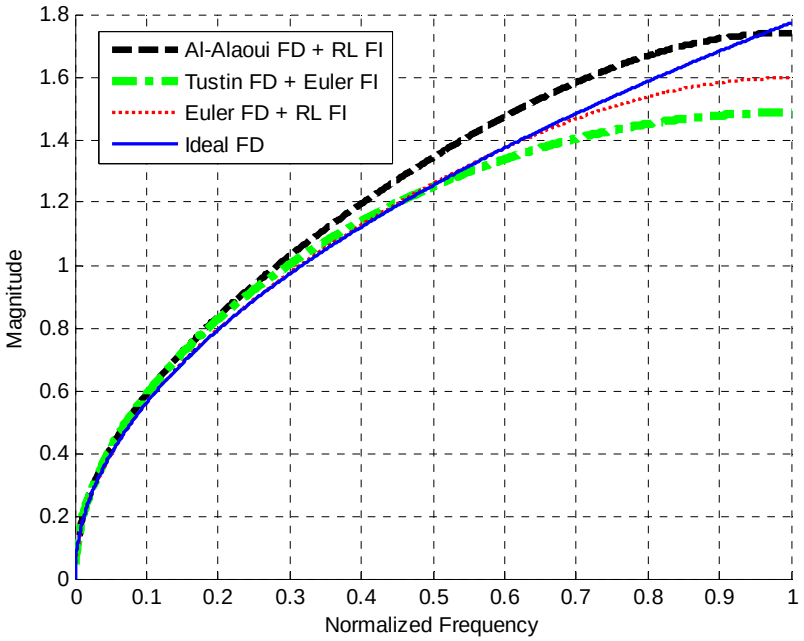

Figure 4.10 *Magnitude response of the feedback systems constructed with different fractional differentiators and fractional integrators.*

The second examples of the FD are constructed as: a) Al-Alaoui fractional differentiator and Riemann-Liouville fractional integrator with $K = 0.4$ b) Tustin FD and Euler FI, with $K = 5$; c) Euler fractional differentiator and Riemann-Liouville fractional integrator with $K = 0.3$; (see Figure 4.10).

Note that the gains chosen in each case were found experimentally to yield the best performance. In order to apply the two filters, $H_D(z)$ and $H_J(z)$, in feedback systems, they are both transformed from FIR filters to IIR filters, using Prony's method, i.e. using (4.34) and (4.35).

Table 4.2. *Coefficients of the proposed fractional differentiator (constructed from an Euler fractional differentiator and Riemann-Liouville fractional integrator with* $K = 0.3$*)*

Numerator **b**		Denominator **a**	
$b(0) = 1.0606$	$b(6) = 6.0842$	$a(0) = 1.0000$	$a(6) = 2.2568$
$b(1) = -6.5215$	$b(7) = -1.4923$	$a(1) = -5.5882$	$a(7) = -0.3743$
$b(2) = 17.4250$	$b(8) = 0.2098$	$a(2) = 13.3879$	$a(8) = 0.0233$
$b(3) = -26.4796$	$b(9) = -0.0144$	$a(3) = -17.9144$	$a(9) = 0.0010$
$b(4) = 25.1405$	$b(10) = 0.0003$	$a(4) = 14.5993$	$a(10) = -0.0001$
$b(5) = -15.4126$		$a(5) = -7.3913$	

The very low d.c. gain (0.0523), obtained by setting $z = 1$ is consistent with a differentiator characteristic. This, along with the pole positions indicates a differentiator-like operator.

As expected, Figure 4.9 and Figure 4.10 show that the magnitude response performance of the fractional differentiators constructed by the feedback system is dependent on both the type of fractional differentiator/fractional integrator, and the proportional gain, K. The fractional differentiator with this feedback system is unconditionally stable when $K > 0$, because all the poles are inside the unit circle. For comparison, the plots also include some traces typical of the outputs of some traditional types of fractional differentiators. In particular, the case of the Euler fractional differentiator and Riemann-Liouville fractional integrator, with $K = 0.3$, exhibits the best magnitude response amongst these differentiators. Table 4.2 shows the coefficients of the proposed fractional differentiators, and Figure 4.11 is the associated pole/zero plot, which

exhibits that all the poles are located inside the unit circle, so that the feedback system is stable.

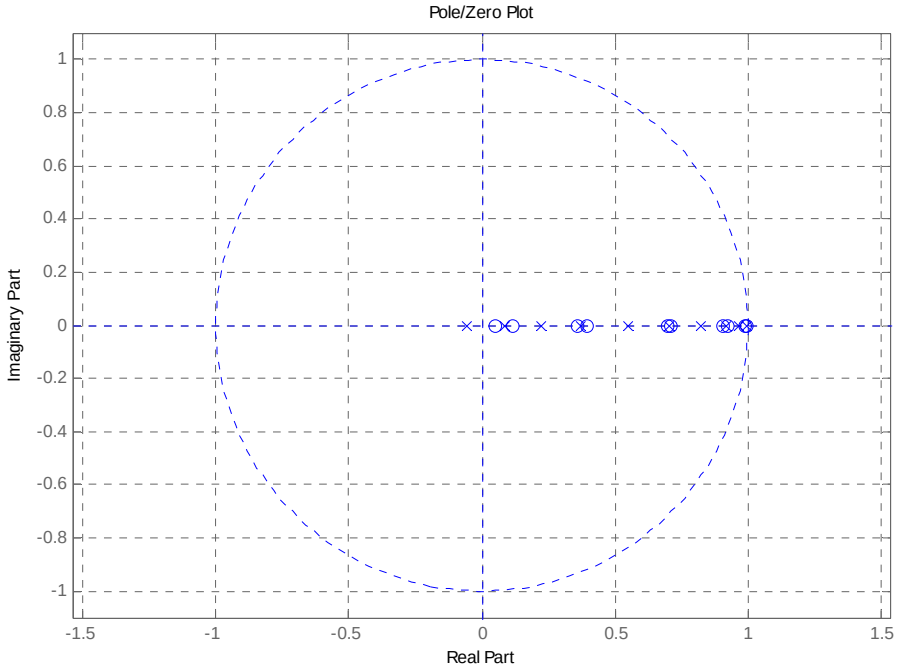

Figure 4.11 *Pole/zero Plot of the proposed fractional differentiator (constructed by an Euler fractional differentiator, and Riemann-Liouville fractional integrator).*

In order to test the differentiator performance in the time-domain, a sample period of $T = 0.01\,\mathrm{s}$ has been chosen. The fractional differentiators described above (i.e. constructed by an Euler fractional differentiators and an Riemann-Liouville fractional integrator with $K = 0.3$, and a standard Euler fractional differentiator (without feedback), are used. A standard time-domain function $x(t) = t^p \ (t > 0)$ is used as the input. Choosing $p = 1.5$, the ideal output should be: $y(t) = D^{0.5}(x(t)) = 1.3293\,t$.

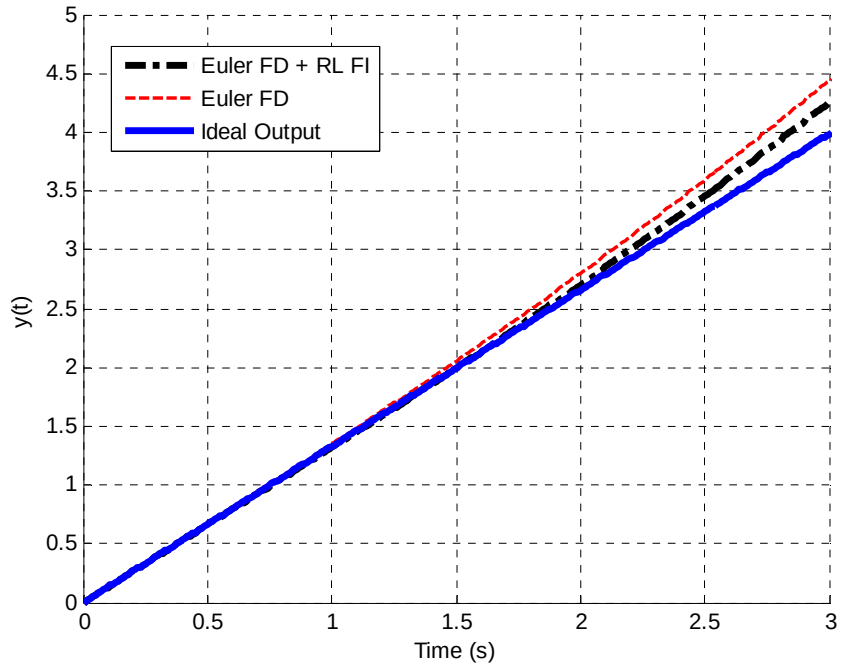

Figure 4.12 Fractional derivative of $x(t) = t^{1.5}$ for order $v = 0.5$.

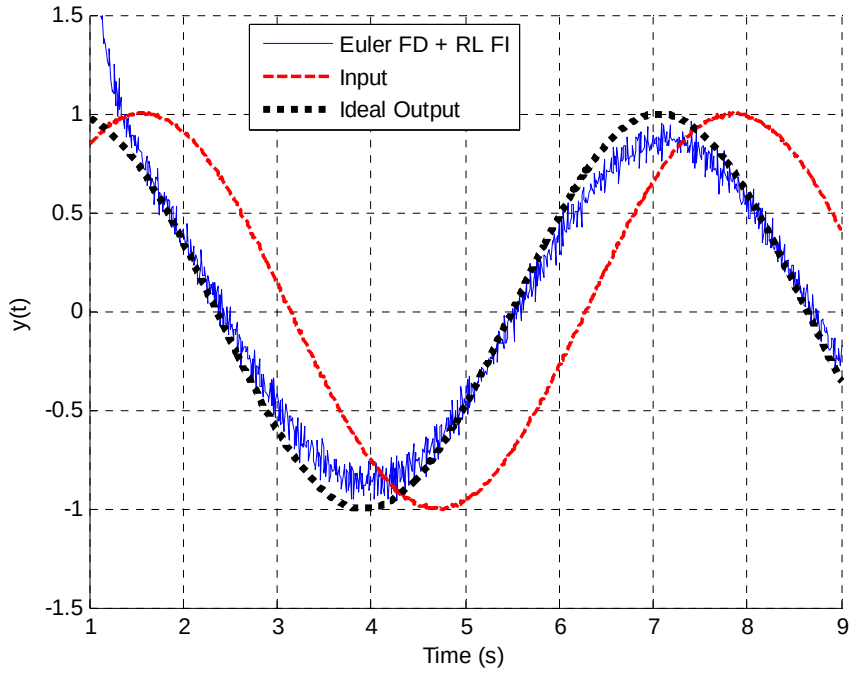

Figure 4.13 *Fractional derivative of* $y(t) = \sin(t)$ *with addition of white Gaussian noise* $(SNR = 45\,\mathrm{dB})$ *and order* $v = 0.5$.

As a further test, a sine wave with added white Gaussian noise defined by signal-to-noise ratio of $SNR = 45\text{db}$, is inputted to the differentiator. If the input sine function is $y(t) = \sin(t)$, $t > 1s$ and zero otherwise, the ideal fractional derivative, after initial transients have decayed, is:

$$D^{v}(y(t))\sin(t + v\frac{\pi}{2}) \tag{4.44}$$

Figure 4.12 and Figure 4.13 show the time-domain performance of the fractional differentiators constructed by the feedback system. When compared to a standard Euler fractional differentiator, the fractional differentiators constructed by the feedback system exhibit better performance in the time-domain (Figure 4.12), especially when $t > 1s$. Figure 4.13 shows that the system responds well to a noisy input (for which $SNR = 45\text{ dB}$), providing a good verification of the system's stability.

From the above example, the fractional differentiator constructed by an Euler fractional differentiator and an Riemann-Liouville fractional integrator, with a proportional controller $(K = 0.3)$, was shown to provide better magnitude response performance than standard fractional differentiators (i.e. Euler, Al-Alaoui and Tustin fractional differentiators).

It is noteworthy that many of the time-domain outputs of fractional differentiators presented in many journal and conference papers that consider the RL or GL definitions of fractional differentiators, as a means of illustrating the veracity of the implementation being proposed, would actually show huge disparities between actual and desired outputs if the plot have been extended over a longer time interval. An example was shown earlier in Figure 4.12, with significant error occurring when the time $t > 1.5\text{s}$ (about 150 samples) for a 150th order FIR fractional differentiator. For this FIR fractional differentiator,

the output is a function only of the past 150 samples. The physical fractional degree system is known to be a function of the initial value and derivatives, but these are not captured by the FIR approximation. For this example, when $t < 1.5\text{s}$, the FIR approximation is shown to lead to an output with little error due to the fact that it implicitly assumes zero initial conditions, but this assumption will lead to a large error when $t > 1.5\text{s}$.

A fractional differentiator can only be approximated by an FIR filter, as the output of the physical system will depend on the value and derivatives at the initial time, i.e. for a particular waveform to be processed by a fractional differentiator, a different initial (start) time will cause a different output waveform.

To research this topic, a function $f(t) = (t-1)^{1.5} \quad t = 1:6$ second, is given as the input, but with different lower limits $a_1 = 1$ and $a_2 = 3$. The fractional derivative with fractional degree $v = 0.5$ of the input is obtained using the Grunwald-Letnikov definition (4.21) directly. The result on Figure 4.14 illustrates, (as expected) that the fractional derivatives are different when the lower limit, or initial conditions, are different.

In [40], the Grunwald-Letnikov fractional derivative ${}_aD_t^v f(t)$ of the power function $f(t) = (t-a)^p$, where p is a real function, is given by the formula:

$$ {}_aD_t^v (t-a)^p = \frac{\Gamma(p+1)}{\Gamma(-v+p+1)} (t-a)^{p-v} \tag{4.45} $$

where $(v < 0,\ p > -1)$ or $(0 < m \le v \le m+1, \quad p > m)$, and m is an integer number. It can be found from (4.45) that the required lower limit is a for the

Grunwald-Letnikov fractional derivative for the input power function $f(t)=(t-a)^p$. Therefore, for the given function $f(t)=(t-1)^{1.5}$ presented above, the output with lower limit $a_1=1$ gives the correct Grunwald-Letnikov fractional derivative.

When the fractional derivative is obtained using an FIR fractional differentiator, the effective lower limit a will change with time. Therefore, huge disparities tend to occur between the actual and desired outputs when the plot is extended over a longer time interval. One can conclude that great care must be taken when utilizing time-domain traces to illustrate the veracity of a fractional-degree system, and the effects of the signal and its derivatives must be considered carefully.

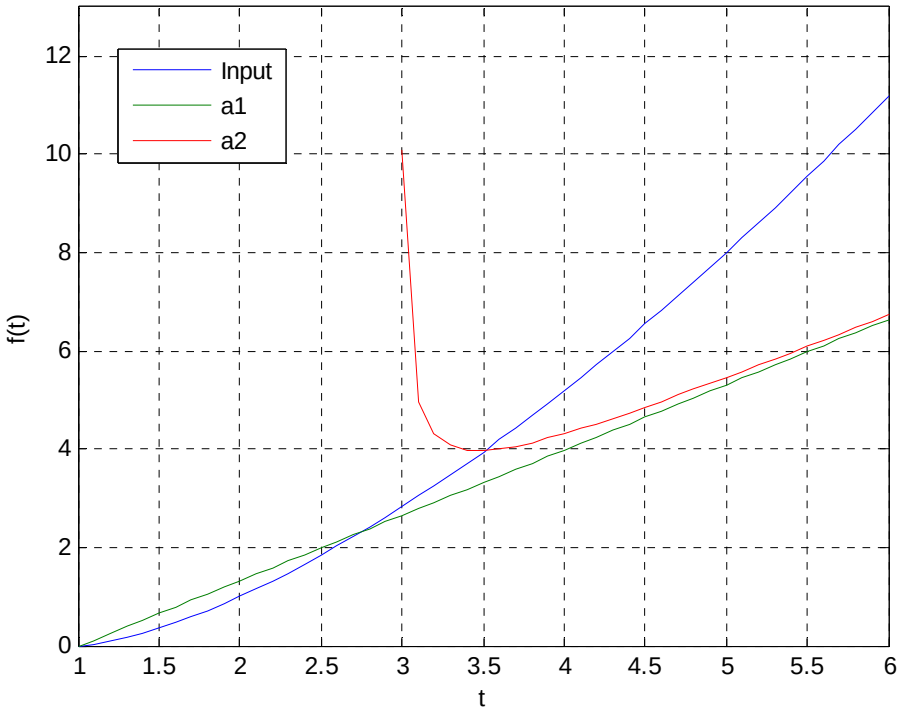

Figure 4.14 *Inputs and outputs for fractional derivative of degree* $v=0.5$ *for different lower limit when using the* Grunwald-Letnikov *definition.*

4.4 Discussion on Caputo fractional degree differentiators, and future work

In many practical applications, such as in solid mechanics, rheology, and those relating to viscoelasticity, mathematical modeling naturally leads to differential equations of fractional degree, and these involve the formulation of initial conditions to such equations. The utilization of physically interpretable initial conditions is required by some applied problems [40]. The initial conditions of Riemann-Liouville fractional derivatives only contain the limit values at the lower terminal $t = a$, for example

$$\begin{aligned} &\lim_{t\to a} {}_aD_t^{\nu-1} f(t) = k_1, \\ &\lim_{t\to a} {}_aD_t^{\nu-2} f(t) = k_2, \\ &\cdots \\ &\lim_{t\to a} {}_aD_t^{\nu-n} f(t) = k_n \end{aligned} \tag{4.46}$$

where k_i, $i = 1, 2, \cdots n$ are given constants. Though the initial value problem can be solved mathematically, the solutions are practically useless, because when a real physical application is considered, the physical meaning of such fractional derivatives can be unknown, or very difficult to estimate [30].

The Laplace transform formula for the Caputo definition, with a limit of $a = 0$, is given by [40]:

$$L\left\{ {}_0^C D_t^{\nu}(t) \right\} = s^{\nu} F(s) - \sum_{k=0}^{m-1} s^{\nu-k-1} f^{(k)}(0) \tag{4.47}$$

where $m - 1 < \nu \le m$. The Laplace transform of the Riemann-Liouville derivative is:

$$L\left\{{}_0D_t^{v}(t)\right\} = s^{v}F(s) - \sum_{k=0}^{m-1} s^{k}\,{}_0D_t^{v-k-1} f(t)\big|_{t=0} \tag{4.48}$$

where $m-1 < v \le m$. The main advantage of the Caputo derivative is that only the initial conditions: $f(0)$, $f^{'}(0), \cdots$, $f^{(m-1)}(0)$, i.e. the initial value of the function value itself and its integer-degree derivatives, have to be specified. Conversely, for the Riemann-Liouville derivative, the values of certain fractional derivatives at the initial point $t = 0$ need to be specified.

Another significant difference between the Riemann-Liouville and Caputo definitions is that, for a constant input (for example of magnitude K_c), the output of the Caputo definition is 0, unlike that of the Riemann-Liouville definition, for which

$${}_0D_t^{v}(K_c) = \frac{K_c t^{-v}}{\Gamma(1-v)} \tag{4.49}$$

As an example, let $f(t) = 3$ as the input function, the output being shown in Figure 4.15. The output corresponding to the Riemann-Liouville definition is calculated as $y(t) = 1.6926t^{-0.5}$. It is noteworthy that, taking the lower terminal $a \to -\infty$ for both Riemann-Liouville definition and Caputo definition, the two definition are the same [40]. It means that for the study of steady state dynamical processes, the two definitions must give the same results.

When designing fractional degree differentiators, it is clear that the outputs of differentiators based on the Riemann-Liouville definition and those based on the Caputo definition differentiator differ when the initial value of the input does not equal zero. It can be surmised that Caputo based fractional differentiators have better performance in time-domain of the reducing

transient effects, especially for a constant input signal and/or, more generally, when the initial value of the input differs from zero.

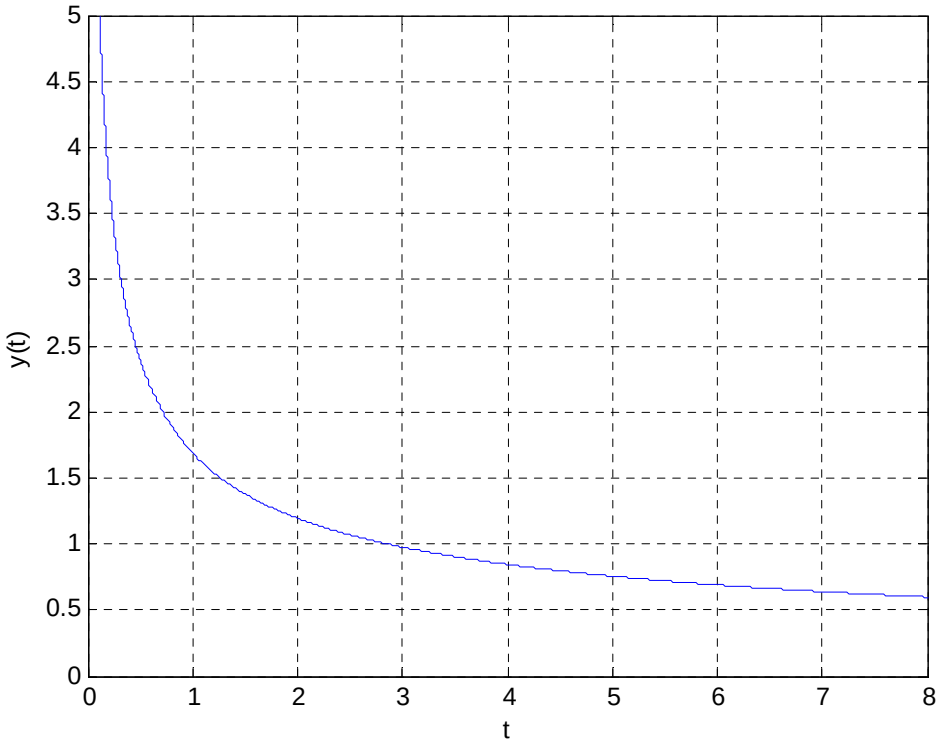

Figure 4.15 *Output of fractional derivative of degree 0.5 for a constant input, when using the Riemann-Liouville definition.*

In [55], the relationship between the Caputo fractional derivative and the Riemannn-Liouville fractional derivative is given by:

$$ {}_aD_t^v y(t) = {}_a^C D_t^v y(t) + \sum_{i=1}^{m-1} \frac{y^{(i)}(a)}{\Gamma(i-v+1)} (t-a)^{i-v} \qquad (4.50) $$

where $m-1 < v \le m$, and a is the initial value of the input function. In particular, for a the case of $0 < v < 1$, $m = 1$, this definition can be simplified to:

$$ {}_aD_t^{0.5}y(t) = {}_a^CD_t^{0.5}y(t) + \frac{y(a)}{\Gamma(-v+1)}(t-a)^{-0.5} \tag{4.51} $$

Therefore, a Caputo fractional differentiator can be designed as follows:

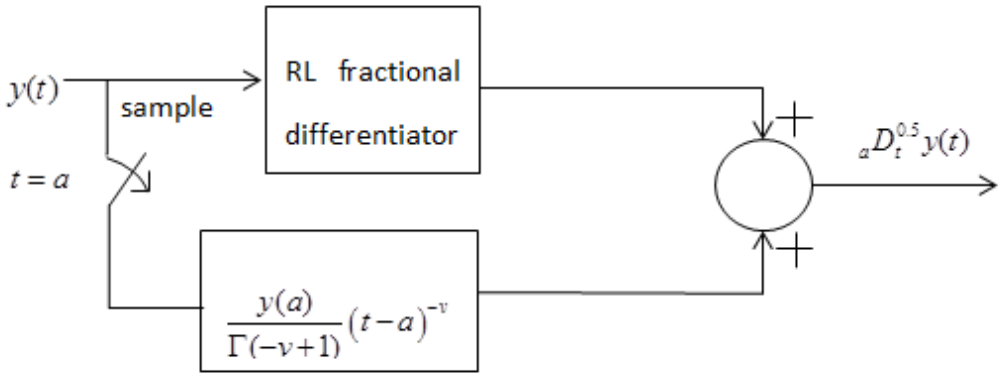

Figure 4.16 *Proposed Caputo fractional-degree differentiator structure.*

where the initial condition $y_{\text{int}}(t) = -\big(y(a)/\Gamma(-v+1)\big)(t-a)^{-v}$. To test the performance, a RL fractional differentiator of degree $v = 0.5$ bas been chosen from (4.27) with order $N = 150$. The RL fractional differentiator is tested to provide a comparison with the Caputo fractional differentiator. The ideal output is computed from the definition directly, in (4.22), with the lower limit of $a = 0$.

To illustrate the application of the Caputo fractional differentiator, its response to a number of typical inputs was considered:

$$ \begin{aligned} f_1(t) &= 3, \\ f_2(t) &= t^{1.5}, \\ f_3(t) &= t^{1.5} + 30, \\ f_4(t) &= \sin(0.5t) + 10, \end{aligned} $$

where $t = 0:150$.

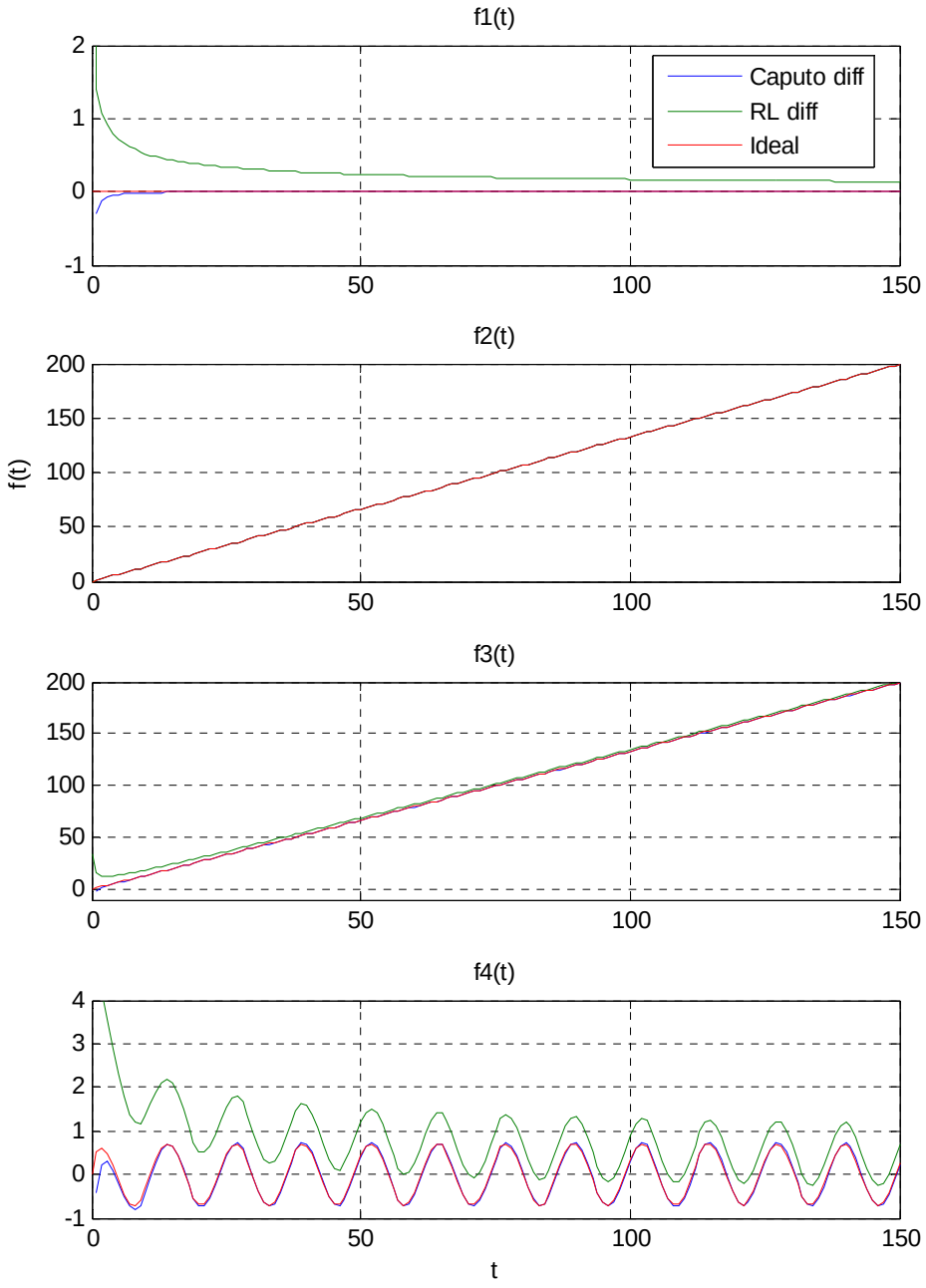

Figure 4.17 *Outputs of fractional derivative of degree* $v = 0.5$ *for different inputs when using the Caputo and Riemann-Liouville definitions.*

The outputs of fractional derivative of degree $v = 0.5$ are shown on Figure 4.17. As expected, the output of the Caputo differentiator for a constant $f_1(t)$ is zero, with a transient time of approximately 15 second. For the case of an input function $f_2(t) = t^{1.5}$, the output of the Caputo differentiator, RL differentiator, and ideal output expected when using the Caputo definition, are almost coincident, because, the initial condition term $y_{\text{int}}(t) = -\big(y(a)/\Gamma(-v+1)\big)(t-a)^{-v}$ of (4.51) is zero when the initial value of the input function, $f(0) = 0$. When the initial value is not zero, a d.c. component is added to the input function $f_3(t) = t^{1.5} + 30$. The Caputo differentiator exhibits almost ideal output, while an obvious difference can be found between the Caputo and RL differentiators. For the case of $f_4(t) = \sin(0.5t) + 10$, the situation is similar to that pertaining to $f_3(t)$, with a difference between the Caputo and RL differentiators, and a non-zero initial condition.

4.5 Conclusion

In this chapter, some concepts and definitions of fractional calculus have been reviewed, the Riemann-Liouville, Grunwald-Letnikov, and Caputo definitions were demonstrated.

As the fractional differentiators to be implemented are to be in the form of FIR or IIR filters, the transfer function and expansion techniques to develop such rational structures were also described, thereby illustrating some existing realizations of fractional differentiators, of the basic Riemann-Liouville-based and Grunwald-Letnikov based differentiators. It is shown that the magnitude response performance at high frequency is not satisfactory, under the above

definitions of the FD. The method of designing FIR fractional degree differentiators based on a Newton-Cotes numerical integration rules is introduced. Then, the transfer function with tuning parameter is given for computing the required filter coefficients. In addition, the FIR differentiators can be transformed to IIR differentiators by using some least-squares methods, such as the Padé approximation or Prony's method.

A new feedback system is constructed in this Chapter, to improve the fractional degree differentiator, both in the frequency-domain and time-domain. Specifically, it is shown that a Riemann-Liouville-based fractional differentiator can perform well in a feedback structure. A fractional differentiator constructed by an Euler fractional differentiator and RL fractional integrator in a feedback structure with a suitably gained proportional controller ($K = 0.3$ for the structure presented) was shown to provide better magnitude response performance than standard fractional differentiators (i.e. Euler, Al-Alaoui and Tustin FD fractional differentiators). The proposed structure shows an unconditionally stable characteristic for a positive proportional feedback constant, $K > 0$. This feedback system was constructed based on the standard Riemann-Liouville and Grunwald-Letnikov definitions, which can be designed and implemented easily.

Then, the Caputo fractional degree differentiator is designed that is based on the RL fractional degree differentiator. The proposed differentiator is obtained by cascading a function that models the behavior of the system at the initial condition to an RL fractional differentiator. Then, some time-domain tests were presented which show that the FIR Caputo fractional differentiator has the desired output, based on the Caputo definition.

A physical understanding of fractional differentiators and the FIR or IIR implementations of such systems has been a focus of research in recent years. In

this chapter some consideration is given to the limitations of some such systems. For example, the problem of huge disparities found between actual and desired outputs of a FIR fractional differentiator (using GL or RL definitions), if the output have been extended over a longer time interval, is discussed. The reason is that the effective initial conditions pertaining to the application of the FIR approximation (or an IIR filter that is based on the FIR sequence) of the differentiator changes as time increases.

Chapter 5 Applications of Digital Differentiators

There are many applications of digital differentiators. In this chapter, two important applications will be introduced. Specifically, the first of these involves the application of second degree differentiators in the estimation of the frequency components of a power system, while the second example concerns the application of fractional differentiators for image processing, edge detection applications.

5.1 Frequency estimation using second-degree differentiator

Good-quality frequency estimation of signals is pertinent to power system operation, control and protection. Therefore, algorithms to implement such estimation systems are frequently used. In [56], a novel algorithm for an IIR second-degree differentiator has been developed and implemented for on-line estimation of the fundamental frequency of non-sinusoidal signals. This method has a simple structure, wide range of application, and good robustness against sampling frequency variation. The authors point out that compared with other methods of frequency estimation (e.g. enhanced phase-locked-loop systems, as proposed by Karimi-Ghartemani and Iravani [57][58][59][60]), the only limitation of Karimi-Ghartemani and Iravani's proposed method is its slightly reduced accuracy (maximum error of approximately 3 mHz) under static sinusoidal conditions.

5.1.1 Review of second-degree IIR differentiator based algorithms

This section provides an overview of the second-degree IIR- differentiator-based algorithm for frequency estimation, as described in [56].

Let, $s(t)$ represent a continuously-measured non-sinusoidal signal:

$$s(t) = \sum_k S_{\max_k} \sin(2\pi kft + \alpha_k) + \xi(t) \tag{5.1}$$

where $\xi(t)$ represents zero-mean random noise, f is the fundamental frequency, and $S_{\max_k}$ and α_k are the peak value and phase angle of the k^{th} harmonic of the signal. A pre-filter was added to reduce the effect of harmonics and of additive noise. Therefore, the signal can be rewritten, approximately, as:

$$s_F(t) = S_{\max 1} \sin(2\pi kft + \alpha_F) + \xi_F(t) \tag{5.2}$$

where α_F and $\xi_F(t)$ are the new phase angle and noise of $s_F(t)$, respectively.

The second-degree differentiation of (5.1) is:

$$s_{FD}(t) = -4\pi^2 f^2 S_{\max 1} \sin(2\pi kft + \alpha_F) + \xi_{FD}(t) \tag{5.3}$$

where $\xi_{FD}(t)$ is the noise signal after second-degree differentiation.

If the waveform above is discretized with a finite number of significant harmonics (with maximum order M) at sampling frequency f_s, (5.1), (5.2) and (5.3) can be rewritten as:

$$s(n) = \sum_{k=1}^{M} S_{\max_k} \sin(2\pi kfn + \alpha_k) + \xi(n) \tag{5.4}$$

$$\begin{aligned} s_F(n) &= S_{\max 1} \sin(2\pi kfn + \alpha_F) + \xi_F(n) \\ &= s_{FT}(n) + \xi_F(n) \end{aligned} \tag{5.5}$$

$$\begin{aligned} s_{FD}(n) &= -4\pi^2 f^2 S_{\max 1} \sin(2\pi kfn + \alpha_F) + \xi_{FD}(n) \\ &= s_{FDT}(n) + \xi_{FD}(n) \end{aligned} \tag{5.6}$$

where

$$s_{FT}(n) = S_{\max 1} \sin(2\pi kfn + \alpha_F) \tag{5.7}$$

and

$$s_{FDT}(n) = -4\pi^2 f^2 S_{\max 1} \sin(2\pi kfn + \alpha_F) \tag{5.8}$$

$s_{FT}(n)$ and $s_{FDT}(n)$ are the true samples of $s_F(n)$ and $s_{FD}(n)$, respectively, showing the theoretically correct sinusoidal values. The discrete errors $\xi(n)$, $\xi_F(n)$ and $\xi_{FD}(n)$ correspond to the values of $\xi(t)$, $\xi_F(t)$, and $\xi_{FD}(t)$ at discrete time index n, with additional noise because of quantization.

Sarkar and Sengupta, [56], outline an algorithm that achieves fundamental frequency estimation:

$$f(n) = \frac{1}{2\pi} \sqrt{\frac{\sum_{j=0}^{A-1} \left| s_F(n-j) \left[-s_{FD}(n-j) \right] \right|}{\sum_{j=0}^{A-1} \left(s_F(n-j) \right)^2}} \tag{5.9}$$

where A is a constant that plays an important role in the accuracy and computational load associated with the proposed algorithm. The authors point out that the variation of estimation errors is a function of the variation of a

parameter A, which is cyclic in nature, and is a minimum when the number of samples per cycle is an integer. The corresponding value of A is defined as:

$$A(n) = \text{round}\left(\frac{f_s}{2f(n-1)}\right) \quad \text{to} \quad \text{the} \quad \text{nearest} \quad \text{integer} \qquad (5.10)$$

In the numerator of (5.9), the absolute value has been considered, in order to avoid any discrepancy because of slight phase angle error. The block diagram of the fundamental frequency estimation algorithm is shown in Figure 5.1.

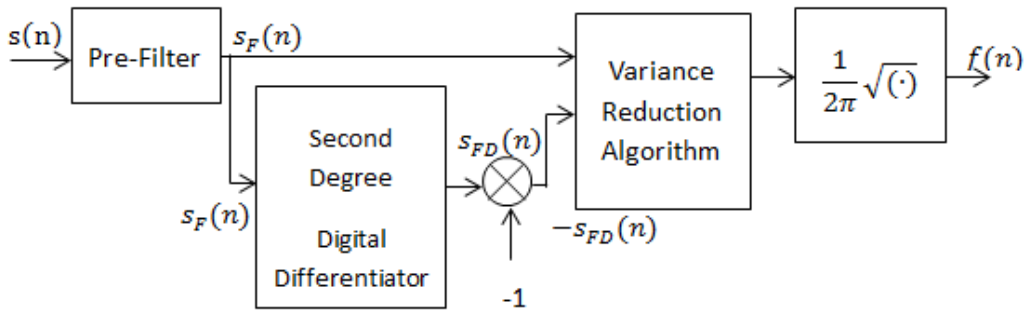

Figure 5.1 *Block diagram of the frequency estimation algorithm.*

The following elements are considered when designing the frequency estimator:

- The pre-filter utilizes a low-pass Chebychev-1, filter of order four, with a pass-band ripple of 0.001 dB, and a cut-off frequency of 50 Hz. A sample frequency 6.4 KHz is chosen.

- Use is made of the second-degree low-pass differentiator introduced in [11], for which the transfer function is:

$$H_{SDDD}(z) = \frac{1}{T_s^2} G \frac{(1-z^{-2})^2}{(1+r_2 z^{-1})^4} = \frac{3.72 - 7.44z^{-2} + 3.72z^{-4}}{1 + 3.8569z^{-1} + 5.5785z^{-2} + 3.586z^{-3} + 0.8644z^{-4}}$$

when $(G = 3.72 \quad r_2 = 0.9642358)$ and when it is assumed that $T_s = 1$

- The sample frequency is selected to be 6.4 *K*Hz. For a typical fundamental sinusoidal signal of frequency 50 Hz, this corresponds to :

$$A(n) = \frac{f_s}{2f(n-1)} = \frac{6400}{2 \times 50} = 64$$

A simulation of the algorithm is presented below. The results generated by the simulation are used to evaluate the performance of the system. In this test, sinusoidal signals with unity amplitude, and frequencies of 50 Hz, 51 Hz and 40 Hz, have been provided as inputs to the algorithms, as shown in Figure 5.2.

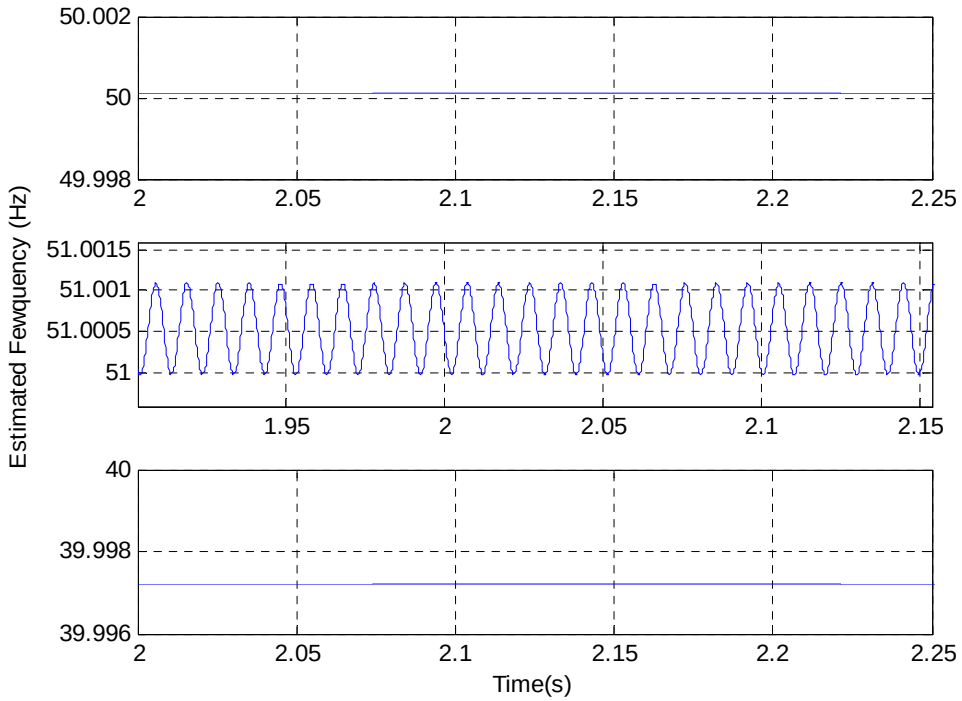

Figure 5.2 *Frequency estimates obtained from the algorithm of Sarkar and Sengupta for 50 Hz, 51 Hz and 40 Hz static sinusoidal signal inputs.*

For the 50 Hz sinusoidal test signals, the proposed method provides almost zero steady-state error. However, for input frequencies of 51 Hz and 40 Hz, the results show small oscillatory outputs in steady-state and/or offset errors, respectively. Specifically, a small offset error will exist, and in the case of a 51 Hz input, a small oscillatory component exists in the steady-state frequency estimate. This is because, from (5.10), the value of A chosen will be calculated using a floor or ceiling function, so that the estimate of A will be in error when $f_s / 2f(n-1)$ is not an integer. In this case, a small oscillation will be evident in the output of the algorithm, such as when the frequency is 51 Hz. The steady-state error that occurs at an input frequency of 40 Hz, is caused by the pre-filter, which has a pass-band ripple of 0.001 dB in this case.

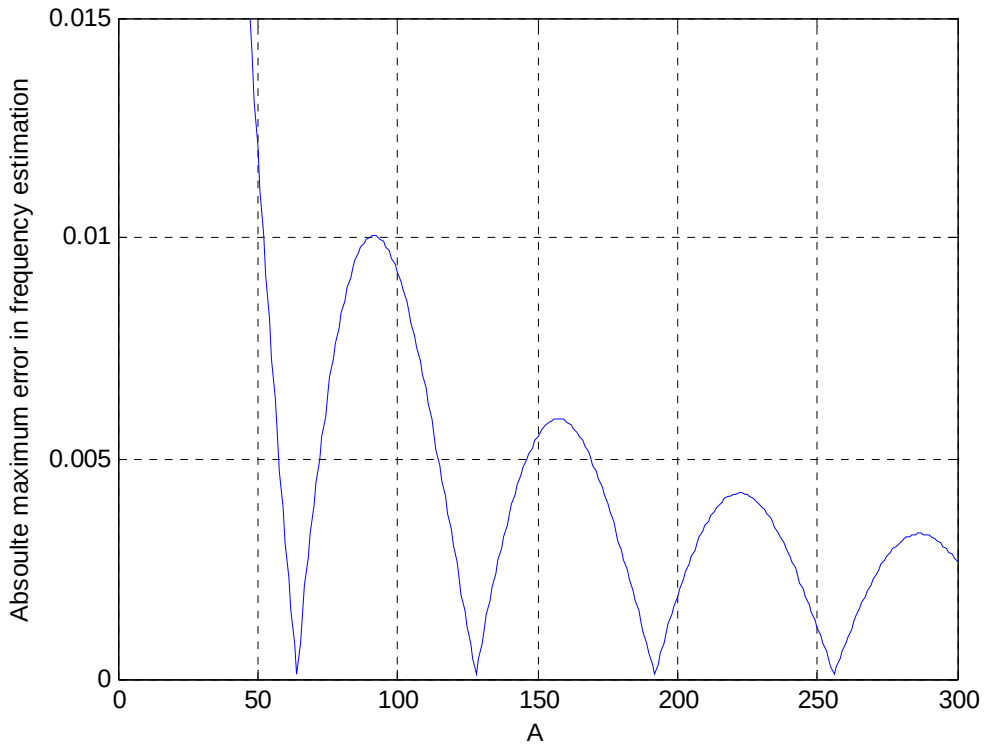

Figure 5.3 Absolute maximum error in frequency estimates of 50Hz sinusoidal signals as *A is allowed to vary.*

Figure 5.3 shows the absolute maximum error of the input of 50 Hz sinusoidal signals. As the described in above section, the error is minimum when the number of samples per cycle is an integer.

Another test is used which considers a step change of the input frequency. A sinusoid of unity amplitude, for which the frequency drops suddenly from 50 Hz to 40 Hz at time $t = 3s$ is used for this test. The resultant plot, Figure 5.4, shows that the proposed method provides fast convergence, and a response time of less than 50 ms.

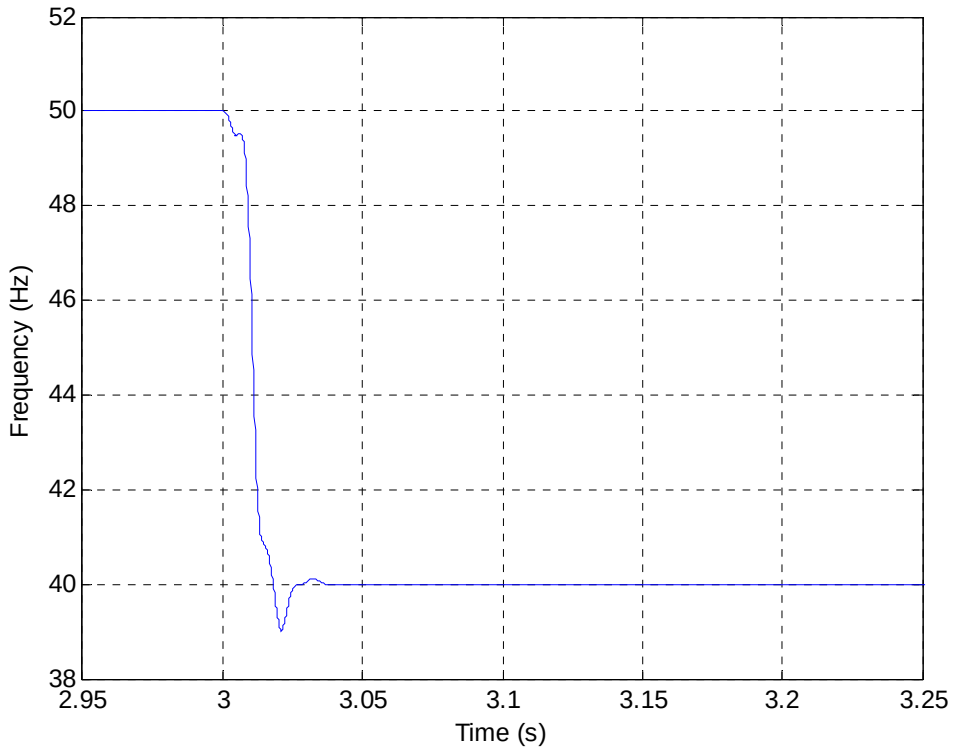

Figure 5.4 *Frequency estimates during a step change in frequency.*

5.1.2 Improved design of second-degree differentiator based algorithms

In [56] the algorithm of Sarkar and S. Sengupta, described in the previous section, the authors proposed the use of a the minimum-phase second-degree IIR differentiator to obtain the double derivative signal $s_{FD}(t)$. There is a small, but variable group delay, for this minimum phase differentiator (about 0.04 samples), as shown in Figure 5.5. This delay between the input signal $s_F(t)$ and its double derivative signal $s_{FD}(t)$, and more particularly its variation, will cause some error for the algorithm (5.9).

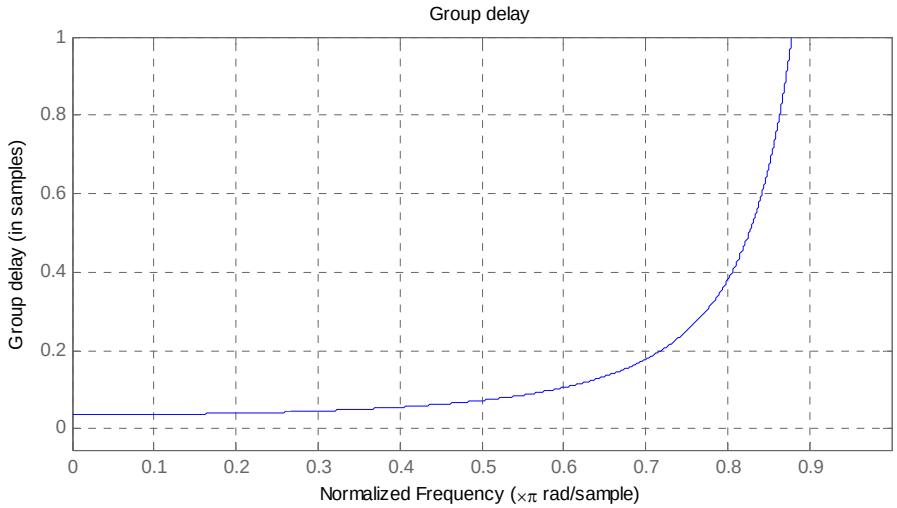

Figure 5.5 *Group delay of the minimum-phase second-degree IIR differentiator.*

To solve this problem, the IIR differentiator is replaced by a linear phase second-degree FIR differentiator. As shown in Figure 5.6, a delay must be added to the input signal to eliminate the effect of the group delay of the second-degree FIR differentiator. The error caused by the delay can be fully

removed because the FIR differentiator has constant group delay. Note that the frequency estimation output of the algorithm is not operating in a high-frequency closed-loop control system, so a small constant delay is immaterial to the application of the frequency estimator.

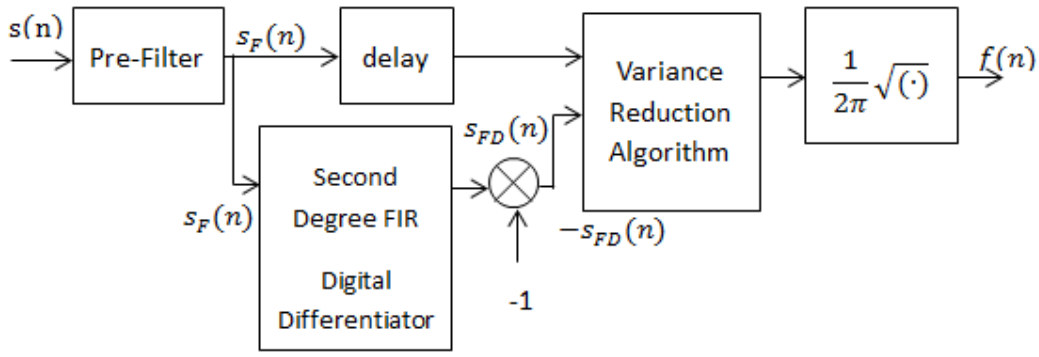

Figure 5.6 *Block diagram of the frequency estimation for the improved algorithm.*

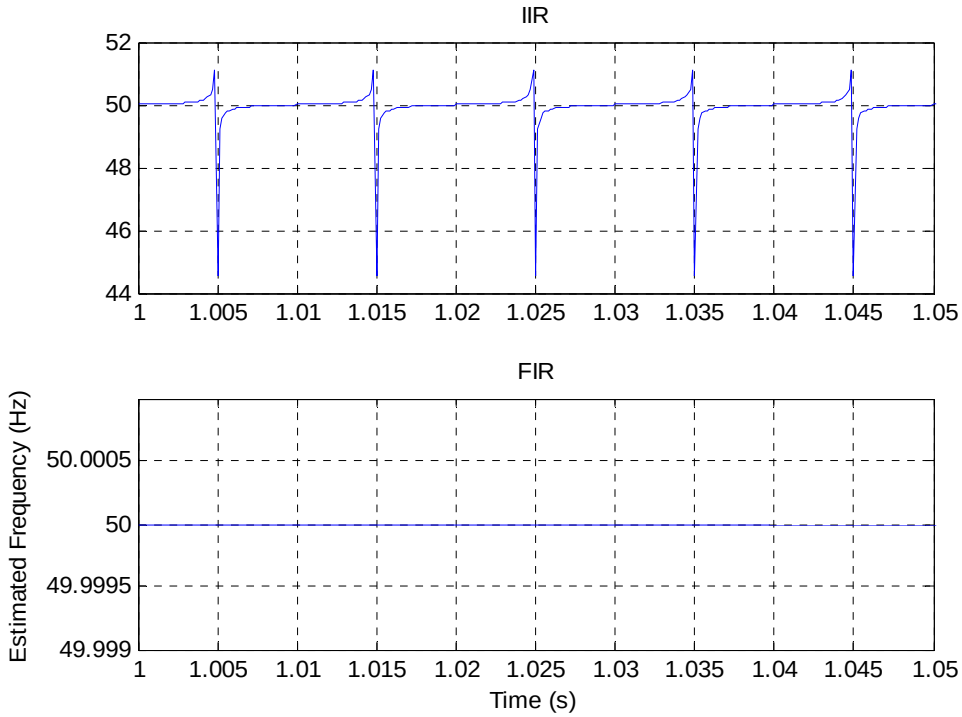

Figure 5.7 *Comparison of frequency estimates of 50 Hz sinusoidal signals of IIR differentiator and FIR differentiator, for the case of* $A = 1$.

For example, a 20th order second-degree FIR differentiator, with normalized frequency 0.2, is used in this test. This differentiator was described in Section 3.3. The proposed FIR differentiator has a constant group delay of ten samples. The pre-filter utilizes a low-pass Chebychev-1 filter, of order four, with a pass-band ripple of 0.001 dB, and a cut-off frequency of 50 Hz. This filter matches that proposed by Sarkar and S. Sengupta in [56].

In the first test, the value of A was chosen as one. This choice implies that no averaging effect is included in the *A*-based algorithm. As shown in Figure 5.7, the frequency estimates obtained through use of an FIR differentiator provides zero steady-state error. The equivalent method that makes use of an IIR differentiator exhibits large errors with a period (for a 50 Hz input), of 0.01 s, which always correspond to half a signal period. It can be concluded that for this type of input, at least, the error caused by the delay can be fully removed when using the linear FIR differentiator.

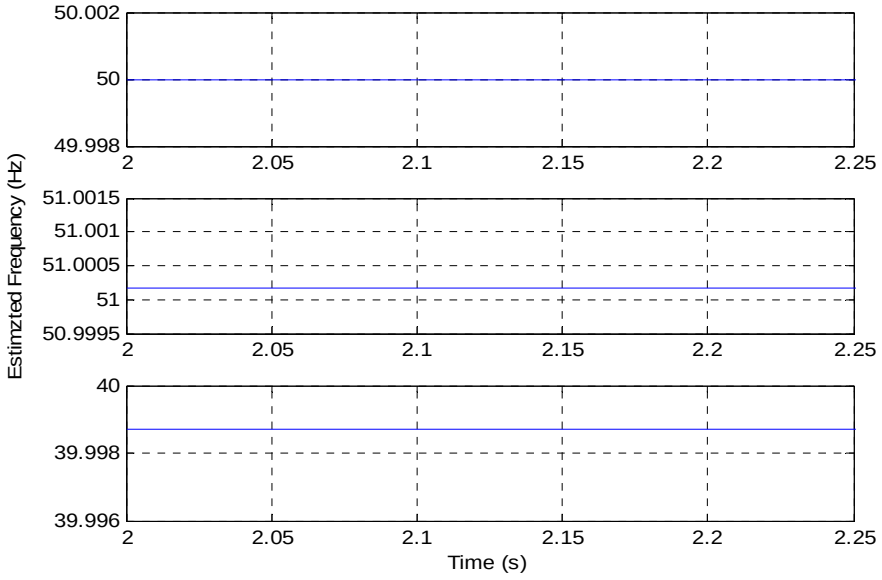

Figure 5.8 *Frequency estimates provided by new algorithm of 50 Hz, 51 Hz and 40 Hz static sinusoidal signals, using linear phase second-degree FIR differentiator.*

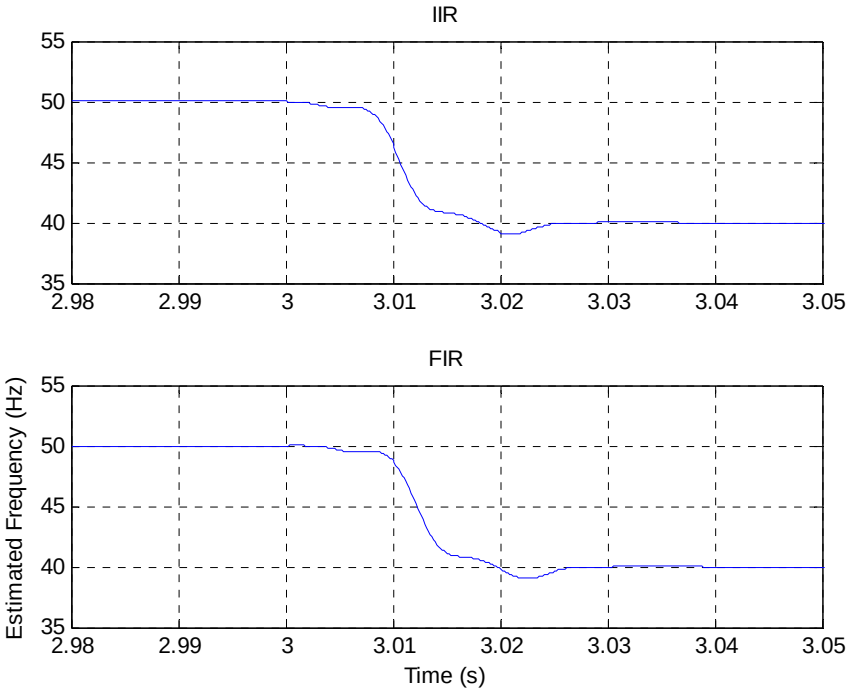

Figure 5.9 *Comparison of frequency estimates during step frequency change (at* $t = 3s$*).*

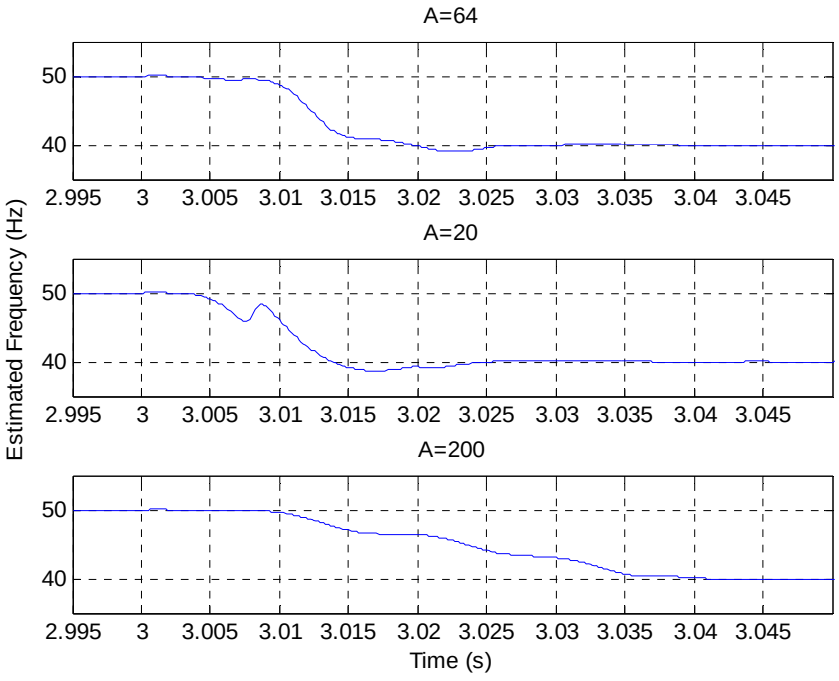

Figure 5.10 *Comparison of frequency estimates during step frequency change with different values of* A*, assuming an FIR differentiator.*

Figure 5.9 shows the comparison of frequency estimates during step frequency changes. There is very little difference between the methods using an IIR differentiator and FIR differentiator. However, the FIR-based method does have a specific delay, due to the group delay of the FIR differentiator being ten samples.

In another test, the averaging value of A is changed, using $A=64$ as a base (initial) value, then choosing $A=20$ and $A=200$, to investigate the influence of A. The FIR differentiator has been chosen. It is shown on Figure 5.10 that, the smaller the value of A, the faster the convergence of the algorithm, and the smoother the transition.

In order to evaluate the sensitivity of the algorithm to input noise, a further test was implemented. A sinusoidal 50 Hz signal with zero-mean white Gaussian noise (signal to noise ratio, $SNR=30$) has been used as input test signals. The result, shown on Figure 5.11, makes it clear that increasing A results in a reduced absolute maximum steady-state error.

It can be concluded from the results above that the choice of A plays an important role in this algorithm. Compared with the use of IIR differentiator, the FIR-based method exhibits better selectively on the choice of value of A. A large value of A provides small maximum steady-state errors, with an improved noise tolerance of the frequency estimation algorithm, and a smooth transition band, but it is associated with a slow convergence, due to the effective averaging being over an extended period.

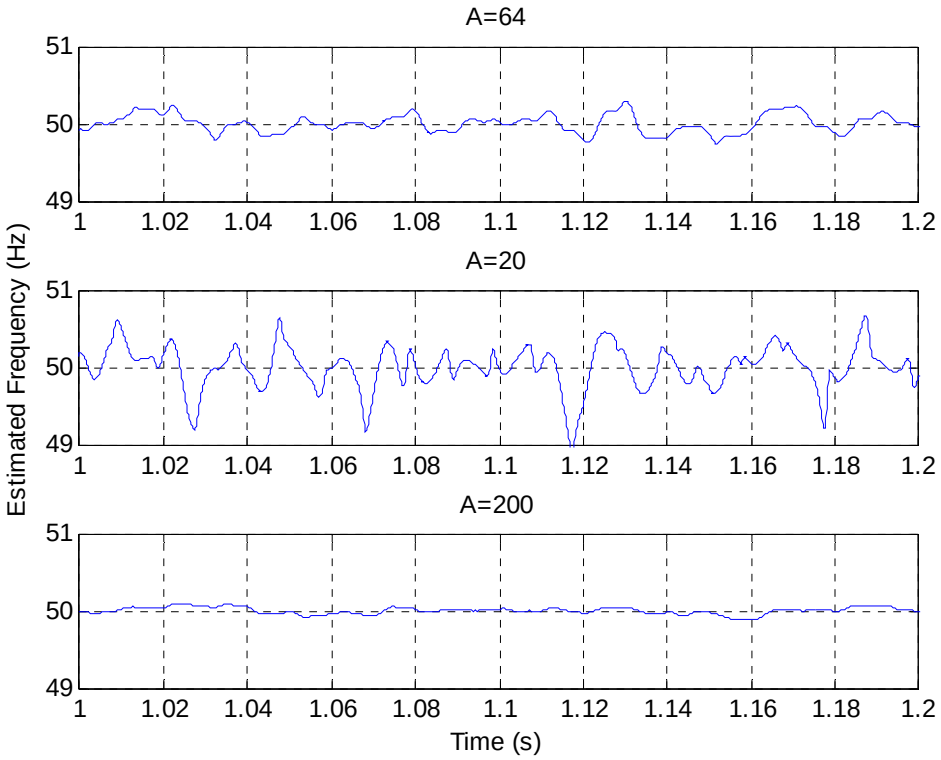

Figure 5.11 *Comparison of frequency estimates of 50Hz sinusoidal signal with added white-noise, for different values of* A*, when using the FIR-based frequency estimation algorithm.*

To investigate the effect of harmonics on the performance of the proposed method, an input of 50 Hz, with additional harmonic components, has been used, as follows:

$$v(t) = \sin\left(\omega t + 15^\circ\right) + 0.2\sin\left(3\omega t + 145^\circ\right) + 0.1\sin\left(5\omega t + 75^\circ\right) + 0.05\sin\left(\omega t + 115^\circ\right) \quad (5.11)$$

The pre-filters have chosen as following Table:

Table 5.1. Filter parameter of pre-filter

Pre-filter	Order	Pass-band ripple	Stop-band ripple	Cut-off frequency
LP Chebyshev Type 1	$N = 4$	0.001 dB	N/A	50 Hz
LP Elliptic	$N = 4$	1 dB	80 dB	50 Hz
BP Chebyshev-Type 1	$N = 4$	0.001 dB	N/A	40 Hz to 60 Hz

In the above tests, the LP Chebyshev-Type 1 filter was chosen as the pre-filter used in [56].

It is shown in Figure 5.12 that the Elliptic pre-filter provides the least minimum steady-state error amongst these filters. This is because the harmonic components have been effectively removed by the pre-filters. For example, the normalized frequency of third harmonic component of the input signal is at a normalized frequency $3\omega/(\text{sample} \quad \text{frequency}/2) = 3\times 50/(6400/2) = 0.0469$. For the selected filters, it can be found from Figure 5.13 that the magnitude responses at a normalized frequency of 0.0469 are -4.5db, -54.6db and -19db respectively. The elliptic pre-filter can best remove the harmonic components. When deciding on a rule for the choice of the pre-filter, can be concluded that: (1) the accuracy of the frequency estimate depends on the magnitude of the pre-filter attenuation at the fundamental frequency (for the constant frequency, sinusoidal inputs); and (2) for signals with significant harmonics and/or noise, the attenuation of the pre-filter at higher frequencies is also important.

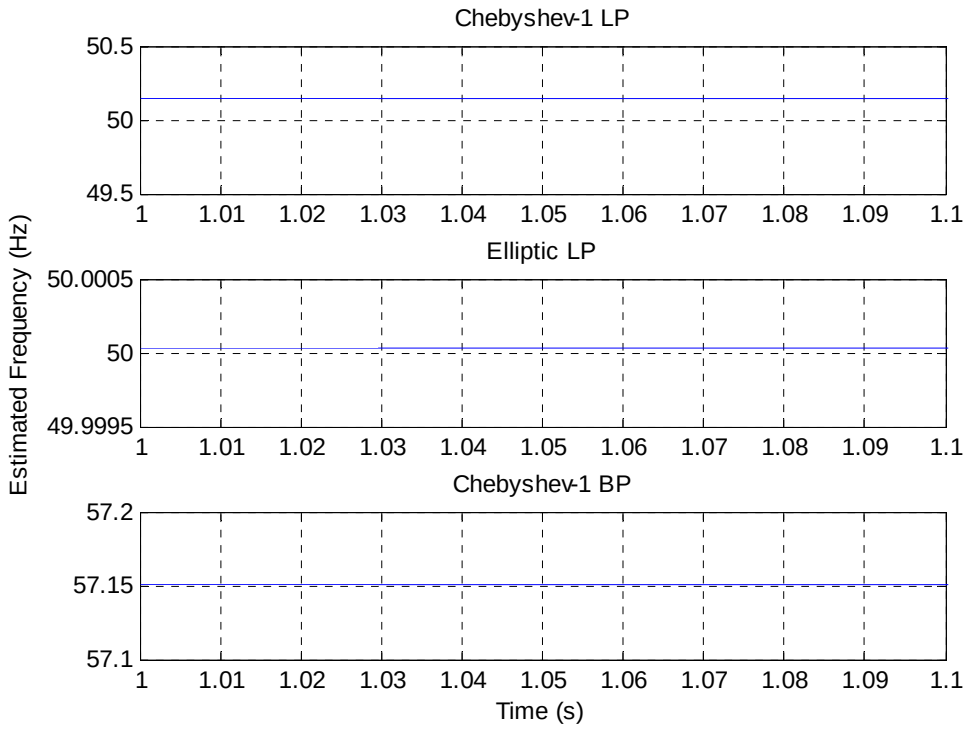

Figure 5.12 *Comparison of frequency estimates for 50 Hz input, with different pre-filters.*

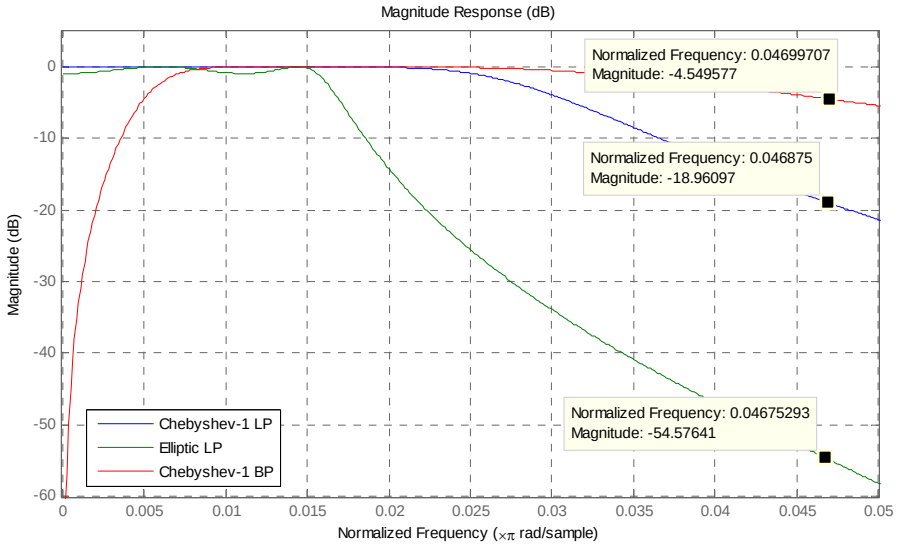

Figure 5.13 *Magnitude response of the pre-filters used in the frequency estimators.*

5.2 Image Edge detection using differentiator

Edge detection of an image is one of the most important tasks in digital image processing. It is the foundation of high-level image processing, incorporating the understanding and analysis of images, and computer vision [62]. The basic idea of most available edge detectors is to locate some local object-boundary information in an image, by the thresholding and skeletonizing of the pixel-intensity variation map [69]. The edge detection process serves to simplify to analysis of images by drastically reducing the amount of data to be processed, while at the same time preserving useful structural information about object boundaries [61]. Therefore, in image processing, methods obtaining the image edge remain a focus for research.

In image processing, edge detection often utilizes integer-degree differentiation operators, such as first degree operators that use the gradient or second degree operators via the Laplacian [61] [63] [65]. In [62] [34] [64], some methods based on fractional degree operators are introduced.

5.2.1 Review of frequency-estimation algorithms based on second-degree IIR differentiators

In this section, some classical and recently-reported edge detectors are introduced, including the Prewitt [68], Sobel [67], Alaoui FIR [65] and Alaoui IIR [66]. Most of the edge detectors need to compute the derivatives of the image intensity function. It is assumed that the distance between two samples is the same along the horizontal and vertical directions, equal to Δ. The following are

the approximations of the first-degree derivative:

$$\begin{aligned}
&\frac{1}{\Delta}\{f(n\Delta+\Delta)-f(n\Delta)\} \quad \text{Forward difference} \\
&\frac{1}{\Delta}\{f(n\Delta)-f(n\Delta-\Delta)\} \quad \text{Backward difference} \\
&\frac{1}{\Delta}\{f(n\Delta+\Delta)-f(n\Delta-\Delta)\} \quad \text{Central difference.}
\end{aligned} \tag{5.12}$$

Unlike the forward and backward differences, the central difference is symmetric and provides a more precise approximation of the first derivative [1].

5.2.1.1 Sobel and Prewitt edge detector

The Sobel [67] and Prewitt [68] edge detectors represent the most basic masks used in edge detection. These can be applied by smoothing the image before computing the derivatives, in the direction perpendicular to the derivative. In many applications, the operators are used for standard gradient computation, to retrieve the image gradient and edges. A Sobel edge detector is given as follows:

$$G_{Sx} = \begin{bmatrix} -1 & 0 & 1 \\ -2 & 0 & 2 \\ -1 & 0 & 1 \end{bmatrix} \tag{5.13}$$

This filter computes the partial derivative in the x (horizontal) direction. Similarly, a similar filter can compute the partial derivative in the y (vertical) direction:

$$G_{Sy} = \begin{bmatrix} -1 & -2 & -1 \\ 0 & 0 & 0 \\ 1 & 2 & 1 \end{bmatrix} \tag{5.14}$$

The Prewitt edge detector is obtained in the same fashion as the Sobel mask in the x (horizontal) direction:

$$G_{Px} = \begin{bmatrix} -1 & 0 & 1 \\ -1 & 0 & 1 \\ -1 & 0 & 1 \end{bmatrix} \tag{5.15}$$

and in the y (vertical) direction:

$$G_{Sy} = \begin{bmatrix} -1 & -1 & -1 \\ 0 & 0 & 0 \\ 1 & 1 & 1 \end{bmatrix} \tag{5.16}$$

Both of the above edge detectors are based on the discrete approximation of the central differentiators. The Prewitt edge detector is based on the central difference differentiator of coefficients $h = [-1 \quad 0 \quad 1]$, with a low-pass smoothing filter, $[1 \quad 1 \quad 1]$. The Sobel edge detector is obtained from the same differentiator, with a differentiator smoothing filter of $[1 \quad 2 \quad 1]$.

The gradient magnitude is obtained by combining the partial derivative in the x and y directions, as

$$G = \sqrt{(G_x * I_m)^2 + (G_y * I_m)^2} \tag{5.17}$$

where I_m is the gradient of a given image, and $*$ is the signal convolution operation.

5.2.1.2 Al-Alaoui IIR edge detector

Traditional edge detection relies on mask edge detectors based on low-order FIR differentiators to perform efficient edge detection. In [66], Al-Alaoui presented a method of employing a direct approach to edge detection, to perform edge detection without using masks.

Some IIR differentiators are given in [66], which are obtained by interpolating two Newton-Cotes numerical integration rules, as described in Section 2.2.6. The transfer functions of the IIR differentiators are:

$$H_{Alaoui1}(z) = \frac{0.3638(z-1)}{z+1/7} \tag{5.18}$$

$$H_{Alaoui2}(z) = \frac{(z^2-1)}{z^2+0.611z+0.0932} \tag{5.19}$$

$$H_{Alaoui3}(z) = \frac{3(z^2-1)}{3.7321(z^2+0.5358z+0.0718)} \tag{5.20}$$

The The edge detectors are achieved by computed the partial derivatives in the x - and y- directions, and then combining them using (5.17).

5.2.1.3 Al-Alaoui FIR edge detector

Al-Alaoui approximated the Al-Alaoui first-order IIR differentiator via an FIR filter. The FIR approximation of the Al-Alaoui IIR differentiator 1 (the transfer function is given in (5.18)) is designed in [65]. The resulting transfer function of the FIR Al-Alaoui differentiator is given:

$$H_{ALaoui}(z) = 0.36z^2 - 0.42z + 0.06 \tag{5.21}$$

Therefore, the Al-Alaoui edge detectors can be obtained from (5.21), with smoothing filters $[1 \quad 1 \quad 1]$, $[1 \quad 2 \quad 1]$ and $[1 \quad 3 \quad 1]$. In this section, the Al-Alaoui edge detector includes the smoothing filter. For example, the smoothing filter $[1 \quad 1 \quad 1]$ leads to the following mask in the *x* direction:

$$G_{Alaouix} = \begin{bmatrix} 0.36 \\ -0.42 \\ 0.06 \end{bmatrix} \begin{bmatrix} 1 & 1 & 1 \end{bmatrix} = \frac{6}{100} \begin{bmatrix} 6 & 6 & 6 \\ -7 & -7 & -7 \\ 1 & 1 & 1 \end{bmatrix} \tag{5.22}$$

And for y direction

$$G_{Alaouiy} = \begin{bmatrix} 1 \\ 1 \\ 1 \end{bmatrix} \begin{bmatrix} 0.36 & -0.42 & 0.06 \end{bmatrix} = \frac{6}{100} \begin{bmatrix} 6 & -7 & 1 \\ 6 & -7 & 1 \\ 6 & -7 & 1 \end{bmatrix} \tag{5.23}$$

5.2.1.4 CRONE edge detector

The CRONE edge detector is introduced in [34], which based on fractional degree differentiation. The CRONE edge detector with mask size $2m+1$ in horizontal direction can be written as:

$$\begin{bmatrix} +a_m & \cdots & +a_1 & 0 & -a_1 & \cdots & -a_m \end{bmatrix} \tag{5.24}$$

and for the vertical direction:

$$\begin{bmatrix} +a_m & \cdots & +a_1 & 0 & -a_1 & \cdots & -a_m \end{bmatrix}^T \tag{5.25}$$

where

$$a_k = (-1)^k \binom{v}{k} = (-1)^k \frac{v(v-1)\cdots(v-k-1)}{k!} \tag{5.26}$$

The coefficients of the CRONE edge detector utilize the Grunwald-Letnikov fractional derivative, as provided in (4.16). v is the fractional degree, which can be a value between 1 and 2 to improve edge detection selectivity, and it can also be a number between -1 and 1 favors robustness of immunity to noise.

5.2.1.4 Edge detector results

In this Section, a noise-free grayscale Lena image is considered as the input image. In Figure 5.14, Figure 5.15 and Figure 5.16, the output results corresponding to the edge detectors are shown. All the edge detectors performed edge detection successfully, and with seemingly good performance. In Figure 5.14, the Al-Alaoui IIR edge detector 1 show worse sensitivity of edge detection compare with other Al-Alaoui IIR edge detectors. In Figure 4.16, the Al-Alaoui FIR edge detector also has the same disadvantage, because it is based on the Al-Alaoui IIR edge detector 1. Figure 5.16 is the comparison of CRONE edge detectors with different fractional degree. It can be concluded that a CRONE detector with high fractional degree is sensitivity to the detail, but miss some particular edges. Although many edge detection methods have developed in the past years [69][70][71], the performance evaluation of the edge detector results is still a challenging problem.

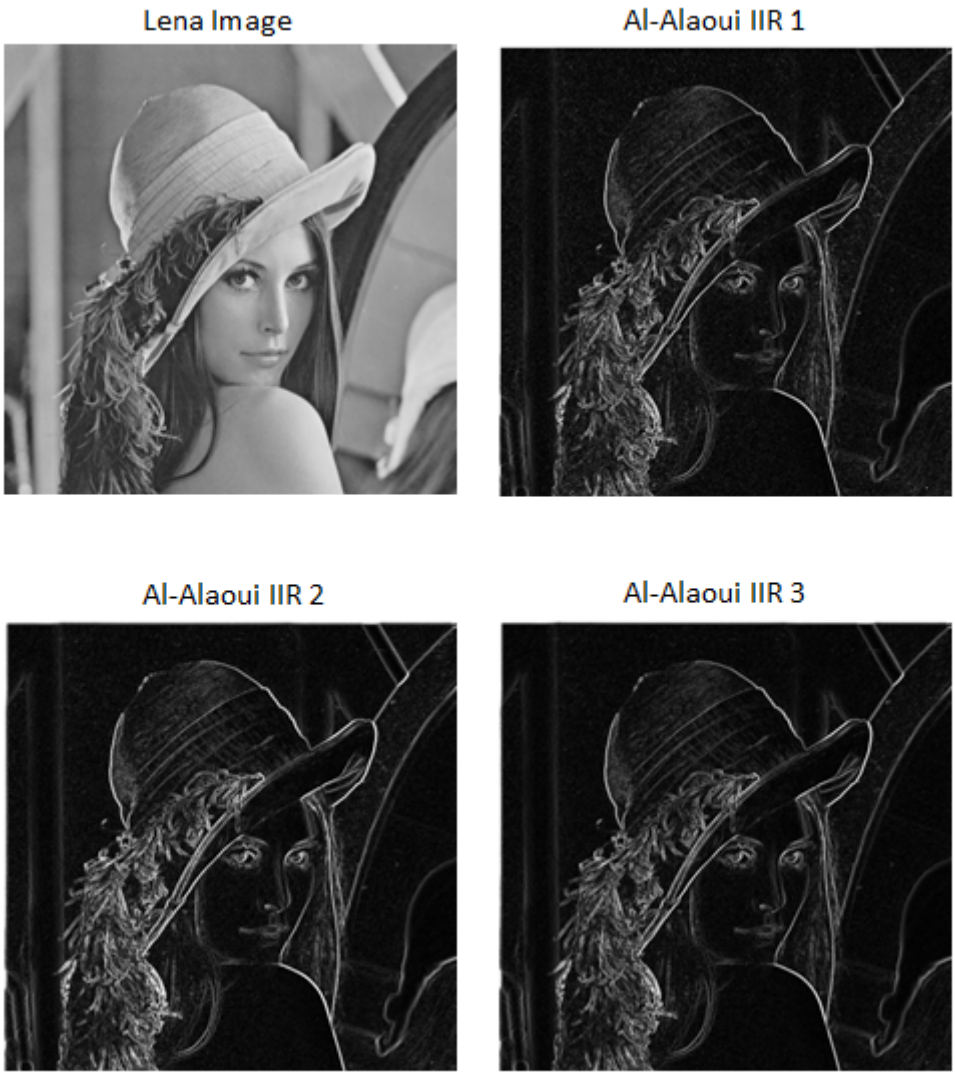

Figure 5.14 *Edge detection results of Al-Alaoui IIR edge detector.*

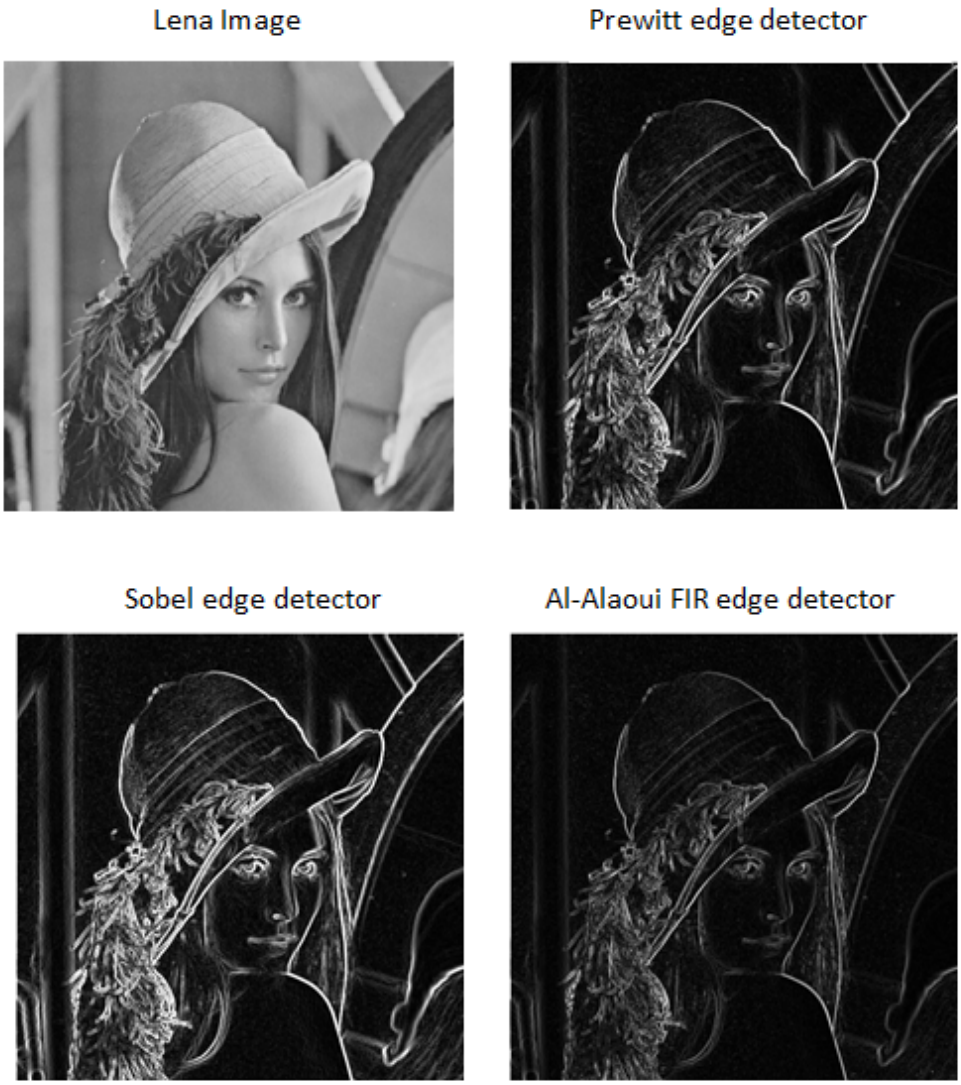

Figure 5.15 *Edge detection results using mask.*

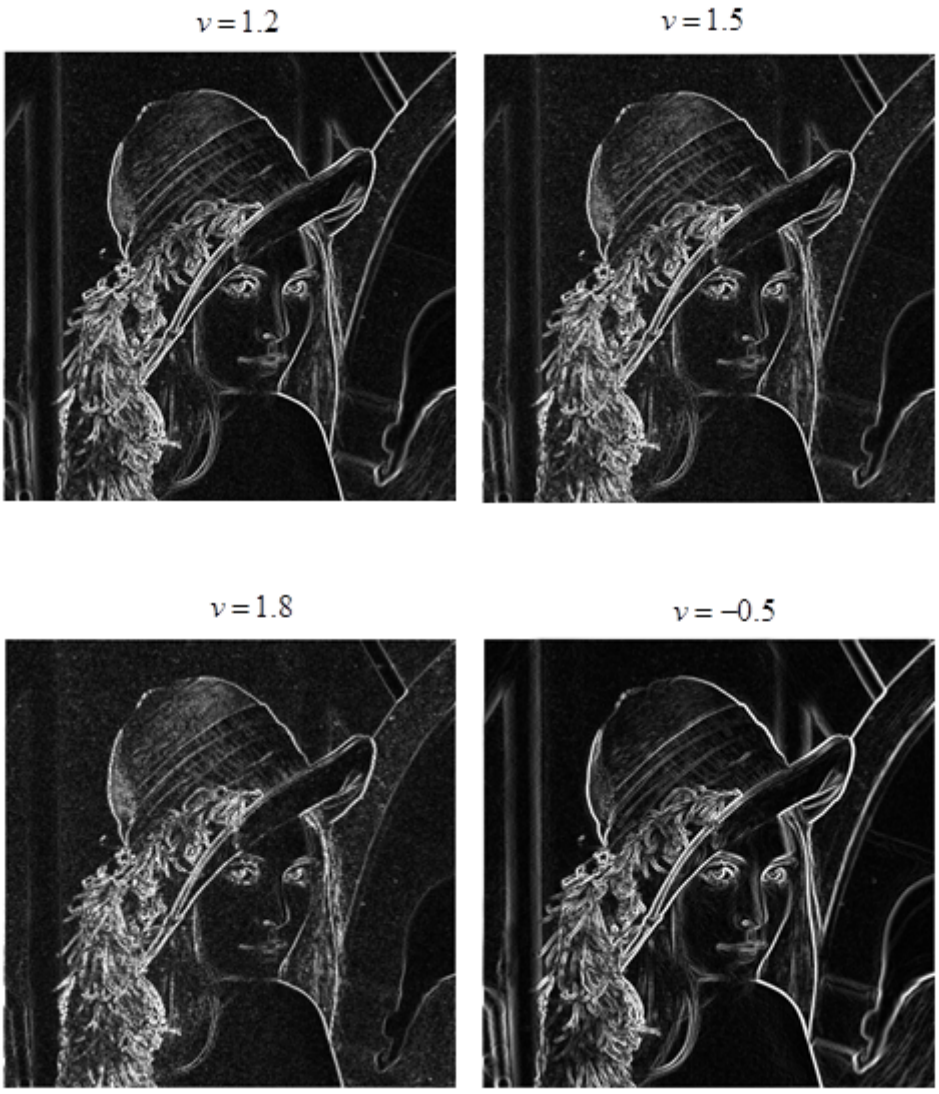

Figure 5.16 *Edge detection results for the CRONE mask.*

5.2.2 Direct Approach to Image Edge Detector Using IIR Fractional Differentiators

The method to design in [66] is based on the first-degree differentiator. In this Section, the first-degree differentiators will be replaced to fractional differentiators.

In the first example, fractional differentiators with different degree, $v = 0.4$, $v = 0.8$, $v = 1.2$ and $v = 1.6$ are selected to design the edge detectors. The coefficients of FIR Grunwald-Letnikov fractional differentiators can be computed from (4.26), then transferred to IIR filters using (4.34) and (4.35) with fifth order $m = n = 5$.

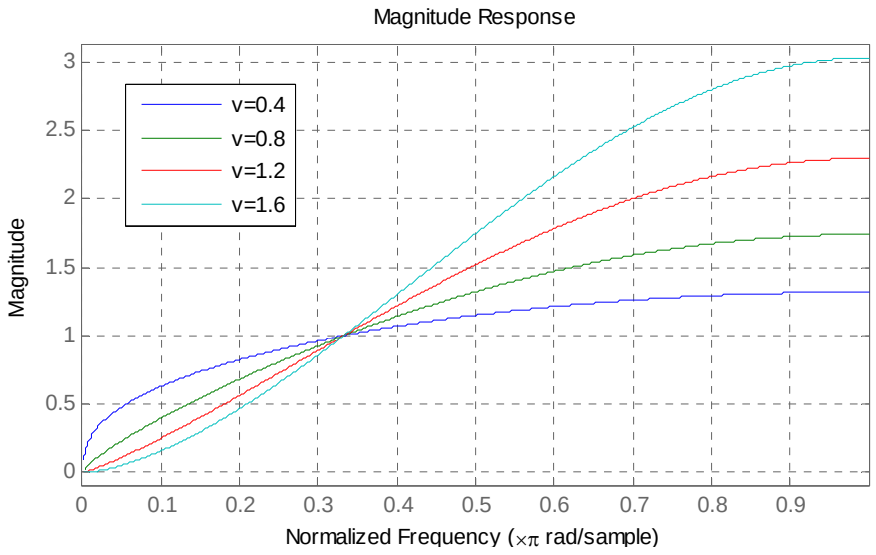

Figure 5.17 *Magnitude response of IIR Grunwald-Letnikov fractional differentiators with different degree.*

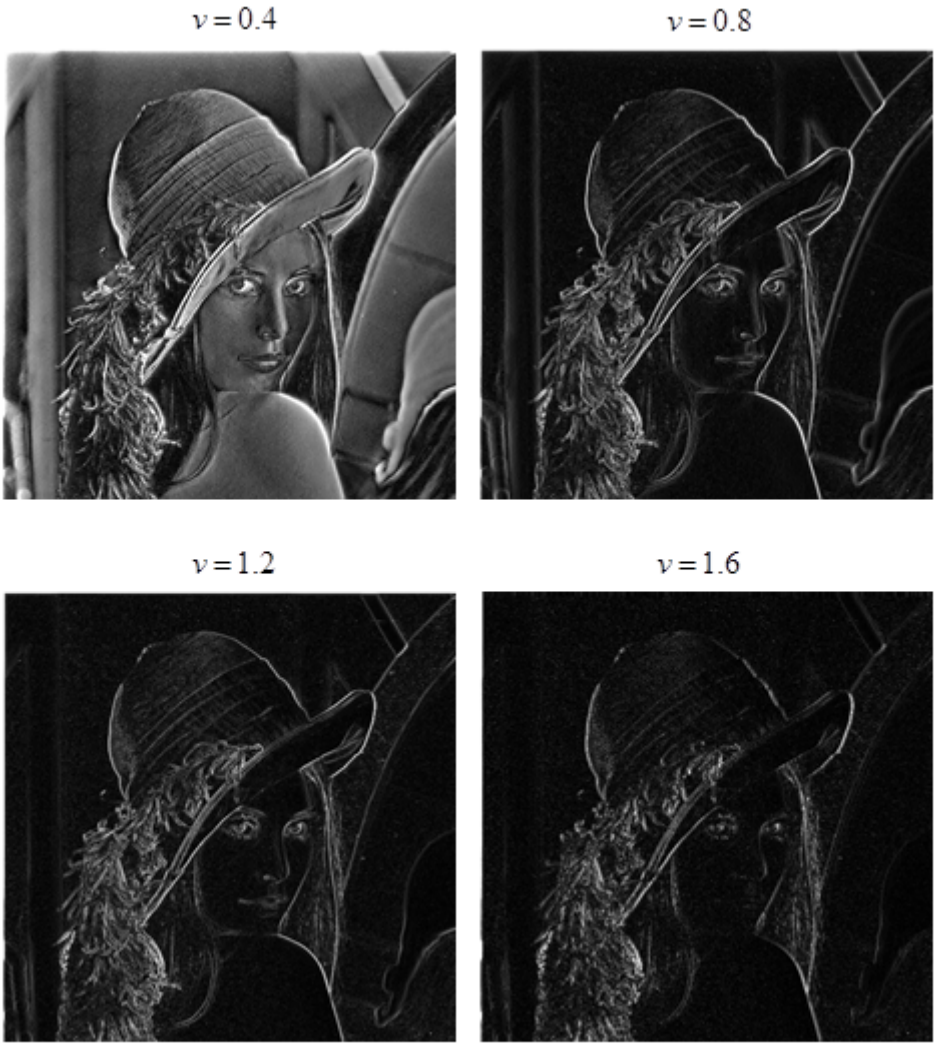

Figure 5.18 *Edge detector based on Grunwald-Letnikov fractional differentiators with different degree.*

Figure 5.17 shows the magnitude characteristics of the fractional differentiators, while Figure 5.18 shows the performance of the corresponding fractional differentiators for edge detection applications. The fractional differentiators with low degree can exhibit more detail of the original image characteristic, such as for $v=0.4$, and the fractional differentiators with high degree show the characteristic of the accuracy edge information. A beneficial characteristic of using a fractional differentiator of low degree for edge detection is that the viewer can still see many of the characteristics of the

original image, while edges are enhanced. A fractional differentiator with high degree has large magnitude response at high frequencies, as is evident in Figure 5.17. Therefore, the fractional differentiator with degree $v = 0.8$ is a suitable solution for edge detection.

The next example compares the first-degree IIR differentiator labelled by Al-Alaoui as differentiator 3, defined in [66] with transfer function (5.20), and two Grunwald-Letnikov fractional differentiators with degree $v = 0.8$, one of which is a third order FIR fractional differentiator (the length of mask will be 5), while the other is a fifth order IIR fractional differentiator. A low-pass first degree differentiator with cut-off frequency $\omega_c = 0.52$ is also adding to the comparison, for which the filter coefficients are taken from Table 2.3.

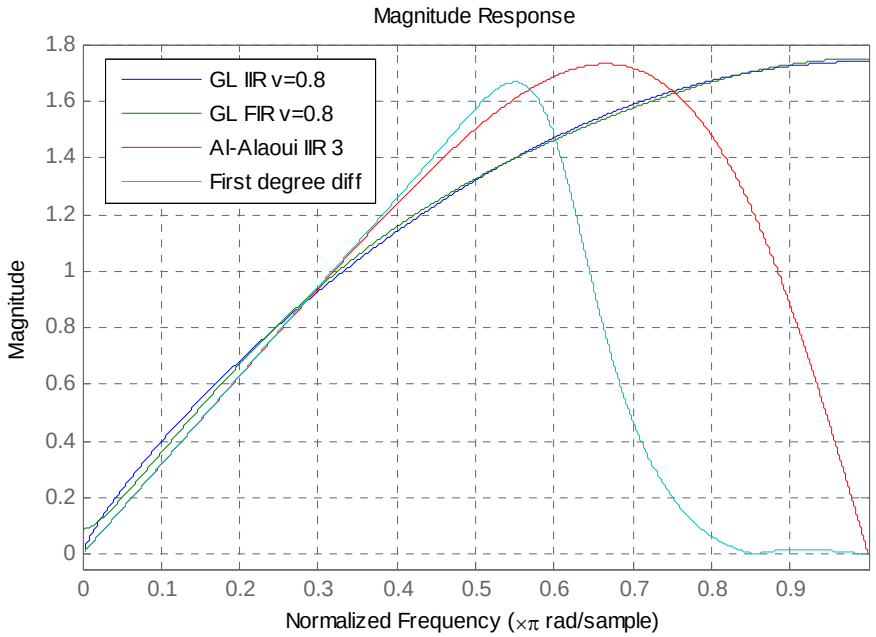

Figure 5.19 *Magnitude response of IIR differentiators.*

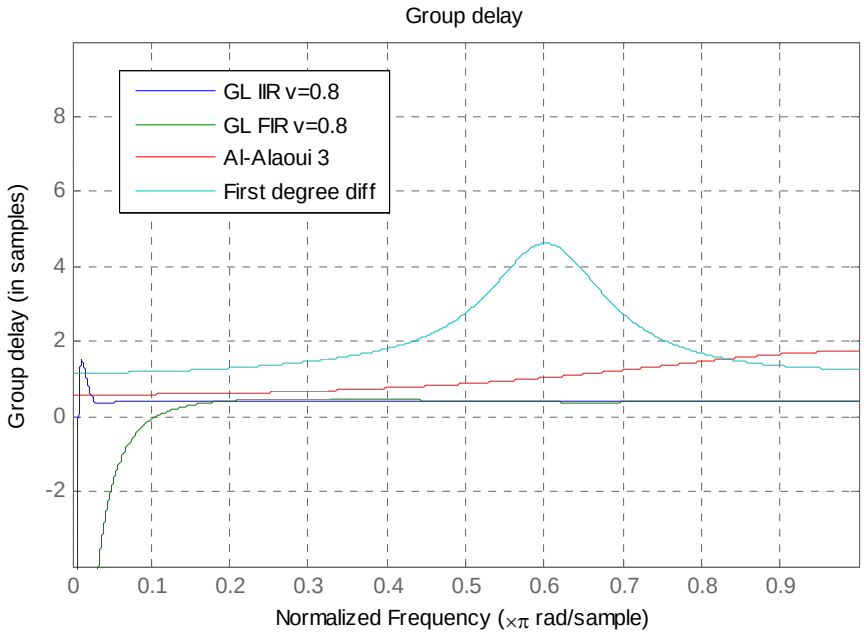

Figure 5.20 *Group delay of IIR differentiators.*

The Figure 5.19 shows the magnitude responses of the IIR differentiators, which have similar magnitude response in the high frequency range. However, the Figure 5.20 shows that these IIR differentiators have different group. The Grunwald-Letnikov fractional IIR differentiator shows better frequency responses than the FIR one, as expected due to the relative low order of the latter.. The fractional differentiators have the smallest group delay amongst the differentiators considered, about 0.5 samples, while the first degree differentiator shows about 1 sample delay at low frequencies. This will cause a problem when computing the gradient using (5.17). The position of corresponding edge pixel detected will be shifted because of the group delay of the differentiators. The bigger the delay is, the lower the detection accuracy is. That is the reason why the Al-Alaoui IIR edge detectors look more indistinct than

the edge detectors using masks that were considered in Section 5.2.1.4. [1]The resulting images are shown in Figure 5.21. The Grunwald-Letnikov FIR edge detector is a CRONE edge detector. When compared with the Grunwald-Letnikov IIR edge detector, the CRONE edge detector exhibits almost the same detection accuracy.

[1] While zero-phase filtering has a useful role in the filtering of off-line data, it is not applicable to real-time signals. However, zero-phase high-pass filtering is worthy of consideration for the processing of static images.

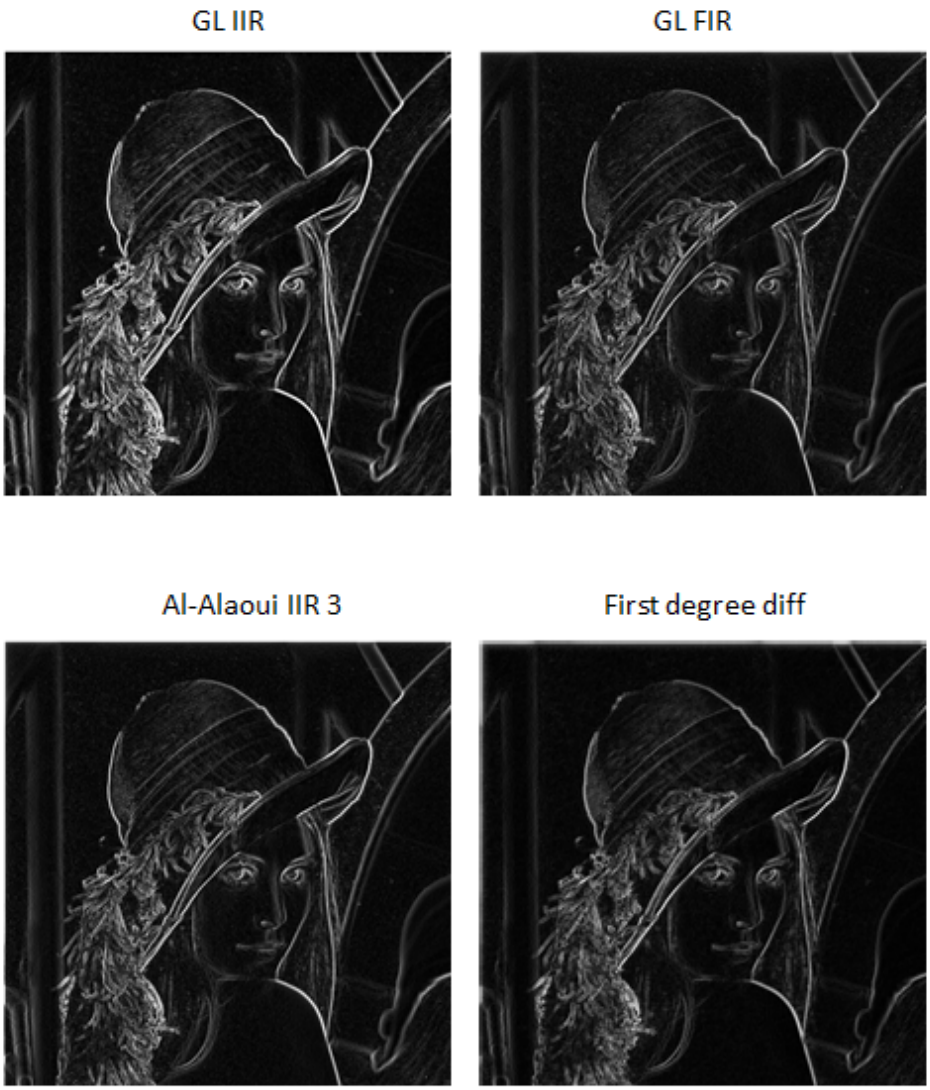

Figure 5.21 *Edge detector based on IIR and FIR differentiators.*

The last example is the comparison of fractional differentiators with different definitions, specifically the Riemann-Liouville definition and Caputo definition. The coefficients of the Riemann-Liouville fractional differentiator can be computed from (4.27), and the coefficients of the Caputo differentiator from (4.50) with degree $v = 0.8$.

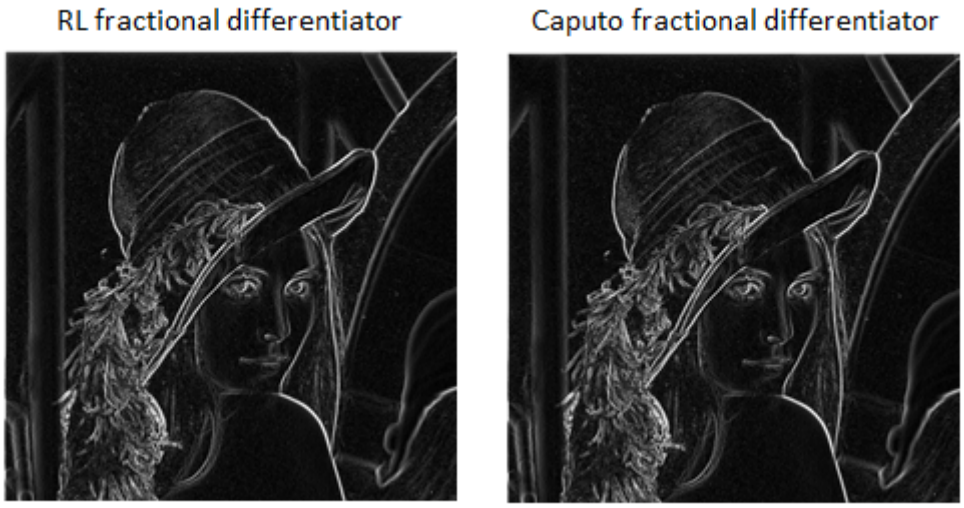

Figure 5.22 *Edge detector based on Riemann-Liouville fractional differentiator and Caputo fractional differentiator.*

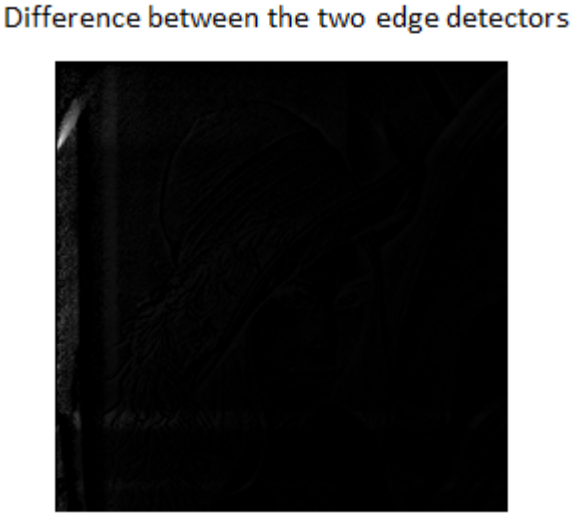

Figure 5.23 *Difference between the Riemann-Liouville and Caputo fractional differentiators.*

It is hard to find the differences between the two edge detectors from Figure 5.22. Thus, the Figure 5.23 shows the difference between the edge detectors. There are some “white pieces” on the left of Figure 5.23. On one-dimensional differences, an initial value of an image is usually not zeros. It is shown on Section 4.4 that the Caputo derivative has better performance when the initial condition has a DC component. The Caputo derivative can reach steady-state with a shorter transient (than that proposed in other works). Therefore the Caputo edge detector has a better visual appearance than the Riemann-Liouville edge detector.

Figure 5.24 *Original image of bike.*

Another image is used to test the performance of the edge detectors. The original image is shown in Figure 5.24. The edge detectors to be tested include the Prewitt edge detector, Al-Alaoui IIR edge detector (5.18), Al-Alaoui FIR dege detector (5.22), CRONE edge detector (5.24), Grunwald-Letnikov IIR edge

detector Caputo edge detector, and the fractional edge detectors considered, with degree $v = 0.8$. Figure 5.26 shows the resulting image with a threshold of 0.15, (so that each pixel with gray value between 0.15 and 1 is displayed with a value of 1. Theoretically, the resulting images of the Al-Alaoui IIR and Al-Alaoui FIR edge detectors, CRONE and GL IIR edge detectors should have the same result, because they are based on the same transfer function. However, some differences can be found on Figure 5.25 and Figure 5.26. Because a low-order IIR filter can outperform a higher order FIR filter, the IIR detector is more sensitive to the detail. Figure 5.27 shows the edge detection of a noisy image (noise has zero mean and a variance of 0.03). The CRONE edge detector show better noise reduction, but some edge information is missing. The IIR GL edge detector and the Caputo edge detector show similar resulting image, but the Caputo edge detector has better performance at the edge of the image. If the edge detector is to retain more details, the noise of the image cannot be effectively suppressed. As expected, the stronger is the noise immunity, the lower is the detection accuracy.

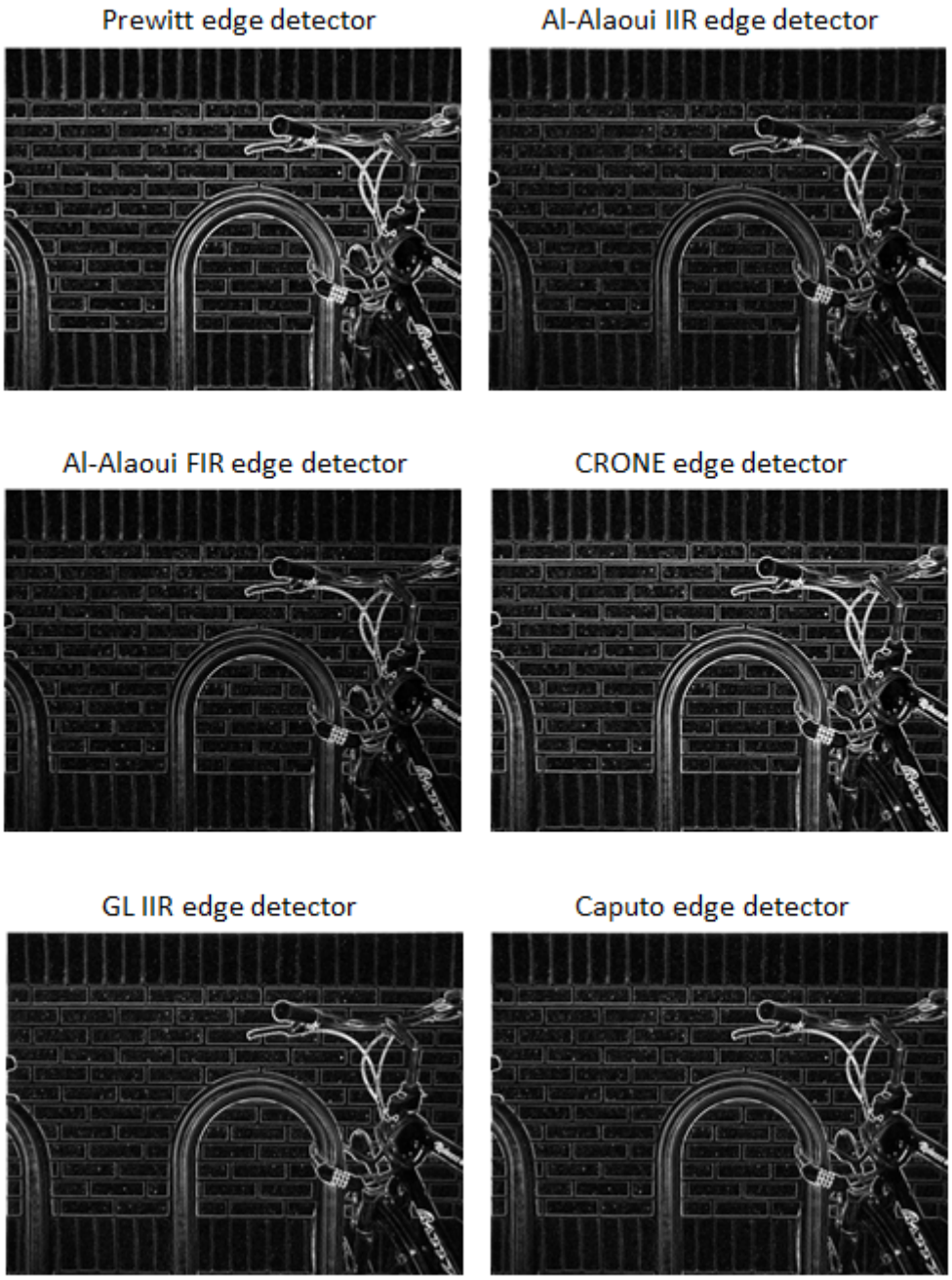

Figure 5.25 *Edge detection results.*

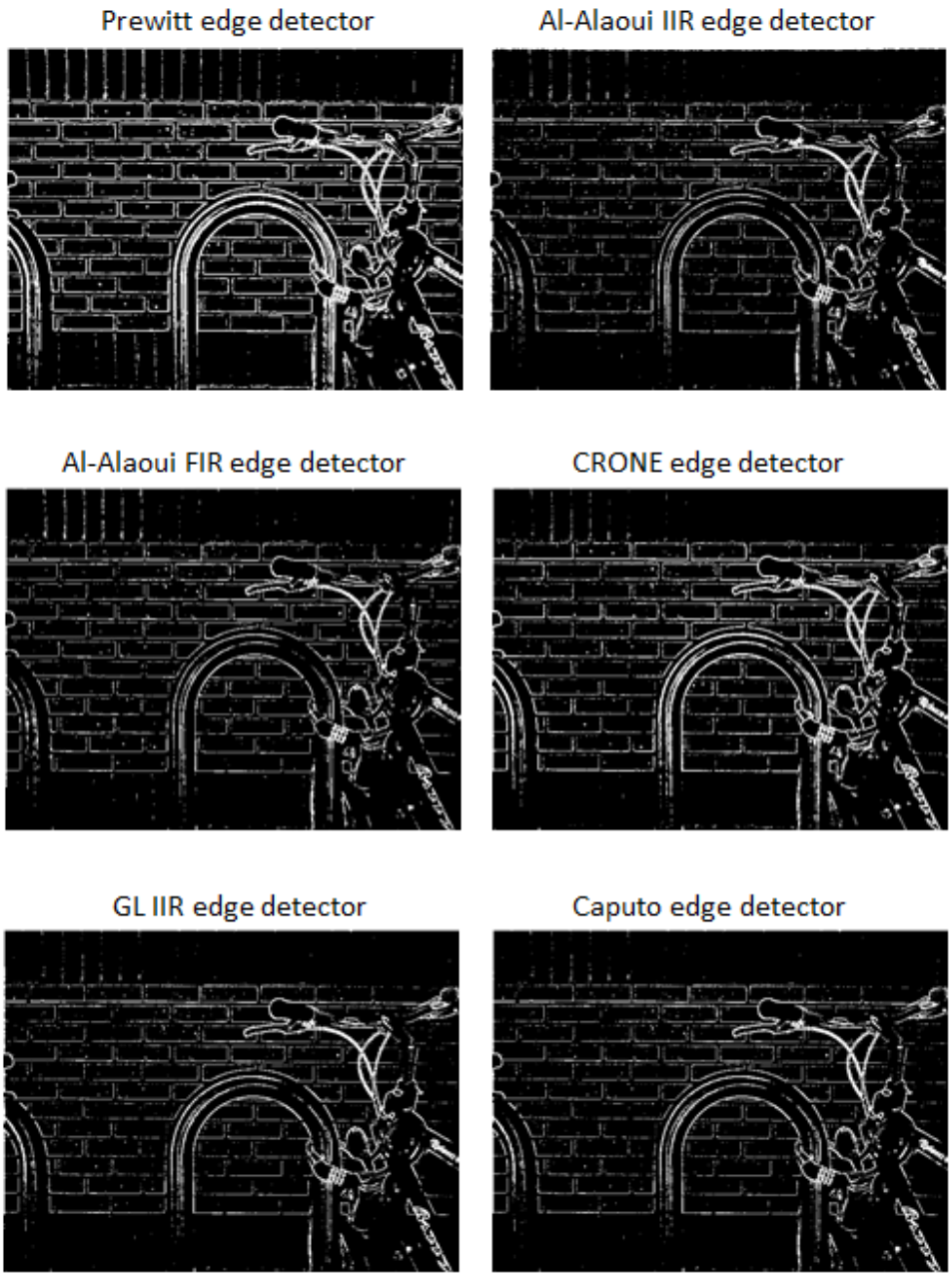

Figure 5.26 *Edge detection results with Threshold = 0.15.*

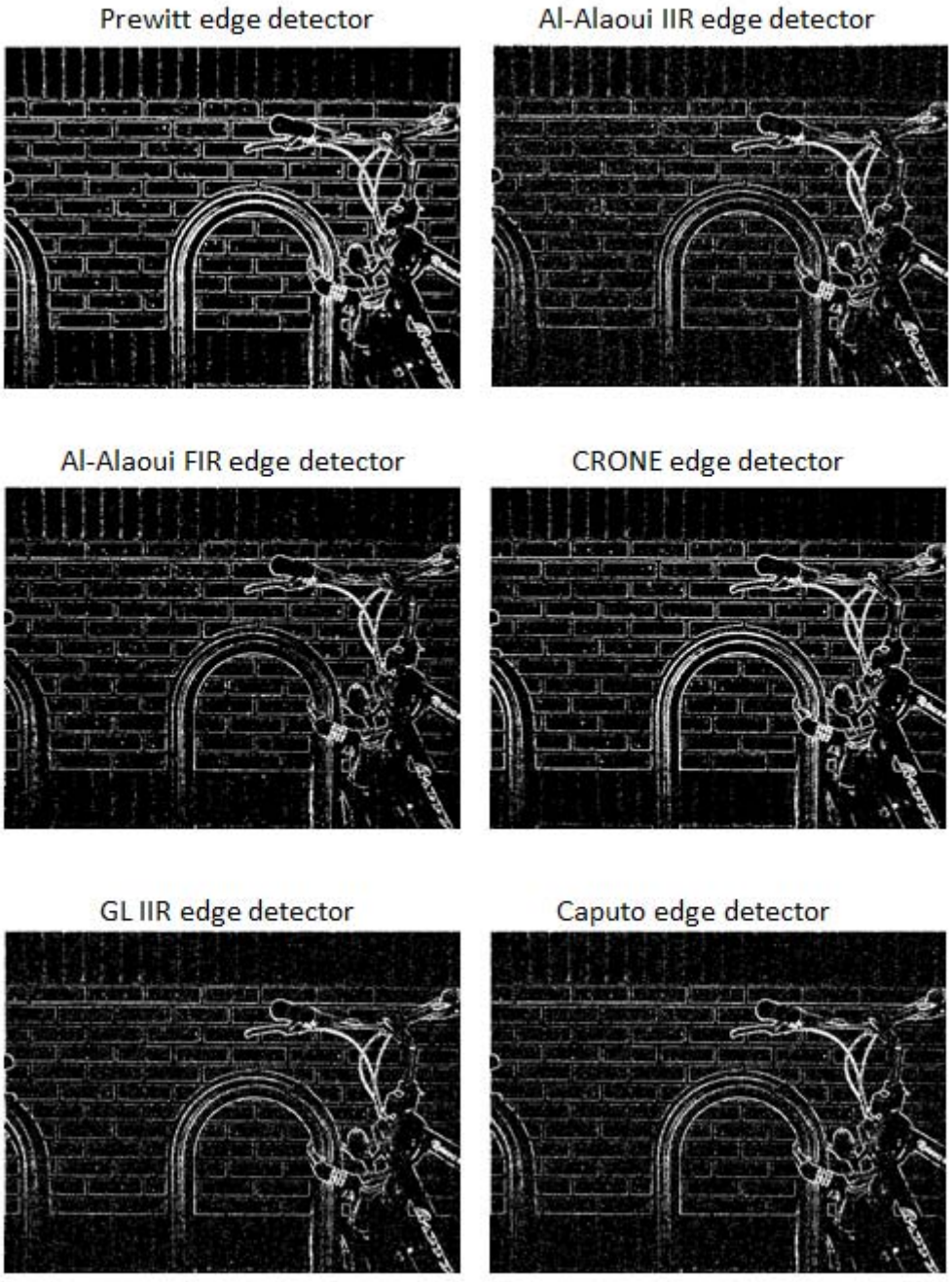

Figure 5.27 *Edge detection results with Threshold = 0.15 for noisy image (mean 0 and variance 0.03).*

5.3 Conclusion

In this chapter, two applications of the digital differentiator are introduced. The first application concerns the frequency estimation of a power system using second degree differentiators. A novel algorithm using an IIR second-degree differentiator has been developed and implemented by A. Sarkar and S. Sengupta [56]. In this algorithm, the performance of the frequency estimator depends on the pre-filter, second-degree differentiator and the value of the parameter A, which is a constant that plays an important role in the accuracy and computational load associated with the proposed algorithm. There is a small, but variable group delay, for the second-degree IIR differentiator, which is the main reason that the frequency estimator provides an oscillatory output error, which is frequency dependent. To overcome this problem, a linear phase, FIR second-degree differentiator is used instead of the IIR differentiator, and the frequency estimation algorithm is improved by adding the known and constant delay associated with the FIR filter. The result shows that the FIR based method exhibits better selectively on the choice of the user-chosen parameter A.

The other application considered is of edge detection using a differentiator. In Section 5.2, some edge detectors have been introduced. A direct approach method to design the edge detector based on an IIR differentiator was introduced by Al-Alaoui [66]. Comparison with some classical, mask-based edge detectors showed that the IIR edge detectors perform better than the FIR edge detectors, though (and because) the IIR filter can have a lower order. From the comparisons shown in this chapter, the FIR edge detector, using a mask, exhibits a clearer edge, because of the gradient of the IIR edge detector using (5.17). The position of corresponding pixel gradient in x direction and y

direction will shift due to the group delay of the differentiators. Therefore, a fractional degree differentiator is using in this method to instead the first degree IIR differentiator. The proposed fractional differentiator has very small group delay, about 0.5 samples, which leads to better performance of the edge detector. Another advantage of using the fractional differentiator is that the filter can be changed to suit the given image. For the lena image, the fractional differentiator of degree $v = 0.8$ shows best performance for edge detection. When examining images, one possible optimization technique would be to use a slider to allow an operator to see the effect of varying the degree.

The use of the Caputo edge detector is designed to improve to performance of edge detection, especially for the edge of an image. Fractional edge detectors have better selectivity than classical edge detector with integer degree. The GL IIR fractional edge detector is more sensitive to detail than the CRONE edge detector with same degree and mask length. When compared to previous applications of fractional differentiators for edge detection, it is found that the Caputo edge detector can improve the edge detection because of the faster attenuation of initial transients caused by non-zero initial conditions. This is of concern for real-time application of edge-detection algorithms.

Chapter 6 Conclusion and Future Work

This thesis will conclude by discussing the advantages of some of the new algorithms and techniques suggested in this work, as well as some suggestions for future work that will build upon that reported in the previous chapters. The thesis concentrates on four topics.

Firstly, when considering first degree and second degree differentiators, the proposed low-pass differentiators were designed by optimizing the magnitude response, group delay and variance. The particular transfer functions of the proposed differentiator are given in (2.39) and (3.21). Because a number of desired characteristics of a differentiator were assumed in advance (e.g. sum of the coefficients, the response to an input of constant slope, or the anti-symmetry of coefficients implicit in a linear-phase FIR or close-to-linear phase IIR differentiator, the number of filter coefficients to be optimized was minimized. The proposed low-pass differentiators exhibit many advantages in the frequency domain, such as high accuracy in the pass band, steep roll-off, and almost linear phase response for IIR differentiators. In particular, when compared with the Al-Alaoui low-pass differentiator, for which the filter coefficients are listed in Table 2.1, the proposed differentiators show better accuracy in the pass band, and steeper roll-off.

There are some previously described methods of designing differentiators based on optimization technology, for which the magnitude response over the full frequency band is obtained by approximating some existing differentiators. Examples include the maximally flat low-pass digital differentiator, or the differentiator design based on the Chebyshev method.

Because the low-pass characteristic of the proposed differentiator is achieved by minimizing the weight vectors relating to the various filter characteristics, including the variance of the filter (which is the measure of the average power output for a white-noise input), the new method has better selectivity in the design of the frequency response. Compared with the maximally flat, low-pass digital differentiators, the proposed differentiators show worse accuracy in the pass band. However, both the proposed and maximally flat designs show small passband error, so that it is shown in both cases that error due to coefficient quantization in a fixed-point system is likely to be the limiting factor for the accuracy of the differentiator output.

Chapter 3 of this thesis concentrated on second-degree differentiators, a topic that has not been widely studied to date. It was found that some new design rules relating to the required time-domain performance of such differentiators (e.g. for constant slope and parabolic inputs), and the application of the optimization algorithm, facilitated the design of new second-degree differentiators for both FIR and IIR systems. As with the first-degree differentiators, time- and frequency-domain results show the good performance of the proposed systems.

A second topic of interest in the design of digital differentiators concerns the optimization algorithm chosen for obtaining the coefficients of the proposed low-pass differentiators. In this work, they are obtained by an algoithm which is based on a sequential quadratic programming (SQP) method. This algorithm is achieved by the solver fgoalattain, which can be found in the Matlab Optimization toolbox. The advantage of using this optimization algorithm is that various objectives are considered in the optimization, with different weight vectors. Therefore, the resulting differentiator will have exactly constrained magnitude and phase response performance, as desired. However, a potential

problem of using this optimization algorithm is the need to find suitable starting points (initial 'guess' for the filter parameters), in order to guard against the problem of local minima. A simple and practical method of achieving this for the differentiators studied was outlined in Chapter 2. It would be useful if a more general and provable technique of selecting these start points could be found. Other potential future work associated with this optimization work would consider the application of some other algorithms, such as a genetic algorithm, simulated annealing or neural networks, as alternative means of solving this problem.

The next topic considered involved the design of fractional degree differentiators. In this chapter, a new feedback system was constructed to improve the fractional degree differentiator in terms of both the frequency domain and time domain performance. Additionally, a Caputo fractional degree differentiator was designed, that is based on the RL fractional degree differentiator, with an additional term based on the initial conditions. The fractional differentiator can be very sensitive to the filter coefficients, i.e. a small change of the coefficients can cause a large error in time-domain output. A differentiator design using an optimization technique was chosen to ensure good performance in the frequency domain. However, this technique produced differentiators that showed large output errors when tested in the time domain. Hence, the optimization technique that proved successful in the design of integer degree differentiators was not utilized for the design of fractional differentiators. It is shown that the FIR model of a fractional differentiator based on the RL or GL definition may not produce the desired output in the time domain when the initial conditions of the differentiator differ from those that would pertain in a steady-state system. The problem has been shown to be particularly acute when the integration of output errors is considered over a

long time interval. Future work in this field will involve the consideration of a feedback system to reduce or eliminate this problem.

The thesis also contains the description of two applications for which the new differentiators presented prove advantageous relative to prior work. The first application of the differentiator is the estimation of the frequency components of a power system using a second degree differentiator. A linear phase FIR second degree differentiator is designed to replace the IIR differentiator previously used in the given algorithm. The results show that the FIR based method can reduce the error caused by the non-constant group delay of the IIR differentiator. Therefore the proposed frequency estimator provides a more accurate output.

Finally, the application of image edge detection using a differentiator is introduced and discussed. The edge detectors chosen are designed using fractional IIR differentiators, based on Grunwald-Letnikov and Caputo definitions. The proposed edge detectors are compared with some other edge detectors and show good results. However, many suggestions for future work can be suggested. In this work, there is no clear standard method proposed for the evaluation of different edge detectors. As is common, a qualitative method is used to permit the reader to decide which outputs are visually most pleasing and which are deemed to be most suitable for the user's application. An associated problem is that it is difficult to choose an appropriate performance measure for the edge detector, especially for the fractional-degree edge detector. In this work, a threshold of 0.15 is applied for generating the resultant image, but it can be important to choose an appropriate threshold for the edge detector. A low threshold may miss some edges, and a high threshold may cause excessive noise in the resulting image. Thus, a thresholding algorithm can be advantageous, and will be considered in future work on this topic. Finally, an

edge detector based on an IIR differentiator was designed. It was observed that the position of the corresponding pixel gradient in the x and y directions will effectively shift due to the group delay of the IIR differentiators. Zero-phase filtering can have a useful role in the filtering of off-line data, but it is not applicable to real-time signals. However, zero-phase high-pass filtering is worthy of consideration for the processing of static images.

Bibliography

[1] Bose. T, *Digital Signal and Image Processing*, Wiley, 1st edition, 2003.

[2] Ovaska, S. J., Vainio, O., and Laakso, T. I, “Design of predictive IIR filters via feedback extension of FIR forward predictors”, *IEEE Trans. IMS,* vol. 46, no. 5, pp. 1196-1201 1997.

[3] Al-Alaoui, M. A, “Linear phase low-pass IIR digital differentiators”, *IEEE Trans. Signal Processing,* vol. 55, no. 2, pp. 697-706, 2007.

[4] Markell. R, “‘Better than Bessel’ Linear Phase Filters for Data Communications”, *Linear Technology,* Application Note 56, 1994.

[5] Murthy, H. A. and Gadde, V, “The modified group delay function and its application to phoneme recognition”, *Int. Conf. on Acoustics, Speech, and Signal Processing*, vol. 1, Hong Kong, China, 2003, pp. I-68-71.

[6] Brayton, R.K., S.W. Director, G.D. Hachtel, and L. Vidigal, "A New Algorithm for Statistical Circuit Design Based on Quasi-Newton Methods and Function Splitting," *IEEE Trans. on Circuits and Systems*, vol. CAS-26, pp 784-794, 1979.

[7] Grace, A.C.W., "Computer-Aided Control System Design Using Optimization Techniques," *Ph.D. Thesis*, University of Wales, Bangor, Gwynedd, UK, 1989.

[8] Diniz P. S. R., da Silva E. A. B. and Netto, S. L., *Digital Signal Processing:*

System Analysis and Design, Cambridge University Press, 2nd edition, 2010.

[9] Vainio. O, Renfors. M, and Saramaki. T, "Recursive Implementation of FIR Differentiators with Optimum Noise Attenuation", *IEEE Trans. Instrum and Meas,* vol. 46, no. 5, pp. 1202-1207, 1997.

[10] Al-Alaoui, M. A, "Novel digital integrator and differentiator", *IEE Electron. Lett*, vol. 29, no.4, pp. 376-378, 1993.

[11] Al-Alaoui, M. A, "A Class of Second Order Integrators and Low-pass Differentiator", *IEEE Trans. Circuit Syst I, Fundam. Theory Appl*, vol. 42, no.4, pp. 220-223, 1995.

[12] Al-Alaoui, M. A, "Class of digital integrators and differentiators", *IET. Signal Processing,* vol. 5, no. 2, pp. 251-260, 2011.

[13] Chien-Cheng Tseng, "Stable IIR digital differentiator design using iterative quadratic programming approach", *Signal Processing*, vol. 80, no. 5, pp. 857-866, 2000.

[14] Wei Zhu, Zhezhao Zeng and Yongqing Zhou, "Optimal design of High-Order Digital Differentiator", *Signal Processing, ICSP 2008 Int. Conf*, pp 2892-2895.

[15] Carlsson, B., "Maximum flat digital differentiator," *Electron. Lett.*, vol. 27, no.8, pp. 675-677, 1991.

[16] Khan, I.R. and Ohba, R. , "New design of full band differentiators based on Taylor series", *IEE proceedings- Vision, image and Signal Processing,* vol. 146, pp. 185-189, 1999.

[17] Soo-Chang Pei and Peng-Hua Wang, “Closed-form design of maximally flat FIR Hilbert transformers, differentiators, and fractional delayers by power series expansion”, *IEEE Trans. on Circuits and Systems I*, vol. 48, pp. 389-398, 2001.

[18] Selesnick, I.W, “Maximally flat low-pass digital differentiator”, *IEEE Trans. on Circuits and Systems II*, vol. 49, no. 3, pp. 219-223, 2002.

[19] Rabiner, L., Bell Laboratories, Murray Hill, N.J. and McClellan, J.H. ; Parks, T.W., “FIR digital filter design techniques using weighted Chebyshev approximation”, *IEEE Proceedings*, vol.63, no.4,pp. 595-610, 1975.

[20] Al-Alaoui, M. A, “Novel approach to designing digital differentiators”, *Electronics letters*, vol.28, no15, pp. 1376-1378, 1992.

[21] Al-Alaoui, M. A, “Novel IIR differentiator from the Simpson integration rule”, *IEEE trans on Circuits and Systems I*, vol. 41, no. 2, pp. 186-187, 1994.

[22] Tahmasbi, A. ; Shokouhi, S.B., “New optimized IIR Low-Pass Differentiators”, *Int. Conf. on Signal Acquisition and Processing*, Bangalore, India, pp. 205-209, 2010.

[23] Astrom, K. J., Jury, E. I., and Agniel, R. G, “A numerical method for the evaluation of complex integrals”, *IEEE trans. Automatic Control,* vol. 15, no 4, pp 468-471 1970.

[24] Kavanagh, R. C., “FIR Differentiators for Quantized Signals”, *IEEE Trans. Sig processing*, vol. 49, no. 11, 2001.

[25] Steven N .R, Richard. S, Gabor C .T, *Delta-Sigma Data Converters*. New York, IEEE Press, 1996.

[26] Skolnik .M.I, *Introduction to Radar Systems*, McGraw-Hill, New York, 1980.

[27] Cong Yin, Xiaojun Zhou, Zhiyao Zhang, Shenghui Shi, and Yong Liu, "Second-order optical differentiator based on a mechanically-induced LPFG with a single π-shift", *IEEE SOPO Symposium,* 2012.

[28] Mark G. Frei, Ruslan L, Davidchack and Ivan Osorio, "Least Squares Acceleration Filtering for the estimation of Signal Derivatives and Sharpness at Extrema", *IEEE Trans. Biom Eng*, vol. 46, No. 8, pp. 971-977,1999.

[29] Chien-Cheng Tseng and Su-Ling Lee, "Design of second order digital differentiator using Richardson extrapolation and fractional delay", *IEEE Int. Conf. Symposium on Circuits and Systems*, Seattle, USA, 2008, pp. 1120-1123.

[30] Cafagna .D, "Fractional calculus: A mathematical tool from the past for present engineers", *IEEE Industrial Electronics Magazine,* vol. 1, no. 2, pp 35-40, 2007.

[31] Yang Quan Chen, Petras .I, Dingyu Xue, "Fractional order control - A tutorial", *In American Control Conference*, pp. 1397-1411, 2009.

[32] Oustaloup .A, Melchoir .P, Lanusse .P, Cois .C, and Dancla .F, "The CRONE toolbox for Matlab", *In Proceedings of the 11th IEEE international Symposium on Computer Aided Control System Design,* Anchorage, USA, Sep 2000, pp 190-195.

[33] Podlubny .I, “Fractional-order systems and $PI^{\lambda}D^{\mu}$ controllers”, *IEEE Trans, Automatic Control*, vol. 44, no. 1, pp 208-214, Jan 1999.

[34] Mathieu .B, Melchior .P, Oustaloup .A, Ceyral .Ch, “Fractional differentiation for edge detection”, *Signal Processing*, vol. 83, no. 11, pp 2421-2432, Nov 2003.

[35] Hilfer R, *Applications of Fractional Calculus in Physics*, Singapore: World Scientific, 2000.

[36] Sebaa .N, Fellah Z. E. A., Lauriks .W, Depollier .C, “Application of fractional calculus to ultrasonic wave propagation in human cancellous bone”*, Signal Processing archive,* vol. 86, no. 10, pp 2668-2677, 2006.

[37] Assaleh .K; Ahmad W.M., ”Modeling of speech signals using fractional calculus” *9th International Symposium on Signal Processing and Its Applications*, pp 1 – 4, 2007.

[38] Kulish V. V. and Jose L. “Application of Fractional Calculus to Fluid Mechanics”, *J. Fluids Eng*, vol. 124, no. 3, pp 803, 2002.

[39] Soczkiewicz .E, “Application of fractional calculus in the theory of viscoelasticity”, *Molecular and Quantum Acoustics*, vol.23, pp 397-404, 2002.

[40] Podlubny .I, *Fractional Differential Equations*, *Academic Press,* San Diego,

1999.

[41] Samko S. G., Kilbas A. A., Marichev O. I., *Fractional Integrals and Derivatives: theory and applications, Gordon and Breach*, Amsterdam, 1993.

[42] Chien-Cheng Tseng, "Improved design of digital fractional-order differentiators using fractional sample delay", *IEEE Circuits and System I*, vol. 53, no. 1, pp 193-203, 2006.

[43] Diethelm .K, Ford .N. J, Freed .A. D, Luchko .Yu, "Algorithms for the fractional calculus: a selection of numerical methods", *Computer Methods in Applied Mechanics and Engineering,* vol. 194, pp 743-773, 2005.

[44] Aoun .M, Amairi .M,.; Najar, S.; Abdelkrim, M.N, "Simulation method of fractional systems based on the discrete-time approximation of the Caputo fractional derivatives", In *8th Intl Multi-Conference on Systems, Signals and Devices*, pp 1 – 6, 2011.

[45] Odibat .Z, "Approximations of fractional integrals and Caputo fractional derivatives", *Applied Mathematics and Computation,* vol. 178, no. 2, pp 527-533, 2006.

[46] Petras .I, "Fractional-order feedback control of a DC motor", *Journal of Electrical Engineering,* vol. 60, no. 3, pp 117-128, 2009.

[47] Smith J.M, *Mathematical Modeling and Digital Simulation for Engineers and Scientists*, 2nd ed., Wiley, New York, 1987.

[48] Machado .J.A.T, “Discrete-Time Fractional Order Controller”, *Journal of fractional Calculus & Applied Analysis*, vol.4, no. 1, pp.47-66, 2001.

[49] Chien-Cheng Tseng, “Design of Fractional Order Digital FIR Differentiators”, *IEEE Signal processing letters*, vol. 8, no. 3, pp 77-79, 2001.

[50] Barbosa R.S., Tenreiro Machado J.A., Silva M.F., “Time domain design of fractional differintegrators using least-squares”, *Signal Processing,* vol. 86, no. 10, pp 2567-2581, 2006.

[51] YangQuan Chen, Blas M. Vinagre, “A new IIR-type digital fractional order differentiator”, *Signal Processing,* vol. 83, no. 11, pp 2359-2365, 2003.

[52] Yang Zhu Zhong, Zhou Ji Liu, “An Improved Design for the IIR-Type Digital Fractional Order Differential Filter”, *2008 International Seminar on Future BioMedical Information Engineering*, pp 473-476, USA, 2008.

[53] Lorentzen L., Waadeland H., *Continued Fractions with Applications*, Addison-Wesley, North-Holland, Amsterdam, 1992.

[54] Trigeassou J.C., Maamri N., Oustaloup A., “Automatic initialization of the Caputo fractional derivative”, *In IEEE Decision and Control and European Control Conf*, Orlando, Dec. 2011, pp 3362-3368.

[55] Thabet Abdeljawad, “On Riemann and Caputo fractional differences”, *Special Issue on Advances in Fractional Differential Equations II*, vol. 62, no.

3, pp 1602-1611, 2011.

[56] Sarkar .A and Sengupta .S, “Second-degree digital differentiator-based power system frequency estimation under non-sinusoidal conditions”, *Science, Measurement & Technology, IET*, vol. 4, 2010, pp 105-114.

[57] Karimi-Ghartemani and Iravani, “A new phase-locked loop (PLL) system”, *Proc. 44th IEEE 2001 Midwest Symp. on Circuits and Systems*, vol. 1, Dayton , pp. 401– 424, 2001.

[58] Karimi-Ghartemani, M and Iravani, M.R., “A nonlinear adaptive filter for online signal analysis in power systems: applications”, *IEEE Trans. Power Deliv*, vol. 17, no. 2, pp 617-622, 2002.

[59] Karimi-Ghartemani, M and Iravani, M.R., “Robust and frequency-adaptive measurement of peak value”, *IEEE Trans. Power Deliv*, vol. 19, no. 2, pp 481-489, 2004.

[60] Karimi-Ghartemani, M and Iravani, M.R., “Measurement of harmonics /inter-harmonics of time-varying frequencies”, *IEEE Trans. Power Deliv*, vol. 20, no. 1, pp 23-31, 2005.

[61] Canny, J, “A Computational Approach to Edge Detection” , *IEEE Trans. PAMI,* vol. 8, no. 6, pp. 679-698, 1986.

[62] Gao, C.B. ; Zhou, J.L. ; Hu, J.R. ; Lang, F.N, “Edge detection of colour image

based on quaternion fractional differential", *Image Processing, IET,* vol. 5, no. 3, pp. 679-698, 2011.

[63] Deriche .R, "Using Canny's criteria to derive a recursively implemented optimal edge detector", *Intl. J. Comput. Vision,* vol. 1, no.2, pp 167-187,1987.

[64] Haibo Yang ; Yongqiang Ye ; Danwei Wang ; Bin Jiang, "A novel fractional-order signal processing based edge detection method", 11th *International Conference on Control Automation Robotics & Vision (ICARCV)*, pp 1122-1127, 2010, Singapore.

[65] Al-Alaoui, M. A, "Novel FIR approximations of IIR differentiators with applications to image edge detection", *International Conference on Electronics, Circuits and Systems (ICECS),* pp 554-558, 2011, Beirut.

[66] Al-Alaoui, M. A, "Direct approach to image edge detection using differentiators", *17th IEEE International Conference on Electronics, Circuits, and Systems (ICECS)*, pp 154-157, 2010.

[67] SobeL. I, "Neighborhood coding of binary images for fast contour following and general array binary processing", *Computer Vision, Graphics and Image Processing*, vol. 8, pp 127-135, 1978.

[68] Prewitt J.M.S, "Object enhancement and extraction", *Picture Processing and Psychopictorics*, pp 75-149, 1970.

[69] SongWang, Feng Ge, and Tiecheng Liu, "Evaluating Edge Detection through

Boundary Detection", *EURASIP Journal on Applied Signal Processing*, vol. 2006, pp1-15.

[70] Heath .M. D, Sarkar .S, Sanocki .T, and Bowyer .K. W, "A robust visual method for assessing the relative performance of edge-detection algorithms," *IEEE Transactions on Pattern Analysis and Machine Intelligence*, vol. 19, no. 12, pp. 1338–1359, 1997.

[71] Baker .S and Nayar .S. K, "Global measures of coherence for edge detector evaluation," in *Proceedings of IEEE Computer Society Conference on Computer Vision and Pattern Recognition (CVPR '99)*, vol. 2, pp. 373–379, Fort Collins, Colo, USA, 1999.

[72] Laakso .T. I, Valimaki .V, Karjalainen .M and Laine .U.K, "Splitting the unit delay: tool for fractional delay filter design," *IEEE Signal Processing Magazine*, pp.30-60, 1996.